NUMERICAL ANALYSIS OF TURBULENT FLOW AND HEAT TRANSFER WITH NANOFLUID IN ELLIPTICAL CROSS-SECTIONED DUCT

KAĞAN PENEKLİOĞLU

FEBRUARY 2017

NUMERICAL ANALYSIS OF TURBULENT FLOW AND HEAT TRANSFER
WITH NANOFLUID IN ELLIPTICAL CROSS-SECTIONED DUCT

A THESIS SUBMITTED TO
THE GRADUATE SCHOOL OF NATURAL AND APPLIED
SCIENCES OF
ÇANKAYA UNIVERSITY

BY
KAĞAN PENEKLİOĞLU

IN PARTIAL FULFILLMENT OF THE REQUIREMENTS FOR THE
DEGREE OF
MASTER OF SCIENCE
IN
THE DEPARTMENT OF
MECHANICAL ENGINEERING

FEBRUARY 2017

Title of the Thesis: **Numerical Analysis of Turbulent Flow and Heat Transfer with Nanofluid in Elliptical Cross-Sectioned Duct**
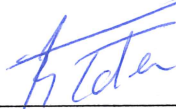
Submitted by **Kağan Peneklioğlu**

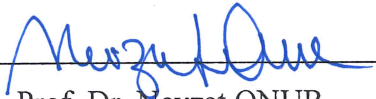Approval of the Graduate School of Natural and Applied Sciences, Çankaya University.

_____

Prof. Dr. Halil Tanyer EYYUBOĞLU

Director

I certify that this thesis satisfies all the requirements as a thesis for the degree of Master of Science.

_____

Prof. Dr. Sıtkı Kemal İDER

Head of Department

This is to certify that we have read this thesis and that in our opinion it is fully adequate, in scope and quality, as a thesis for the degree of Master of Science.
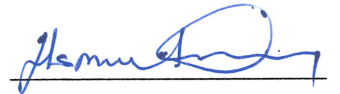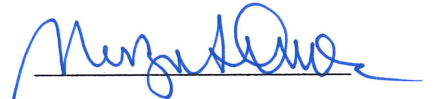
_____

Prof. Dr. Nevzat ONUR

Supervisor

Examination Date: 10.02.2017

Examining Committee Members (first name belongs to the chairperson of the jury and the second name belongs to supervisor)
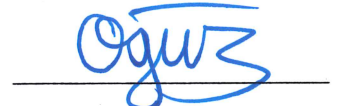
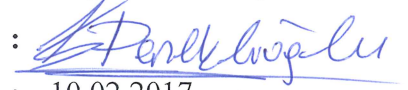|		
Prof. Dr. Haşmet TÜRKOĞLU	(Çankaya Univ.)	_____
Prof. Dr. Nevzat ONUR	(Çankaya Univ.)	_____
Assoc. Prof. Dr. Oğuz TURGUT	(Gazi Univ.)	_____

STATEMENT OF NON-PLAGIARISM PAGE

I hereby declare that all information in this document has been obtained and presented in accordance with academic rules and ethical conduct. I also declare that, as required by these rules and conduct, I have fully cited and referenced all material and results that are not original to this work.

Name, Last Name : Kağan Peneklioğlu

Signature :

Date : 10.02.2017

ABSTRACT

NUMERICAL ANALYSIS OF TURBULENT FLOW AND HEAT TRANSFER WITH NANOFLUID IN ELLIPTICAL CROSS-SECTIONED DUCT

Peneklioğlu, Kağan

M.Sc., Department of Mechanical Engineering

Supervisor: Prof. Dr. Nevzat ONUR

February 2017, 133 pages

In this study, varying major to minor axis ratio in an elliptic tube has been investigated numerically under the steady state, forced convection with turbulent heat flow conditions. Constant wall temperature was applied to tube wall. Mainly, hydrodynamically and thermally developed turbulent flow has been investigated. To obtain fully turbulent flow, study was performed Reynolds numbers between 10000 and 100000. Water was used as working fluid in the first part of study. ANSYS Fluent 17.0 tool was used for all simulations. After the end of numerical results, average Nusselt numbers and average friction factors were obtained and they were compared with correlations which are commonly used in the literature.

Al$_2$O$_3$ / Water nanofluid was used as working fluid in the second part of study and all simulations were repeated. It is noticed that using of nanofluid increases average Nusselt number significantly. However, it leads to an increase in pressure drop inside the tube. As a result, it causes an increase in average friction factor. According to the results of the study, using of nanofluid increases average Nusselt number almost 13% in all models. At the same time, it causes an increase in average friction factor around 1.7%. It is noticed that different major to minor axis ratios have no significant effect on average Nusselt number and average friction factor. Also, correlations in the form of $Nu = a_1 \times Re^{b_1}$ and $f = a_2 \times Re^{b_2}$ are obtained for average Nusselt number and average friction factor in all models.

Keywords: Elliptic Channel, Turbulent Flow, Forced Convection, Numerical Heat Transfer Analysis, Nanofluids

ÖZ

ELİPTİK KESİTLİ BİR KANAL İÇERİSİNDEKİ ISI TRANSFERİNİN TÜRBÜLANSLI KOŞULLAR ALTINDA VE NANO-AKIŞKAN KULLANIMIYLA BERABER SAYISAL OLARAK İNCELENMESİ

Peneklioğlu, Kağan

Yüksek Lisans, Makine Mühendisliği Anabilim Dalı

Tez Yöneticisi: Prof. Dr. Nevzat ONUR

Şubat 2017, 133 sayfa

Bu çalışmada, a / b oranları değişen eliptik kesitli kanal içerisindeki zorlanmış taşınım ve ısı transferi türbülanslı akış koşullarında nümerik olarak incelenmiştir. Kanal duvarına sabit yüzey sıcaklığı sınır şartı uygulanmıştır. Genel olarak hidrodinamik ve ısıl olarak gelişmiş olan türbülanslı akış şartları kararlı rejim koşullarında incelenmiştir. Tam türbülanslı akış koşullarını elde edebilmek için çalışma, 10000 ile 100000 aralığındaki farklı Reynolds Sayılarında gerçekleştirilmiştir. Çalışmanın ilk bölümünde akışkan olarak su kullanılmıştır. Nümerik analizler ANSYS Fluent 17.0 paket programında yapılmıştır. Nümerik analizler sonucu elde edilen ortalama Nusselt sayıları ve ortalama sürtünme faktörleri literatürde bulunan başka bağıntılar ile kıyaslanmıştır.

Çalışmanın ikinci kısmında, akışkan olarak Al_2O_3 / Su nanoakışkanı kullanılıp, tüm hesaplamalar tekrar edilmiştir. Nanoakışkanın ortalama Nusselt sayısını önemli ölçüde arttırdığı görülmüştür. Ancak nanoakışkan kullanımı içerideki basınç düşümünü de arttırmıştır. Dolayısıyla sürtünme katsayısında da artışa sebep olmuştur. Çalışma sonucunda, nanoakışkan kullanımıyla beraber ortalama Nusselt sayısı tüm modellerde %13 artmıştır. Öte yandan sürtünme katsayısı da aynı şekilde yaklaşık olarak % 1.7 artmıştır. Eliptik kanal için değişen a / b oranlarının ortalama Nusselt sayısı ve Darcy friction factorleri için önemli bir etkisi olmadığı görülmüştür. Ayrıca ortalama Nusselt sayısı için, $Nu = a_1 \times Re^{b_1}$ ve ortalama Darcy sürtünme faktörü için $f = a_2 \times Re^{b_2}$ formunda bağıntılar tüm modeler için elde edilmiştir.

Anahtar Kelimeler: Elliptik kanal, türbülanslı akış, zorlanmış taşınım, sayısal ısı transferi analizi, nanoakışkan

ACKNOWLEDGEMENTS

I wish to express my deepest gratitude to my supervisor Prof. Dr. Nevzat ONUR for his guidance, advice, criticism, encouragements and insight throughout the research.

I would also like to thank Prof. Dr. Haşmet TÜRKOĞLU and Assoc. Prof. Dr. Oğuz TURGUT for their suggestions and comments.

I would also like to thank my family for their support and love.

Finally, and most importantly, I would like to thank my wife, Hale, for sharing my happiest moments and giving me the morale in the most difficult times. I am grateful to her for her endless support, tolerance and patience, which she exhibited throughout study.

TABLE OF CONTENTS

LIST OF FIGURES

xiv

LIST OF TABLES

NOMENCLATURE

a	Major Axis of Ellipse
A_c	Cross-sectional Area
A_s	Surface Area
b	Minor Axis of Ellipse
C_{fx}	Local Darcy Friction Factor
c_p	Specific Heat
D_h	Hydraulic Diameter
D_{np}	Diameter of Nanoparticles
f_m	Average Darcy Friction Factor
h	Local Heat Transfer Coefficient
$\bar{h}$	Average Heat Transfer Coefficient
k-ω	Turbulent Kinetic Energy and Specific Dissipation Rate
L	Length of the Tube
$\dot{m}$	Mass Flow Rate
Nu_m	Average Nusselt Number
Nu_x	Local Nusselt Number
P	Perimeter
Pr	Prandtl Number
q_s''	Local Heat Flux
Re	Reynolds Number
T_i	Inlet Temperature
T_m	Mean Temperature
T_o	Outlet Temperature
T_s	Surface Temperature
T_w	Wall Temperature
u	x component of Velocity
u_i	Inlet Velocity
u_m	Average Velocity in x-direction

v	y component of Velocity
w	z component of Velocity
T	Local Fluid Temperature
k	Thermal Conductivity
ΔT_{lm}	Logarithmic Mean of Temperature Differences
ΔP	Pressure Differences
η	Effectiveness
θ	Dimensionless Temperature
μ	Dynamic Viscosity
ρ	Density
τ_w	Wall Shear Stress
ϕ	Nanoparticles Volume Fraction

Subscripts

bf	base fluid
eff	effective
nf	nanofluid
np	nanoparticle

Abbreviations

CFD	Computational Fluid Dynamics
SST	Shear Stress Transport

1. INTRODUCTION

It has a great importance to determine the amount of heat transfer and the flow behavior in a tube. Removing the heat from the systems which include heat exchangers is crucial in terms of thermal efficiency. In order to make this kind of systems work efficiently, it is necessary to choose a proper tube geometry. In this type of implementations, non-exact circular tube geometries are widely accepted. In recent implementations, heat exchangers with elliptical cross-section have come forward. It has been observed that this type of heat exchangers are thermally more efficient than the heat exchangers with circular cross-section which have the same surface area. Usage of the elliptic pipes instead of the circular pipe is recommended by Shariat et al. especially in heat transfer applications [4]. The tubes with elliptical cross-section which will be examined in this study are preferred in the automotive, energy, and electronic cooling industries.

Another implementation to increase the thermal efficiency of heat exchangers is increasing the heat transfer by changing the thermophysical properties of the fluid in the tube. It has been a well-known method to increase the convection heat transfer by adding small solid particles which have high thermal conductivity into the fluid since 1980s. Until early 2000s, solid particles that are produced were micro-scale. These relatively bigger particles caused corrosion on the tube wall in time. Today, it is possible to produce particles at nano-scale. Using of these ultra-fine particles with conventional fluid together can be defined as nanofluid. Nanofluids are basically defined as mixture of solid nanoparticles and conventional base fluid such as oil, water and ethylene glycol mixture. Nano particles can be easily fluidized with the fluid.

Therefore, using nanofluid does not cause corrosion on the tube surface anymore. It has been observed that using of nanofluid dramatically increases heat transfer.

In the first part of the study, five different major to minor axis ratio in an elliptic tube has been investigated numerically. Length of the tube was chosen to provide hydrodynamically and thermally fully developed flow conditions. Constant surface temperature boundary conditions is applied to tube wall. All numerical studies has been carried out as steady-state and water is used as working fluid in the first part of study. Reynolds Numbers in all simulations kept in the range of $10^4 \leq Re \leq 10^5$. $SST\ k - \omega$ turbulence model was used to solve turbulence equations.

In the second part of the study, Al_2O_3 / Water nanofluid was used as working fluid and all calculations were repeated. Continuity, momentum, energy and turbulence equations were solved by ANSYS Fluent 17.0 which uses using finite volume method to solve numerical equations. After the end of study, the change of average Friction factor and average Nusselt number with respect to Reynolds number has been examined on both part of the study.

2. LITERATURE SURVEY

Numerous experimental, numerical and analytical studies about flow and heat transfer are available in the literature with various geometric cross-sections. In the literature review, studies comparing a channel with an elliptic section and a channel without an elliptical section have been taken into consideration. In addition, many articles have been reviewed in order to understand the effect of nanofluid use on heat transfer applications. The studies reviewed are presented below.

Bianco et al. [1] have shown that the use of nanofluids for laminar flow in a circular duct increases heat transfer. Single phase and two-phase modeling approach was used in this study. They modeled thermophysical properties of the fluid as both constant and varying with temperature. As a result, they noticed that use of nanofluid increases heat transfer. They also stated that single-phase and two-phase modeling approaches give similar results.

Dawood et al. [2] studied heat transfer for different nanofluids for both laminar flow and turbulent flow for an elliptical annulus channel. Four different nanoparticles with different volume fractions were investigated under constant heat flux boundary conditions. The results show that the SiO_2-water nanofluid is the best in terms of thermal performance. It was also found that the increased volume fraction increased the Nusselt number.

Vajjha et al. [3] developed new correlations with numerical analysis performed by using two different nanoparticle (Al_2O_3 and Cuo) and two different base fluid (ethylene glycol and water) under turbulent conditions. They have come to the conclusion that the Nusselt number and friction factor correlations that can be used in nanofluid flows should depend on the particle volume fraction.

Al$_2$O$_3$-water nanofluid in an elliptical tube under laminar and constant heat flux conditions numerically examined by Shariat et al [4]. They used the two-phase modelling approach. The results show that the increasing nanoparticle volume fraction increases Nusselt number while the local skin friction factor decreases. Besides, they also seen that the local skin friction factor increases with the increase of the a / b ratios in the elliptic channel, but the local Nusselt number does not change significantly. They also noticed that usage of the elliptic pipes with a / b = 1.33 instead of the circular pipe is recommended.

Hussein et al. [5] have numerically examined the TiO$_2$ nanofluid in three different tubes (circular, elliptical, flat). As the nanoparticle ratio in the nanofluid increases, the heat transfer improves. They also emphasized that there is a difference of 2% between the experimental study and the numerical study. They indicated that the highest value of the heat transfer coefficient was in the flat tube, followed by elliptical and circular tubes, respectively.

Namburu et al. [6] found a new correlation for viscosity in numerical analysis using three different nanoparticles (CuO, Al$_2$O$_3$, SiO$_2$) and two different base fluids (ethylene glycol, water) under constant heat flux boundary conditions and turbulent flow conditions. The correlation developed according to the nanoparticle volume fraction was confirmed by experimental studies. Moreover, Nusselt numbers in their studies are found to be compatible with the existing correlations in the literature. They also found that nanoparticles with smaller diameters have higher viscosity values and higher Nusselt number.

Yarmand et al. [7] used four different (Al$_2$O$_3$, ZnO, CuO, SiO$_2$) nanoparticle with different volume fractions to study the thermal characteristic of nanofluid in a rectangular channel with constant heat flux boundary conditions and turbulent flow conditions. The results show that the SiO$_2$ nanofluid has the highest Nusselt number. They are also found that Nusselt number increases with increasing nanoparticle volume fraction.

Abdel-Wahed et al. [8] examined the thermal and hydrodynamic behavior of flow in an experiment with an elliptic cross-sectional channel with a / b ratio of 2 in laminar flow conditions. Nusselt number and friction factor were compared with similar studies in the literature.

Ebadian et al. [9] used the successive approximation method to examine convective heat transfer in a elliptic cross-sectional channel under constant wall temperature boundary conditions. The Nusselt number found by analytically solving the elliptic equations was found very close to the exact value.

Analytical and experimental work about laminar flow in elliptical channel by Bhatti [10] was found to be consistent. The Karman-Pohlhausen integral method was used for the analytical study. It has been found that the results are similar under the flow is hydrodynamically fully developed assumption.

The results of heat equation under laminar flow and constant wall temperature boundary conditions were solved numerically by Dunwoody [11]. Results are listed for different aspect ratios. The results show that the Nusselt number decreases with increasing aspect ratio.

Onur et al. [14] numerically examined steady-state forced convection heat transfer and pressure drop characteristics for hydrodynamically fully developed and thermally developing three-dimensional turbulent flow in a horizontal trapezoidal duct. They investigated both experimentally and numerically in the Reynolds number range from $2.6x10^3$ to $67x10^3$. They also found that new equations for average Nusselt number and average Darcy friction factor in the form of $Nu = C_2 Re^{n_1}$ and $f = C_3 Re^{n_3}$. In addition, they compared constants in the equations they were found by using numerous turbulence models. Results have shown that there is a good agreement between experimental and numerical results.

3.   HEAT TRANSFER

Heat transfer is thermal energy transportation between media due to temperature differences. If there is temperature difference, heat transfer must occur from hot media to cold media. There are three different heat transfer mechanism which are conduction, convection and radiation.

Convection heat transfer is the kind of energy transfer between a solid surface and the adjacent fluid (liquid or gas) that is in motion, and it requires the combined effects of conduction and fluid motion. If there is no any bulk fluid motion, heat transfer between a solid surface and the adjacent fluid is by pure conduction. If there is bulk motion in fluid, heat transfer will be increased.

Convection heat transfer can be categorized according to the nature of the flow. In forced convection, flow is triggered by external means, such as by a fan, a pump, or atmospheric winds. In natural convection, buoyancy forces are entirely responsible for fluid motion when the fluid is heated. In other words, an increase in temperature produces a reduction in density, which in turn causes fluid motion due to pressures and forces when fluids of different densities are affected by gravity.

3.1.   Forced Convection

Laminar and turbulent flow

It is important that the flow is laminar or turbulent for the calculations of convection heat transfer. Frictional force, pressure drop and heat transfer phenomena depend on the laminar or turbulent characteristic of the flow. In a fluid, if the fluid particles follow the same direction without any circular movements, this flow is called

laminar flow. If the fluid particles move circularly without following the same direction, this flow is called turbulent flow.

As the fluid moves slowly from the entrance of the tube, flow irregularity begins and as the fluctuations increase, the fluid switches to the turbulent flow. At the end of the boundary layer, the flow is entirely turbulent.

The area which has the turbulent consists of three different layers, which are viscous sublayer, buffer layer, and turbulent region. In the viscous sublayer, the velocity is almost linear.

In order to determine if the flow is laminar or turbulent, it is necessary to calculate Reynolds number. In the tube, the Reynolds number is defined as:

$$Re = \frac{\rho V D_h}{\mu} \qquad\qquad 3.1$$

μ (kg/m.s) represents the dynamic viscosity of the fluid, ρ (kg/m^3) represents the density of the fluid, V (m/s) represents the average velocity of the fluid in the tube, and D_h (m) represents the hydraulic diameter of the tube.

In the flow, the critical Reynolds number is defined as:

$$Re \approx 2300 \qquad\qquad 3.2$$

This value is interval value for laminar and turbulent flow.

For laminar flow, it is defined as:

$$Re \leq 2300 \qquad\qquad 3.3$$

In the same way, for the full-turbulent flow, it is defined as:

$$Re \geq 10000 \qquad\qquad 3.4$$

Length of Hydrodynamic Entrances

In the flow in the tube, in addition to laminar or turbulent flow, entrance and fully-development conditions are also examined. As soon as the fluid enters the tube, it starts to interact with the surface. As a result of this interaction, effects of friction become important and as the fluid moves forward, the boundary layer develops. This development ends when the frictionless flow region becomes smaller and boundary layers merge at the tube axis. At the merge point, friction has an effect through the whole section and the velocity profile does not change in the axial direction any more. Starting from this point, the flow is defined as developed. The distance from the entrance to the point where this condition occurs is defined as length of hydrodynamic entrance$(x_{fd,h})$.

With the help of these results, the length of tube which the hydrodynamic fully-developed area occurs for laminar flow is defined as:

$$\left(\frac{x_{fd,h}}{D_h}\right)_{lam} \approx 0.05 Re \qquad\qquad 3.5$$

On the other hand, there is no general statement for turbulent flow unlike laminar flow. However, it is known that this length is independent from Reynolds number in turbulent flow conditions. The length of the hydrodynamic fully-developed area in turbulent flow conditions is defined as:

$$10 \leq \left(\frac{x_{fd,h}}{D_h}\right)_{turb} \leq 60 \qquad\qquad 3.6$$

For this reason, $(x_{fd,h}/D_h) > 10$ gives the distance on which the hydrodynamic fully-developed conditions are settled in turbulent flow conditions.
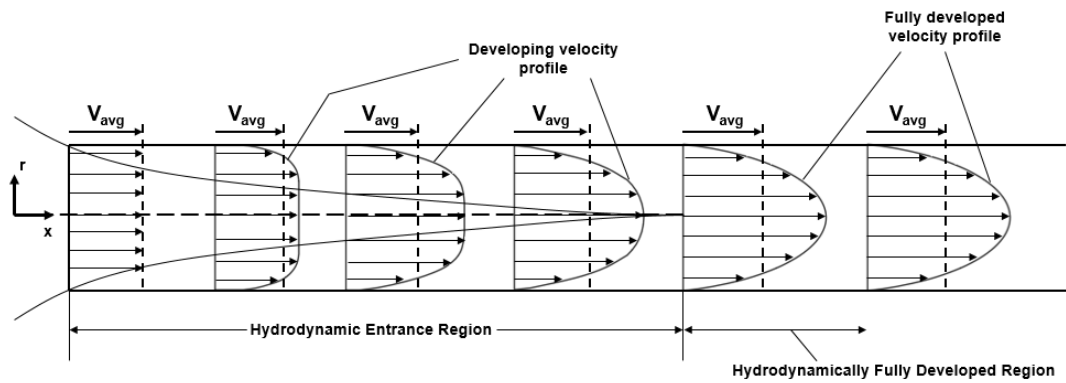
Figure 1. Development of Velocity Boundary Layer

The velocity of a fluid which enters the tube that has a circular section with a uniform velocity profile is zero on walls and as the fluid interacts with the tube walls, the velocity decreases gradually from the middle section to the boundaries. In order to keep the mass flowrate constant, it is required that the velocity in the middle section be higher than the velocity in the boundaries. As a result, velocity profile is constantly developing in the tube.

Length of Thermal Entrances

When a fluid enters the tube with a temperature which is higher than the surface temperature, convectional heat transfer occurs and thermal boundary layer begins to develop. This development of the boundary layer continues until the fully-developed thermal conditions are settled in the tube. Besides, not depending on whether the tube surface boundary condition is constant temperature or constant heat flux, if the tube is long enough, fully-developed thermal conditions are settled. When fully-developed thermal conditions are settled, heat transfer coefficient becomes independent from axial direction.

9
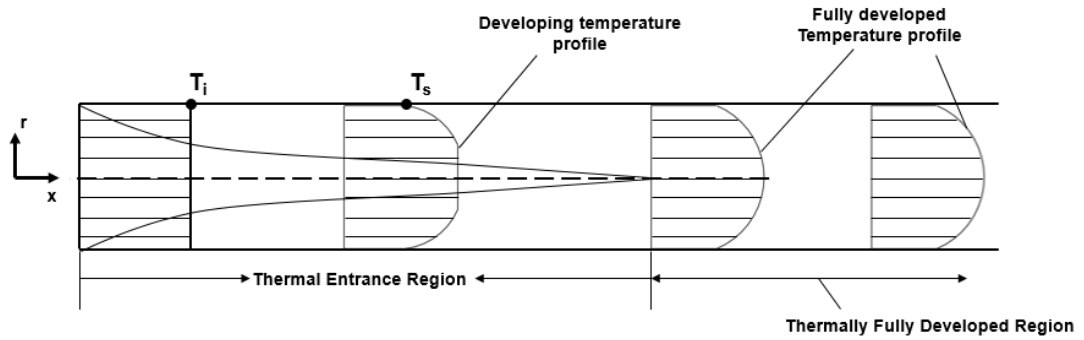
Figure 2. Development of Thermal Boundary Layer

Thermal entrance length for laminar flow is defined as:

$$\left(\frac{x_{fd,t}}{D_h}\right)_{lam} \approx 0.05 RePr \tag{3.7}$$

In addition, for turbulent flow conditions are almost independent from Reynolds and Prandtl numbers and thermal entrance length is generally express as $(x_{fd,t}/D_h) \cong 10$.

If we compare equation 3.5 and 3.7, we can see that if Pr>1, hydrodynamic boundary layer develops faster than thermal boundary layer and if Pr<1, vice versa. For the fluids such as oil which has a big Prandtl number, hydrodynamic boundary layer is much smaller than thermal boundary layer and it is meaningful to assume that fully-developed velocity profile occurs in the whole thermal entrance region.

3.2. The Dimensionless Numbers Used in Numerical Study

The reason why dimensionless numbers are used is to simplify the operations with the dimensionless numbers which include all the parameters instead of dealing with plenty of parameters separately.

Among the dimensionless numbers which are used in forced convection heat transfer, the most common ones are Reynolds number (Re), local Nusselt number (Nu_x), average Nusselt number (Nu_m), local Darcy friction factor (C_{fx}), average Darcy friction factor (f_m), and Prandtl number (Pr).

When these numbers are determined, we can comment on the thermal and flow performance of that flow. In this study, the thermal and flow performance of elliptic tube under different geometric conditions are investigated by calculating the dimensionless numbers.

3.2.1. Reynolds Number

Flow in a tube, Reynolds number, the ratio between inertial forces to viscous forces, is defined as below:

$$Re = \frac{\rho V D_H}{\mu} \tag{3.8}$$

where;

D_h	(m)	hydraulic diameter of the tube,
ρ	(kg/m^3)	density of fluid,
V	(m/s)	mean velocity of flow
μ	(kg/m.s)	dynamic viscosity of fluid

Hydraulic Diameter

The hydraulic diameter given in equation 3.9 is used for noncircular tubes instead of tube diameter.

$$D_h = \frac{4A_c}{P}$$

(3.9)

where,

A_c (m^2)   cross-sectional area of tube

P   (m)   wetter perimeter

Wetted Perimeter and Cross-Sectional Area of Ellipse

In order to calculate Reynolds number, hydraulic diameter must be determined. To do this, wetted perimeter and cross-sectional area of elliptic channel should be calculated. Perimeter of ellipse can be calculated as follows [12]

$$P = \pi(a + b) \sum_{n=0}^{\infty} \binom{0.5}{n}^2 h^n$$

3.10)

where

$$h = \frac{(a - b)^2}{(a + b)^2}$$

(3.11)

12
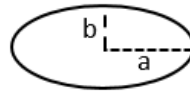
Cross-sectional area of ellipse can be calculated as follows:

$$A_c = \pi a b \tag{3.12}$$

where

a and b are major and minor axis of ellipse, respectively.

Mean Velocity

The average velocity given in equation 3.14 is calculated according to conservation of mass law. It is defined as the following:

$$\dot{m} = \int_{A_c} \rho u(r,x) dA_c \tag{3.13}$$

It is follow that, for incompressible flow in a circular tube,

$$u_m = \frac{\dot{m}}{\rho A_c} = \frac{\int_{A_c} \rho u(r,x) dA_c}{\rho A_c} = \frac{2}{r_o^2} \int_0^{r_o} u(r,x) r dr \tag{3.14}$$

where,

$\dot{m}$ (kg/s)   mass flow rate of flow,
ρ (kg/m^3)   density of fluid,
A_c (m^2)   cross-sectional area of tube,
u_m (m/s)   mean velocity of flow,

The mean velocity is constant for uniform cross-sectional area tube and incompressible flow.

3.2.2. Average Nusselt Number

Average Nusselt number can be defined as the enhancement of heat transfer through a tube as a result of average convection relative to average conduction across the tube.

$$Nu_m = \frac{\bar{h}D_h}{k_f}$$ (3.15)

where,

Nu_m		average Nusselt number
$\bar{h}$	(W/m^2.K)	average heat transfer coefficient
k_f	(W/m.K)	thermal conductivity of fluid
D_h	(m)	hydraulic diameter of the tube

In a flow, the heat transfer with convection is high in high Nusselt numbers.

<u>Newton's Law of Cooling for Internal Flow</u>

In convection heat transfer, Newton's Law of Cooling can be express as

$$q_s'' = h(T_s - T_m)$$ 3.16

where,

q_s''	(W/m^2)	local heat flux
h	(W/m^2.K)	local convection heat transfer coefficient
T_s	(K)	surface temperature
T_m	(K)	mean temperature

3.2.2.1. Logarithmic Mean Temperature Differences Method

In order to calculate average heat transfer coefficient, first of all the log mean temperature differences must be calculated for constant surface temperature condition which is determined for internal flow.
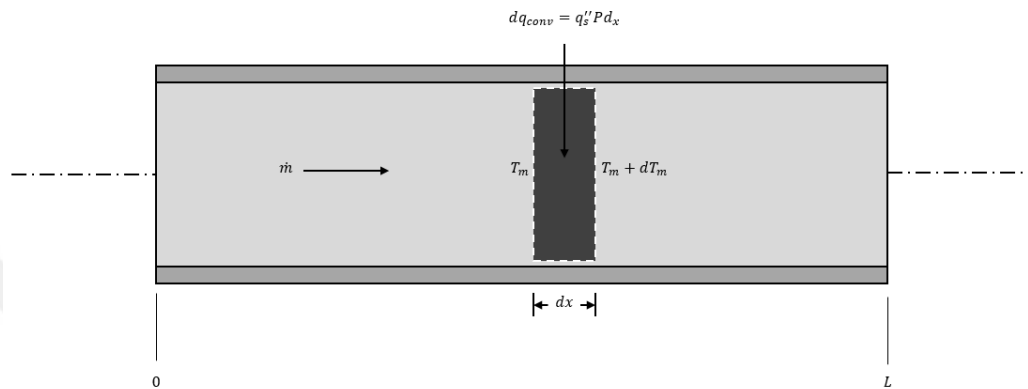
Figure 3. Control Volume for Internal Flow in a Tube

Applying energy balance,

$$\dot{m}c_pT_m + dq_{conv} = \dot{m}c_p(T_m + dT_m) \tag{3.17}$$

$$dq_{conv} = \dot{m}c_p[(T_m + dT_m) - T_m] \tag{3.18}$$

$$dq_{conv} = \dot{m}c_pdT_m \tag{3.19}$$

$$q_s''Pd_x = \dot{m}c_pdT_m \tag{3.20}$$

$$\frac{dT_m}{dx} = \frac{q_s''P}{\dot{m}c_p} \tag{3.21}$$

If we combine Equation 3.16 and Equation 3.21, we can have the equation below:

$$\frac{dT_m}{dx} = \frac{P}{\dot{m}c_p}h(T_s - T_m)$$ (3.22)

The solution of Equation 3.22 for $T_m(x)$ depends on the surface thermal condition.

Defining ΔT as $T_s - T_m$, Equation 3.23 may be expressed as

$$\frac{dT_m}{dx} = -\frac{d(\Delta T)}{dx} = \frac{P}{\dot{m}c_p}h\Delta T$$ (3.23)

Separating variables and integrating from the tube inlet to the outlet,

$$\int_{\Delta T_i}^{\Delta T_o} \frac{d(\Delta T)}{\Delta T} = -\frac{P}{\dot{m}c_p}\int_0^L h\,dx$$ (3.24)

or

$$ln\frac{\Delta T_o}{\Delta T_i} = -\frac{PL}{\dot{m}c_p}\left(\frac{1}{L}\int_0^L h\,dx\right)$$ (3.25)

From the definition of the average convection heat transfer coefficient, Equation 3.25, it follows that:

$$ln\frac{\Delta T_o}{\Delta T_i} = -\frac{PL}{\dot{m}c_p}\bar{h} \qquad T_s = \text{constant}$$ (3.27)

Rearranging,

$$\bar{h} = ln\left(\frac{\Delta T_i}{\Delta T_o}\right)\cdot\frac{\dot{m}c_p}{PL}$$ (3.28)

16

or

$$\bar{h} = \ln\left(\frac{T_s - T_{m,i}}{T_s - T_{m,o}}\right) \cdot \frac{\dot{m}c_p}{PL} \tag{3.29}$$

Average heat transfer coefficient which is required to calculate average Nusselt number can be calculated by using Equation 3.29.

Total heat transfer can be expressed as,

$$Q = \bar{h}A_s\Delta T_{lm}$$

where

A_s m^2 surface area

$\bar{h}$ (W/m^2.K)   average heat transfer coefficient

ΔT_{lm} K   log mean temperature differences

$$\Delta T_{lm} = \frac{\Delta T_o - \Delta T_i}{\ln(\Delta T_o/\Delta T_i)}$$

3.2.3. Local Nusselt Number

Local Nusselt Number is defined as the ratio of the heat transfer which occurs due to the convection on the surface of the tube walls which are x distance from the entrance of the tube to the heat transfer occurs due to the conduction. In the tube, it is calculated as:

$$Nu_x = \frac{h_x D_h}{k_f} \tag{3.30}$$

where

h_x (W/m².K)   local heat transfer coefficient at x location

$$h_x = \frac{q_s''(x)}{T_s - T(x)} \tag{3.31}$$

where,

$q_s''(x)$ (W/m²)   local heat flux at x location

T_s (K)   constant wall temperature

$T(x)$ (K)   mean temperature of fluid at x location

3.2.4. Prandtl Number

It is the ratio between momentum and thermal diffusivities. It is defined as below:

$$Pr = \frac{\mu c_p}{k_f} \tag{3.32}$$

where

μ (kg/m.s)   dynamic viscosity of fluid

c_p (J/kg.K)   specific heat of fluid

k_f (W/m.K)   thermal conductivity of fluid

If Pr=1, hydrodynamic and thermal boundary layer thickness are the same. If Pr<1, hydrodynamic boundary layer thickness is less than the thermal boundary layer thickness. If Pr>1, hydrodynamic boundary layer thickness is more than the thermal boundary layer thickness. The ratio between hydrodynamic and thermal boundary layer is a function of Pr number.

3.2.5. Average Darcy Friction Factor

In engineering applications, it is crucial to know the pressure drop in the tube in order to choose the appropriate pump. Average Darcy friction factor is the resistance against the flow which occurs inside the tube due to the tube geometry and wall structure.

It is necessary this resistance to be broken in order to let the flow occur. Average Darcy friction factor is directly related to the pressure drop which occurs along the tube. It is defined as:

$$f_m = \frac{D_h}{L} \frac{\Delta P}{\frac{1}{2}\rho V^2}$$
(3.33)

where,

f_m average Darcy friction factor

ΔP (Pa)   pressure drop

L (m)   length of the channel

Pressure Drop

The pressure drop given in Equation 3.33 is calculated with equation below.

$$\Delta P = P_i - P_o$$
(3.34)

where,

P_i (Pa)   pressure at inlet

P_o (Pa)   pressure at outlet

3.2.6. Local Darcy Friction Factor

Local Darcy friction factor is the resistance against the flow which occurs in the fluid section which is a certain distance away in the tube due to the tube geometry and wall structure. It is calculated as:

$$C_{f,x} = \frac{\tau_x}{\frac{1}{2}\rho V^2}$$

(3.35)

where

$C_{f,x}$ local Darcy friction factor

τ_x (N/m^2)   wall shear stress at x location

3.2.7. Dimensionless Temperature

Temperature profile in a tube is continuously changing with x. So it is more convenient to work with dimensionless temperature instead of working with temperature profile. Whether the thermally fully developed condition is provided can be determined by examining the change of dimensionless temperature parameter with axial direction.

Dimensionless temperature can be defined as below, [14]

$$\theta = \frac{T_s - T_m(x, y, z)}{T_s - T_i}$$

where

T_s K   tube surface temperature

$T_m(x, y, z)$ K   local mean fluid temperature

T_i K   inlet temperature of fluid

4. HEAT TRANSFER WITH NANOFLUIDS

Nanofluids can be envisioned that fluid in which nanometer-sized particles are suspended in conventional heat transfer basic fluids. Conventional heat transfer fluids, including oil, water and ethylene glycol mixture, are poor heat transfer fluids, since the thermal conductivity of these fluids plays an important role on the heat transfer coefficient between the heat transfer medium and the heat transfer surface. Therefore, there are many research about this issue which is thermal conductivity of these fluids by suspending nano-sized particle materials in base fluids. Nanofluids are basically defined as mixture of solid nanoparticles and conventional base fluid.

Many different solid particle materials are used for nanofluids preparation. Al_2O_3, TiO_2, CuO, TiC, SiC, Au, Ag, Cu and Fe nanoparticles are most common solid particles used in nanofluids research. Their thermal conductivities are significantly higher than the base fluids even at low concentrations, resulting in significant increases in the heat transfer coefficient. Therefore, the effective thermal conductivity and heat-transfer coefficient of nanofluids are expected to enhance the heat transfer compared with conventional heat-transfer liquids. Heat transfer coefficient is the most effective factor in forced convection heat transfer applications such as cooling-heating applications of heat-exchanger including engine and engine systems. [1], [5], [6], [7]

Heat transfer enhancement with nanofluids mainly depends on particle volume concentration, particle material, and particle size and particle shape.

Nanofluids consist homogeneity of base working fluid and solid nanoparticles. Diameters of solid nanoparticles differ from 1 nm to 100 nm. To obtain effective heat transfer enhancement, nanofluids should contain minimum 3% nanoparticles volume fraction. [17]

Producing of Nanoparticles

Typical producing methods for nanoparticles used in nanofluids are mechanical milling, inert-gas-condensation technique, chemical precipitation, chemical vapor deposition, micro emulsions, spray pyrolysis and thermal spraying. Nanoparticles in most materials discussed are most commonly produced in the form of powders [17]. Nanoparticles fluidize easily in the flow due to their small size, and this eliminates the problem of clogging of channels, erosion on the channel walls, and sedimentation.

Accurate prediction of the heat transfer enhancement obtained with nanofluids is necessary for the utilization and application of nanofluids in theoretical and practical applications. So experimental and numerical studies have been developed continuously. In this study, numerical methods are interested. There are two types of numerical simulation approaching to model heat transfer enhancement with nanofluids. The one and simplest method to analyze nanofluids flow and heat transfer is applying single-phase approaches. In this method, nanofluids can be treated as a single phase fluid, and the effects of nanoparticles are taken into account only through the usage of the thermophysical properties of the nanofluids in the associated calculations. The second method to analyze nanofluids is thermal dispersion two phase model approaching. This model takes the effect of improved thermal transport due to the random motion of nanoparticles into account.

Nanofluid thermophysical properties play important roles in the analysis of nanofluid heat transfer enhancement. In this study, single phase approaching was used to determine nanofluid thermophysical properties. Al_2O_3 was selected as nanoparticle and water was selected as working base fluid. 50 nanometer solid nanoparticles diameter and 6% nanoparticles volume fraction was selected to calculate effective thermal properties of nanofluids.

4.1. Thermophysical Properties of Nanoparticle and Nanofluid

In order to carry out simulations for nanofluid, the effective thermophysical properties of nanofluid must be calculated first. The required properties for the simulations which are nanofluid thermal conductivity (k_{nf}), nanofluid dynamic viscosity (μ_{nf}), nanofluid mass density (ρ_{nf}) and nanofluid specific heat (c_{nf}) are given in   Table   1.

Table 1. Thermophysical Properties of Al_2O_3 + Water Nanofluid

Thermophysical Properties	Al_2O_3 Solid Particles	Water	Water + Al_2O_3 Nanofluid
$\rho\ (kg/m^3)$	3970	1000	1178.2
$c_p\ (J/kg \cdot K)$	765	4181	3490.4
$k\ (W/m \cdot K)$	40	0.613	0.67
$\mu\ (Ns/m^2)$	-	0.001	0.0017

Calculations of thermophysical properties of Water + Al_2O_3 nanofluid will be given at Appendix-A / Calculation of Thermophysical Properties of Nanofluid.

4.1.1. Thermal conductivity of nanofluid

The Brownian motion model was used to calculate thermal conductivity of nanofluid. Brownian motion is the random motion of particles suspended in a fluid. The thermal conductivity of nanofluids can be assumed as the combination of two parts [2]:

$$k_{eff} = k_{static} + k_{Brownian} \qquad\qquad 4.1$$

where

k_{static} represents the thermal conductivity enhancement due to the higher thermal conductivity of the nanoparticles [17].

$k_{Brownian}$ takes the effect of the Brownian motion into account, the effect of fluid particles moving with nanoparticles around them [17].

Static thermal conductivity:

$$k_{static} = k_{bf} \left[\frac{(k_{np} + 2k_{bf}) - 2\phi(k_{bf} + 2k_{np})}{(k_{np} + 2k_{bf}) + \phi(k_{bf} + 2k_{np})} \right] \qquad 4.2$$

where k_{np} and k_{bf} are the thermal conductivity of the nanoparticle and the base fluid respectively.

Brownian thermal conductivity:

$$k_{Brownian} = 5 \times 10^4 \beta \phi \rho_{bf} c_{pbf} \sqrt{\frac{kT}{2\rho_{np}R_{np}}} f(T, \phi) \qquad 4.3$$

Modeling function, $f(T, \phi)$ [24]

$$f(T, \phi) = (0.0.028217\phi + 0.003917) \frac{T}{T_o} + (0.030669\phi - 0.00391123) \qquad 4.4$$

where k is the Boltzmann constant, $k = 1.3807 \times 10^{-23} J/K$, T is the fluid temperature and T_o is the reference temperature, R_{np} is the radius of nanoparticle. The term of $f(T, \phi)$ is a function of temperature and particle volume fraction. The correlation of β is a function of the liquid volume that travels with a particle material expressed in table below [2].

Type of particles	β	Concentration	Temperature
Al₂O₃	$8.4407 (100\phi)^{-1.07304}$	$1\% \leq \phi \leq 10\%$	$298K \leq K \leq 363K$

24

4.1.2. Dynamic viscosity of nanofluid

Nanofluid viscosity parameter plays important role in the practical engineering applications because it directly affects the pressure drop. Generally, nanofluid's viscosity is higher than the viscosity of base fluid. Particle volume fraction, particle size and temperature increase viscosity.

For the viscosity of the nanofluid, an empirical correlation was proposed by Nguyen et al. as [17]

$$\mu_{nf} = (1 + 2.5\phi + 150\phi^2)\mu_f \qquad\qquad 4.5$$

4.1.3. Density of nanofluid

The effective density of the nanofluid can be calculated using [2]

$$\rho_{nf} = (1 - \phi)\rho_{bf} + \phi\rho_{np} \qquad\qquad 4.6$$

where

ρ_{nf} and ρ_{bf} are the nanofluid and base fluid densities respectively and ρ_{np} is the density of nanoparticle.

4.1.4. Specific heat of nanofluid

The effective specific heat at constant pressure of the nanofluid $\left(c_p\right)_{nf}$ is computed using the following equation [2]

$$\left(c_p\right)_{nf} = \frac{(1 - \phi)\left(\rho c_p\right)_{bf} + \phi\left(\rho c_p\right)_{np}}{(1 - \phi)\rho_{bf} + \phi\rho_{np}} \qquad\qquad 4.7$$

where

$c_{p_{np}}$ and $c_{p_{bf}}$ are the heat capacity of nanoparticle and base fluid, respectively.

4.2.   Empirical Correlations for Turbulent Forced Convection with Nanofluid

There are many empirical correlations to calculate Nusselt Number for turbulent forced convection with nanofluid for both laminar and turbulent flows. In this study, only correlations for turbulent flows are interested.

The Nusselt numbers of present CFD study were compared with two main correlations which are correlation of Maiga et al. [17] and correlation of Velagapudi et al. [17]. These correlations are most commonly used in literature for turbulent forced convection with nanofluid.

Correlation of Maiga et al.

Nusselt number was proposed for the turbulent flow regime, validity ranges are 10000 < Re < 500000, 6.6 < Pr < 13.9, and ϕ < 10%, as [17]

$$Nu_{nf} = 0.085 Re_{nf}^{0.71} Pr_{nf}^{0.35}$$

Correlation of Velagapudi et al.

A correlation for the turbulent forced convection of nanofluids inside circular tubes was proposed as [17]

$$Nu_{nf} = 0.0256 Re_{nf}^{0.8} Pr_{nf}^{0.4}$$

5.   NUMERICAL STUDY

In this section, the programs which are used in order to model the flow in an elliptical tube, how the flow is modelled, the mathematical formulation which is calculated and how the parameters which effect the results of this study are determined will be examined.

Generally, in the calculation of technical problems, one or some of the analytical, experimental, and numerical methods are used. In this study, numerical methods are focused on.

5.1.   Physical Model

Five different elliptic tube model which has varying major to minor axis ratios are 2.00, 2.25, 2.50, 2.75 and 3.00 were created in ANSYS SpaceClaim. Physical models are given in the Figure 4. Total tube length is 3m in all model.

(a)
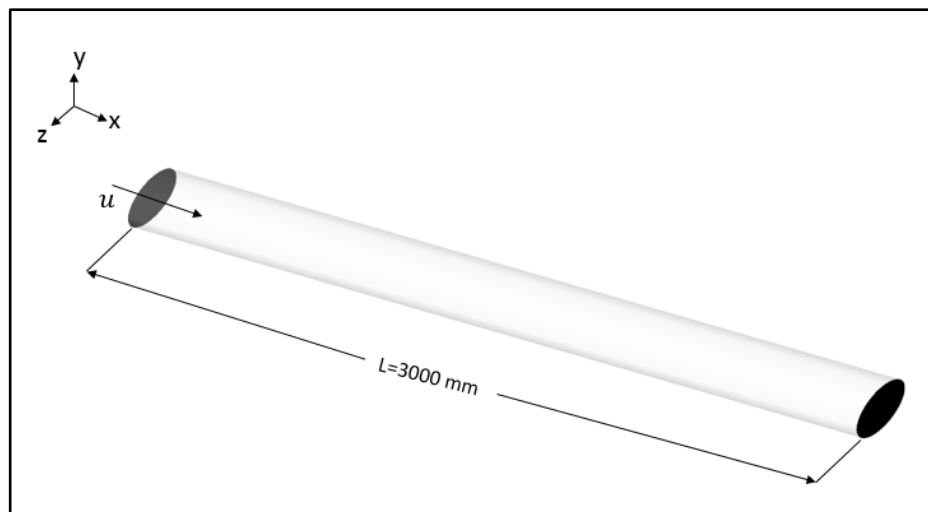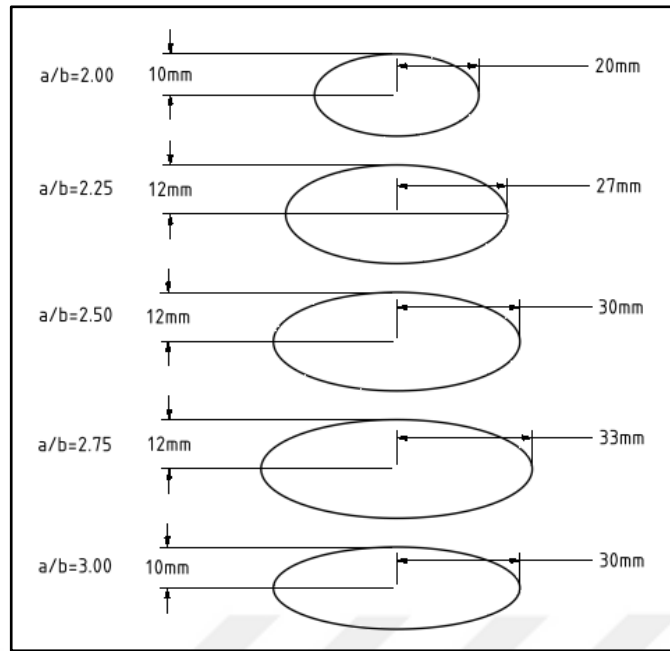
(b)

Figure 4. (a) Isometric View (b) Cross-Sectional View of Elliptic Channels

Definition of Problem

Water and Water + Al$_2$O$_3$ nanofluid are chosen as working fluid in this study. The hydraulic diameters of elliptic tubes change between 26 mm to 33 mm. Velocity and temperature profiles are developing together in the tube. At the end of certain location, velocity and temperature profiles will be fully developed. The length is quite enough to catch hydrodynamically and thermally fully developed conditions. Constant temperature boundary conditions of $T_w = 125°C$ is applied to the tube wall. To determine Reynolds Number, V_i parameter must be calculated before performing all simulations. In this study, the numerical simulations in Reynolds Number between 10000 and 100000 were investigated for elliptic tube in various major-to-minor axis ratio. After the simulations for water, nanofluid studies were performed on every model by using water + Al$_2$O$_3$ as working fluid.

5.2. Governing Equations to be Solved

There is no easy way to fully define fluid properties of turbulent flow because of its complicated and irregular behavior. In the meantime, turbulent flow is very common in engineering applications. Researchers need well defined and applicable calculation methods about turbulent flow. Therefore, they are only interested in time averaged features of turbulent flows in engineering applications. In this approach, time averaged irregular fluctuating terms are added in laminar Navier-Stokes equations and time averaged Navier-Stokes equations are obtained for turbulent flows.

To investigate the effect of fluctuations seen in turbulent flow and derive time averaged Navier-Stokes equations for turbulent flow, averaged value of fluid variable of φ can be defined as $\bar{\varphi}$.

$$\bar{\varphi} = \frac{1}{\Delta t} \int_0^{\Delta t} \varphi(t)dt \tag{5.1}$$

The term of φ is time dependent variable and it is the summation of steady averaged term $\bar{\varphi}$ and average time dependent fluctuating term of φ'.

$$\varphi(t) = \bar{\varphi} + \varphi'(t) \tag{5.2}$$

The term of φ represents velocity components, pressure, temperature variables in flow domain. In other words, x component of average velocity $\bar{u}$, y component of average velocity $\bar{v}$, z component of average velocity $\bar{w}$, fluctuating term of x component u', y component v', z component w' terms can be defined as:

$$u = \bar{u} + u' \tag{5.3}$$

$$v = \bar{v} + v' \tag{5.4}$$

$$w = \bar{w} + w' \tag{5.5}$$

$$p = \bar{p} + p' \tag{5.6}$$

$$T = \bar{T} + T' \tag{5.7}$$

According to the definition, values of time averaged fluctuating terms are zero.

$$\bar{\varphi'} = \frac{1}{\Delta t} \int_0^{\Delta t} \varphi' dt = 0 \tag{5.8}$$

Continuity Equation

The continuity equation for laminar, steady-state, Newtonian, incompressible viscous flow in Cartesian coordinates is expressed:

$$\frac{\partial u}{\partial x} + \frac{\partial v}{\partial y} + \frac{\partial w}{\partial z} = 0 \tag{5.9}$$

If we combine equations between 5.3-5.7 and equation 5.9, we can obtain the equation below.

$$\frac{\partial \bar{u}}{\partial x} + \frac{\partial \bar{v}}{\partial y} + \frac{\partial \bar{w}}{\partial z} + \frac{\partial u'}{\partial x} + \frac{\partial v'}{\partial y} + \frac{\partial w'}{\partial z} = 0 \tag{5.10}$$

If we integrate Equation 5.10 in infinite small interval Δt, the fluctuations terms are dropped and the other terms stayed the same. Equation 5.10 can be represented as:

$$\frac{\partial \bar{u}}{\partial x} + \frac{\partial \bar{v}}{\partial y} + \frac{\partial \bar{w}}{\partial z} = 0 \tag{5.11}$$

Equation 5.11 can be used for expressing continuity equation for turbulent, steady-state, Newtonian, incompressible viscous flow in cartesian coordinates.

<u>Momentum Equations</u>

The momentum equations for turbulent, steady-state, Newtonian, incompressible viscous flow in cartesian coordinates is expressed as

Momentum equation at x direction:

$$u\frac{\partial u}{\partial x} + v\frac{\partial u}{\partial y} + w\frac{\partial u}{\partial z} = f_x - \frac{1}{\rho}\frac{\partial p}{\partial x} + v\left(\frac{\partial^2 u}{\partial x^2} + \frac{\partial^2 u}{\partial y^2} + \frac{\partial^2 u}{\partial z^2}\right)$$
(5.12)

Momentum equation at y direction:

$$u\frac{\partial v}{\partial x} + v\frac{\partial v}{\partial y} + w\frac{\partial v}{\partial z} = f_y - \frac{1}{\rho}\frac{\partial p}{\partial y} + v\left(\frac{\partial^2 v}{\partial x^2} + \frac{\partial^2 v}{\partial y^2} + \frac{\partial^2 v}{\partial z^2}\right)$$
(5.13)

Momentum equation at z direction:

$$u\frac{\partial w}{\partial x} + v\frac{\partial w}{\partial y} + w\frac{\partial w}{\partial z} = f_z - \frac{1}{\rho}\frac{\partial p}{\partial z} + v\left(\frac{\partial^2 w}{\partial x^2} + \frac{\partial^2 w}{\partial y^2} + \frac{\partial^2 w}{\partial z^2}\right)$$
(5.14)

If all equations between 5.3 and 5.7 combined with momentum equations, we can get equations below.

Momentum equation at x direction:

$$(\bar{u} + u')\frac{\partial}{\partial x}(\bar{u} + u') + (\bar{v} + v')\frac{\partial}{\partial y}(\bar{v} + v') + (\bar{w} + w')\frac{\partial}{\partial z}(\bar{v} + v')$$
$$= f_x - \frac{1}{\rho}\left(\frac{\partial \bar{p}}{\partial x} + \frac{\partial p'}{\partial x}\right) + v\left(\frac{\partial^2 \bar{u}}{\partial x^2} + \frac{\partial^2 \bar{u}}{\partial y^2} + \frac{\partial^2 \bar{u}}{\partial z^2} + \frac{\partial^2 u'}{\partial x^2} + \frac{\partial^2 u'}{\partial y^2} + \frac{\partial^2 u'}{\partial z^2}\right)$$
(5.15)

31

After many mathematical operations, Equation 5.15 can be expressed as:

$$\bar{u}\frac{\partial \bar{u}}{\partial x} + \bar{v}\frac{\partial \bar{u}}{\partial y} + \bar{w}\frac{\partial \bar{u}}{\partial z}$$
$$= f_x - \frac{1}{\rho}\frac{\partial \bar{p}}{\partial x} + \frac{1}{\rho}\left[\mu\left(\frac{\partial^2 \bar{u}}{\partial x^2} + \frac{\partial^2 \bar{u}}{\partial y^2} + \frac{\partial^2 \bar{u}}{\partial z^2}\right) - \frac{\partial}{\partial x}\left(\overline{\rho u'^2}\right) - \frac{\partial}{\partial y}\left(\overline{\rho u'v'}\right) - \frac{\partial}{\partial z}\left(\overline{\rho u'w'}\right)\right] \quad (5.16)$$

This equation represents momentum equation at x direction for turbulent flow. If the same mathematical operations are applied for momentum equation at y direction and z direction, momentum equations at y direction and z direction for turbulent flows are obtained.

Momentum Equation at y direction:

$$\bar{u}\frac{\partial \bar{v}}{\partial x} + \bar{v}\frac{\partial \bar{v}}{\partial y} + \bar{w}\frac{\partial \bar{v}}{\partial z}$$
$$= f_y - \frac{1}{\rho}\frac{\partial \bar{p}}{\partial y} + \frac{1}{\rho}\left[\mu\left(\frac{\partial^2 \bar{v}}{\partial x^2} + \frac{\partial^2 \bar{v}}{\partial y^2} + \frac{\partial^2 \bar{v}}{\partial z^2}\right) - \frac{\partial}{\partial x}\left(\overline{\rho u'v'}\right) - \frac{\partial}{\partial y}\left(\overline{\rho v'^2}\right) - \frac{\partial}{\partial z}\left(\overline{\rho v'w'}\right)\right] \quad (5.17)$$

Momentum equation at z direction:

$$\bar{u}\frac{\partial \bar{w}}{\partial x} + \bar{v}\frac{\partial \bar{w}}{\partial y} + \bar{w}\frac{\partial \bar{w}}{\partial z}$$
$$= f_z - \frac{1}{\rho}\frac{\partial \bar{p}}{\partial z} + \frac{1}{\rho}\left[\mu\left(\frac{\partial^2 \bar{w}}{\partial x^2} + \frac{\partial^2 \bar{w}}{\partial y^2} + \frac{\partial^2 \bar{w}}{\partial z^2}\right) - \frac{\partial}{\partial x}\left(\overline{\rho u'w'}\right) - \frac{\partial}{\partial y}\left(\overline{\rho v'w'}\right) - \frac{\partial}{\partial z}\left(\overline{\rho w'^2}\right)\right] \quad (5.18)$$

In order to simplify the notation, tensor notation will be used to define the momentum equations. The convention of this notation is that i or j=1 correspond to x-direction, i or j=2 correspond to y-direction and i or j=3 correspond to z-direction. [16]

In tensor notation, momentum equation is given by Equation 3.19

$$\bar{u}_j \frac{\partial \bar{u}_i}{\partial x_j} = -\frac{1}{\rho}\frac{\partial \bar{p}}{\partial x_i} + \frac{\partial \tau_{vij}}{\partial x} + \frac{\partial \tau_{Rij}}{\partial x} + f_i \qquad (5.19)$$

where τ_{vij} and τ_{Rij} are viscous stress tensor and Reynold stress tensors, respectively.

$$\tau_{vij} = v\left(\frac{\partial \bar{u}_i}{\partial x_j} + \frac{\partial \bar{u}_j}{\partial x_i}\right) \qquad (5.20)$$

$$\tau_{Rij} = -\rho\overline{u_i'u_j'} \qquad (5.21)$$

Extra terms appear in the time-averaged flow equations due to the interactions between various turbulent fluctuations. These extra terms are modelled with classical turbulence models. The six unknown Reynolds stresses $-\rho\overline{u'^2}, -\rho\overline{v'^2}, -\rho\overline{w'^2}, -\rho\overline{u'v'}, -\rho\overline{u'w'}, -\rho\overline{v'w'}$ can be computed by using turbulence model.

Many turbulence models are based upon the Boussinesq hypothesis. Reynolds stress tensor expressed in terms of the time-averaged velocity gradients and the turbulent viscosity. A new quantity the turbulent viscosity or eddy viscosity μ_t appears in the Equation 5.22 [16].

$$-\overline{\rho u'_i u'_j} = \mu_t\left(\frac{\partial \bar{u}_i}{\partial x_j} + \frac{\partial \bar{u}_j}{\partial x_i}\right) - \frac{2}{3}\rho k \delta_{ij} \qquad (5.22)$$

where $k = \frac{1}{2}(\overline{u'^2} + \overline{v'^2} + \overline{w'^2})$ is the turbulent kinetic energy and δ_{ij} is the Kronecker delta ($\delta_{ij} = 1 \; if \; i = j \; and \; \delta_{ij} = 0 \; if \; i \neq j$) [16].

In order to calculate turbulent viscosity in equation 5.22, there are many turbulence models in literature. In this study, $k - \omega$ turbulence model was used. In $k - \omega$ turbulence model, k and ω are calculated separately, and they are used to compute turbulent viscosity μ_t. After calculating turbulent viscosity, equation 5.22 can be calculated and then all momentum equations can be calculated.

$$\mu_t = \alpha^* \rho \frac{k}{\omega}$$

Parameters in above equations computed in $k - \omega$ turbulence model and all equation used in $k - \omega$ turbulence model will be given in next chapter.

Energy Equation

The energy equation for laminar, steady-state, Newtonian viscous flow in cartesian coordinates is expressed as

$$u\frac{\partial T}{\partial x} + v\frac{\partial T}{\partial y} + w\frac{\partial T}{\partial z} = \alpha\left(\frac{\partial^2 T}{\partial x^2} + \frac{\partial^2 T}{\partial y^2} + \frac{\partial^2 T}{\partial z^2}\right) + \frac{v}{c_p}\Phi_v + \frac{u'''}{\rho c_p} \tag{5.23}$$

The term of u''' represents energy generation in the system. The term of α represents thermal diffusivity, and it can be expressed as $\alpha = k/(\rho c_p)$. The term of Φ_v represents dissipation function. There is no energy generation in the system. So last term of the right hand side can be dropped. Also dissipation term can be neglected. Therefore energy equation can be expressed as:

$$u\frac{\partial T}{\partial x} + v\frac{\partial T}{\partial y} + w\frac{\partial T}{\partial z} = \alpha\left(\frac{\partial^2 T}{\partial x^2} + \frac{\partial^2 T}{\partial y^2} + \frac{\partial^2 T}{\partial z^2}\right) \tag{5.24}$$

Likewise in the momentum equations, after integrating time average and many mathematical operations of energy equation, the energy equation for turbulent flow can be obtained as:

$$\bar{u}\frac{\partial \bar{T}}{\partial x} + \bar{v}\frac{\partial \bar{T}}{\partial y} + \bar{w}\frac{\partial \bar{T}}{\partial z}$$

$$= \alpha\left(\frac{\partial^2 \bar{T}}{\partial x^2} + \frac{\partial^2 \bar{T}}{\partial y^2} + \frac{\partial^2 \bar{T}}{\partial z^2}\right) - \left(\frac{\partial}{\partial x}\overline{(u'T')} + \frac{\partial}{\partial y}\overline{(v'T')} + \frac{\partial}{\partial z}\overline{(w'T')}\right) \qquad (5.25)$$

In tensor notation, energy equation is given by Equation 5.26

$$\frac{\partial}{\partial x_i}[u_i(\rho E)] = \frac{\partial}{\partial x_j}\left(k_{eff}\frac{\partial T}{\partial x_j} + u_i\left(\tau_{ij}\right)_{eff}\right) \qquad (5.26)$$

where E is the total energy, k_{eff} is the effective thermal conductivity, and $\left(\tau_{ij}\right)_{eff}$ is the deviatoric stress tensor, defined as

$$\left(\tau_{ij}\right)_{eff} = \mu_t\left(\frac{\partial u_j}{\partial x_i} + \frac{\partial u_i}{\partial x_j}\right) - \frac{2}{3}\mu_t\frac{\partial u_k}{\partial x_k}\delta_{ij}$$

and

$$k_{eff} = k + \frac{c_p\mu_t}{Pr_t}$$

where k is the thermal conductivity, Pr_t is turbulent Prandtl number and its value is 0.85. [21]

5.3.   Boundary Conditions

Fluid enters the tube at temperature of $T_i = 25°C$ and constant velocity. No-slip boundary condition is applied to tube wall. Constant temperature boundary condition of $T_w = 125°C$ is applied to tube wall.

Inlet Boundary Conditions

Velocity components and turbulence parameters (turbulent intensity ratio and turbulent viscosity ratio) in momentum tab were set as inlet boundary conditions. Fluid properties do not change with temperature.

$u = V_i$	at x=0 meter
$v = 0$	at x=0 meter
$w = 0$	at x=0 meter
$T_i = 25°C$	at x=0 meter

where

V_i	is	average inlet velocity
v	is	y component of velocity
w	is	z component of velocity
T_i	is	average inlet temperature

Inlet boundary conditions were taken as above. Also turbulent intensity were calculated as below.

$$I = 0.16(Re)^{-1/8}$$

<u>Wall Boundary Condition</u>

No-slip boundary condition is applied to tube wall. This condition says that velocity is zero on the wall.

$u = v = w = 0$

Constant temperature boundary conditions is applied to tube wall.

$T_w = 125°C$

where

T_w is   constant wall temperature

<u>Outlet Boundary Condition</u>

It is assumed that the pipe exits to atmospheric environment. So pressure outlet boundary condition of $P_o = 0$ Pa (gauge) is applied to outlet of the pipe.

$P_o = 0 \, Pa$ (gauge)

Because of the hydrodynamically and thermally fully developed condition at the outlet,

$\dfrac{\partial u}{\partial x} = 0$

$\dfrac{\partial v}{\partial x} = 0$

$\dfrac{\partial w}{\partial x} = 0$

5.4.   Computational Fluid Dynamics

Although the experimental method, which is one of the calculation methods, gives reliable results, as it requires a certain mechanism, infrastructure, etc., it is an expensive and time-consuming method. On the other hand, there are very few problems which can be solved by using analytical method. Even so, the nonlinear problems which cannot be calculated analytically commonly seen in engineering. Turbulent flow is a good example of this kind of complicated problems. In order to solve this kind of problems by linearized, numerical methods are used. In recent years, with the help of the developments in computer technology, it has become a common way to choose this kind of methods which are completely based on iteration and they have become a solution for many problems.

The reflection of numerical solutions to the fluid dynamics is possible thanks to the computational fluid dynamics. Computational fluid dynamics is the science of predicting fluid flow, heat and mass transfer, chemical reactions, and related phenomena by using numerical methods.

ANSYS Fluent is the most commonly used software to simulate computational fluid dynamics. It is used to determine boundary conditions, do numerical settings and solve the governing equations used in problem. In order to design the model ANSYS Design Modeler is used whereas ANSYS Meshing is used to create the computational mesh domain.

5.4.1. Turbulence Model: Shear Stress Transport (SST) $k - \omega$

For industrial flows, $k - \epsilon$ and $k - \omega$ turbulence models are more accurate than the other models. For separation, transition effects, low Reynolds effects and detailed heat transfer modeling $k - \omega$ models are more accurate than $k - \epsilon$ models.

In this study, SST $k - \omega$ turbulence model was used. SST $k - \omega$ turbulence model is preferred when highly accurate resolution of boundary layers is critical, such as applications involving flow separation or finely resolved heat transfer profiles.

The turbulence kinetic energy, k and the specific dissipation rate, ω are obtained from the following transport equations:

$$\frac{\partial}{\partial t}(\rho k) + \frac{\partial}{\partial x_i}(\rho k u_i) = \frac{\partial}{\partial x_j}\left(\Gamma_k \frac{\partial k}{\partial x_j}\right) + G_k - Y_k \tag{5.26}$$

and

$$\frac{\partial}{\partial t}(\rho \omega) + \frac{\partial}{\partial x_i}(\rho \omega u_i) = \frac{\partial}{\partial x_j}\left(\Gamma_\omega \frac{\partial \omega}{\partial x_j}\right) + G_\omega - Y_\omega \tag{5.27}$$

In these equations, G_k represent the generation of turbulence kinetic energy due to mean velocity gradients. G_ω represents the generation of ω. Γ_k and Γ_ω represent the effective diffusivity of k and ω, respectively. Y_k and Y_ω represent the dissipation of k and ω due to turbulence. All of the above terms are calculated as described below [21].

Modeling the Effective Diffusivity

The effective diffusivities for the $k - \omega$ model are given by

$$\Gamma_k = \mu + \frac{\mu_t}{\sigma_k} \tag{5.28}$$

$$\Gamma_w = \mu + \frac{\mu_t}{\sigma_w} \tag{5.29}$$

Where σ_k and σ_w are the turbulent Prandtl numbers for k and ω, respectively.

The turbulent viscosity μ_t is computed by combining k and ω as follows:

$$\mu_t = \frac{\rho k}{\omega} \frac{1}{\max\left[\frac{1}{\alpha^*}, \frac{SF_2}{a_1 \omega}\right]} \tag{5.30}$$

Where S is the strain rate magnitude, F_2 is given by

$$F_2 = \tanh(\phi_2^2) \tag{5.31}$$

$$\phi_2^2 = \max\left[\frac{2\sqrt{k}}{0.09\omega y}, \frac{500\mu}{\rho y^2 \omega}\right] \tag{5.32}$$

Where y is the distance to the next surface.

$$\alpha^* = \alpha_\infty^* \left(\frac{\alpha_0^* + Re_t/R_k}{1 + Re_t/R_k}\right) \tag{5.33}$$

Where

$$Re_t = \frac{\rho k}{\mu \omega} \tag{5.34}$$

$$R_k = 6 \tag{5.35}$$

$$\alpha_0^* = \frac{\beta_i}{3} \tag{5.36}$$

$$\beta_i = 0.072 \tag{5.37}$$

Modeling the Turbulence Production

The term G_k represents the production of turbulence kinetic energy. From the exact equation for the transport of k, this term may be defined as

$$G_k = -\rho \overline{u'_i u'_j} \frac{\partial u_j}{\partial x_i} \tag{5.38}$$

$$G_\omega = \alpha \frac{\omega}{k} G_k \tag{5.39}$$

The coefficient α is given by

$$\alpha = \frac{\alpha_\infty}{\alpha^*} \left(\frac{\alpha_0 + Re_t/R_\omega}{1 + Re_t/R_\omega} \right) \tag{5.40}$$

where

$$R_w = 3.95$$

Modeling the Turbulence Dissipation

$$Y_k = \rho\beta^* f_\beta k\omega \tag{5.41}$$

Where

$$f_\beta = \begin{cases} 1 & X_k \leq 0 \\ \dfrac{1 + 680X_k^2}{1 + 400X_k^2} & X_k > 0 \end{cases} \tag{5.42}$$

where

$$X_k = \frac{1}{\omega^3} \frac{\partial k}{\partial x_i} \frac{\partial \omega}{\partial x_j} \tag{5.43}$$

and

$$\beta^* = \beta_i^*[1 + \zeta^* F(M_t)] \tag{5.44}$$

$$\beta_i^* = \beta_\infty^* \left(\frac{4/(15 + (Re_t/R_\beta)^4}{1 + (Re_t/R_\beta)^4} \right) \tag{5.45}$$

$$\zeta^* = 1.5$$

$$R_\beta = 8$$

$$\beta_\infty^* = 0.0$$

$$Y_\omega = \rho\beta f_\beta \omega^2$$

where

$$f_\beta = \frac{1 + 70X_\omega}{1 + 80X_\omega} \tag{5.46}$$

$$X_\omega = \left| \frac{\Omega_{ij}\Omega_{ik}S_{ki}}{(\beta_\infty^* \omega)^3} \right| \tag{5.47}$$

$$\Omega_{ij} = \frac{1}{2}\left(\frac{\partial u}{\partial j} - \frac{\partial u_j}{\partial x_i} \right) \tag{5.48}$$

$$F(M_t) = \begin{cases} 0 & M_t \leq 0 \\ M_t^2 - M_{t0}^2 & M_t > 0 \end{cases} \tag{5.49}$$

where

$$M_t^2 = \frac{2k}{a^2}$$

$$M_{t0} = 0.25$$

$$a = \sqrt{\gamma R T}$$

Model Constants

$\sigma_{k,1} = 1.176, \sigma_{\omega,1} = 2.0, \sigma_{k,2} = 1.0, \sigma_{\omega,2} = 1.168$

$a_1 = 0.31, \beta_{i,1} = 0.075, \beta_{i_2} = 0.0828$

$\alpha_\infty^* = 1, \alpha_\infty = 0.52, \alpha_0 = \frac{1}{9}, \beta_\infty^* = 0.09, \beta_i = 0.072, R_\beta = 8$

$R_k = 6, R_\omega = 2.95, \zeta^* = 1.5, M_{t0} = 0.25, \sigma_k = 2.0, \sigma_\omega = 2.0$

5.4.1.1. Wall Modeling Strategies

Velocity profile can be classified as viscous sublayer, buffer layer, fully-turbulent region layer and outer layer. To achieve accurate solution in heat transfer problems, viscous sublayer region should be solved correctly. This region can be labeled as near-wall region.

In the near-wall region, the solution gradients are very high, but accurate calculations in the near-wall region are important to the success of the simulation. Near-wall region can be modeled as 2-way, which are using wall functions and resolving the viscous sublayer.

$k - \epsilon$ turbulence model needs using wall functions. Appropriate wall function should be used for modeling. $k - \omega$ turbulence model does not need wall functions. Resolving the viscous sublayer property is used in this model and it requires very fine mesh near the wall. If the forces or heat transfer on the wall is important, SST $k - \omega$ turbulence model is recommended. To use advantages of the SST $k - \omega$ turbulence model, first grid cell needs to be at about $y^+ \approx 1$. Keeping y^+ value to about 1, first cell height should be calculated before creating mesh elements. [20]

Calculating First Cell Height

In order to create appropriate mesh for SST $k - \omega$ turbulence model, first cell height must be calculated. [20]

$$y^+ = \frac{\rho U_\tau y}{\mu} \tag{5.50}$$

where

y^+		desired y^+ value
U_τ	m/s	frictional velocity
y	m	first cell height

$$U_\tau = \sqrt{\frac{\tau_w}{\rho}} \tag{5.51}$$

where

$$\tau_w = \frac{1}{2} C_f \rho U^2 \tag{5.52}$$

$$C_f = 0.079 Re_D^{-0.25} \qquad \text{for internal flows} \tag{5.53}$$

5.5. Calculation Method

In this study, the flow domain was discretized into a set of control volumes (mesh elements) in order to be able to solve the governing partial differential equations as in the form of algebraic equations. ANSYS Fluent software was used for numerical calculations. It uses finite volume method to solve governing equations. SIMPLE algorithm was used as Pressure-Velocity Coupling method. Both convective and turbulence terms were solved as 2nd order. Pressure parameter was solved by using PRESTO algorithm.

5.5.1. Fluent Calculations for Base Water and Nanofluid

Inlet, outlet and wall boundaries were labelled in ANSYS Meshing and they were used in ANSYS Fluent in boundary conditions window to define boundary conditions. All mesh elements were created in ANSYS Meshing tool. The mesh was imported into ANSYS Fluent and all problem settings were set.

Firstly, analysis type was set as steady-state. Energy equation was activated because problem includes heat transfer. Then, SST $k - \omega$ turbulence model was selected to solve turbulent parameters. After applied appropriate boundary conditions and initialization, the simulation was started.

Before carrying out simulations, inlet velocities must be determined for every different Reynolds number calculations. Sample calculation will be given below.

In order to determine the convergence, residuals are wanted to be reduced below 1×10^{-6} and there was no change in the monitors which were created by the user with respect to iteration were taken into consideration.

After the end of simulation, some parameters such as; outlet temperature of fluid, local heat flux, pressure drop, etc. were obtained from Fluent.

In the presence of nanofluid, higher velocity is required to obtain same Reynolds number because of higher dynamic viscosity.

Convergence Criteria in the Simulations

To check the convergence in all equation sets being solved by ANSYS Fluent, the residuals are wanted to be reduced below 1×10^{-6}. Also monitors of change in outlet temperature of fluid and change in pressure at inlet surface with respect to iterations were followed during simulation. It was expected that no change would occur in these monitors after certain iteration. At this point, it can be said that the analysis was converged.

Residuals monitor with respect to iterations for the numerical simulation in which Reynolds number is 40000 and a/b=2.00 is given in Figure 5. After about 1000 iterations, residuals were reduced below 1×10^{-6} but simulation was not stopped because the other monitors (temperature and pressure) was still changing. Temperature and pressure monitors were fixed after about 1500 iterations. At this point, simulation was stopped.
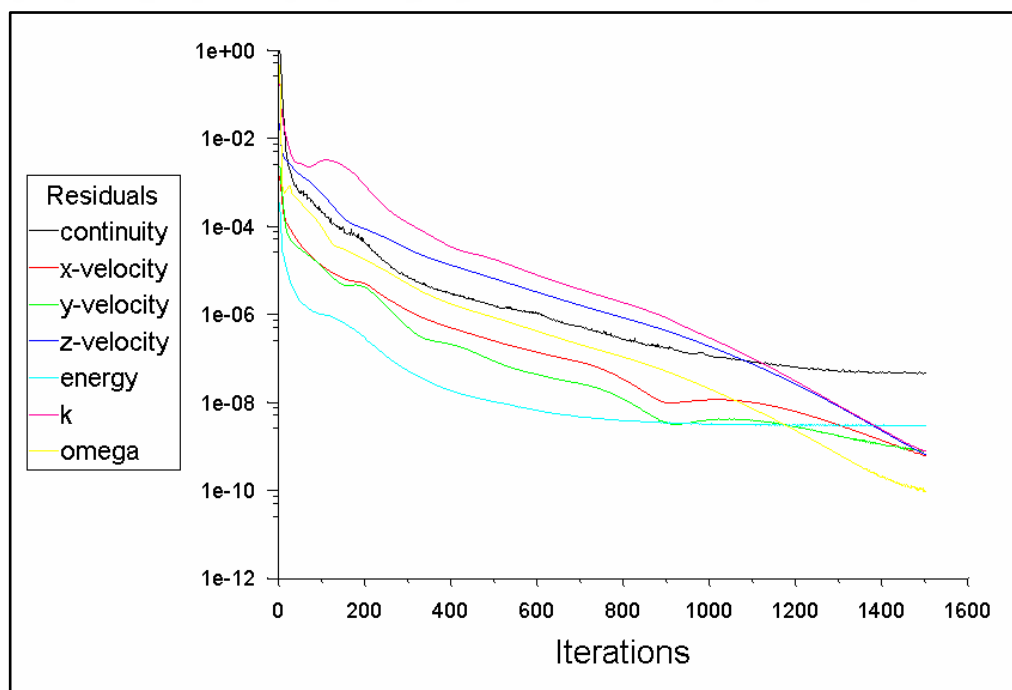

Figure 5. Residual Monitor of The Simulation which is Reynolds Number is 40000 and a/b=3.00

47

Relaxation Factors

Because of the nonlinearity of the equation set being solved by ANSYS Fluent, it is necessary to control the change of solution parameters. This is typically achieved by under-relaxation of variables (also referred to as explicit relaxation), which reduces the change of produced during each iteration [21]. Under relaxation factors are given in Table below.

Table 2. Under-Relaxation Factors used in Simulations

Under- Relaxation Factors	Quantity
Pressure	0.3
Density	1.0
Body Forces	1.0
Momentum	0.7
Turbulent Kinetic Energy	0.8
Specific Dissipation Rate	0,8
Turbulent Viscosity	1,0
Energy	1,0

5.6.   Mesh Independency and Optimization

The first necessary thing to do is to create computational domain. The flow domain was discretized into a set of control volumes (mesh elements) in order to be able to solve the governing partial differential equations as in the form of algebraic equations. In this study, all geometric models were created in ANSYS SpaceClaim tool and all mesh structures were created in ANSYS Meshing tool. y^+ value should be smaller than 1 to obtain correct and accurate results with $SST\ k - \omega$ turbulence model.

So this issue was taken into account while creating the mesh. The created mesh is showed in Figure 6.
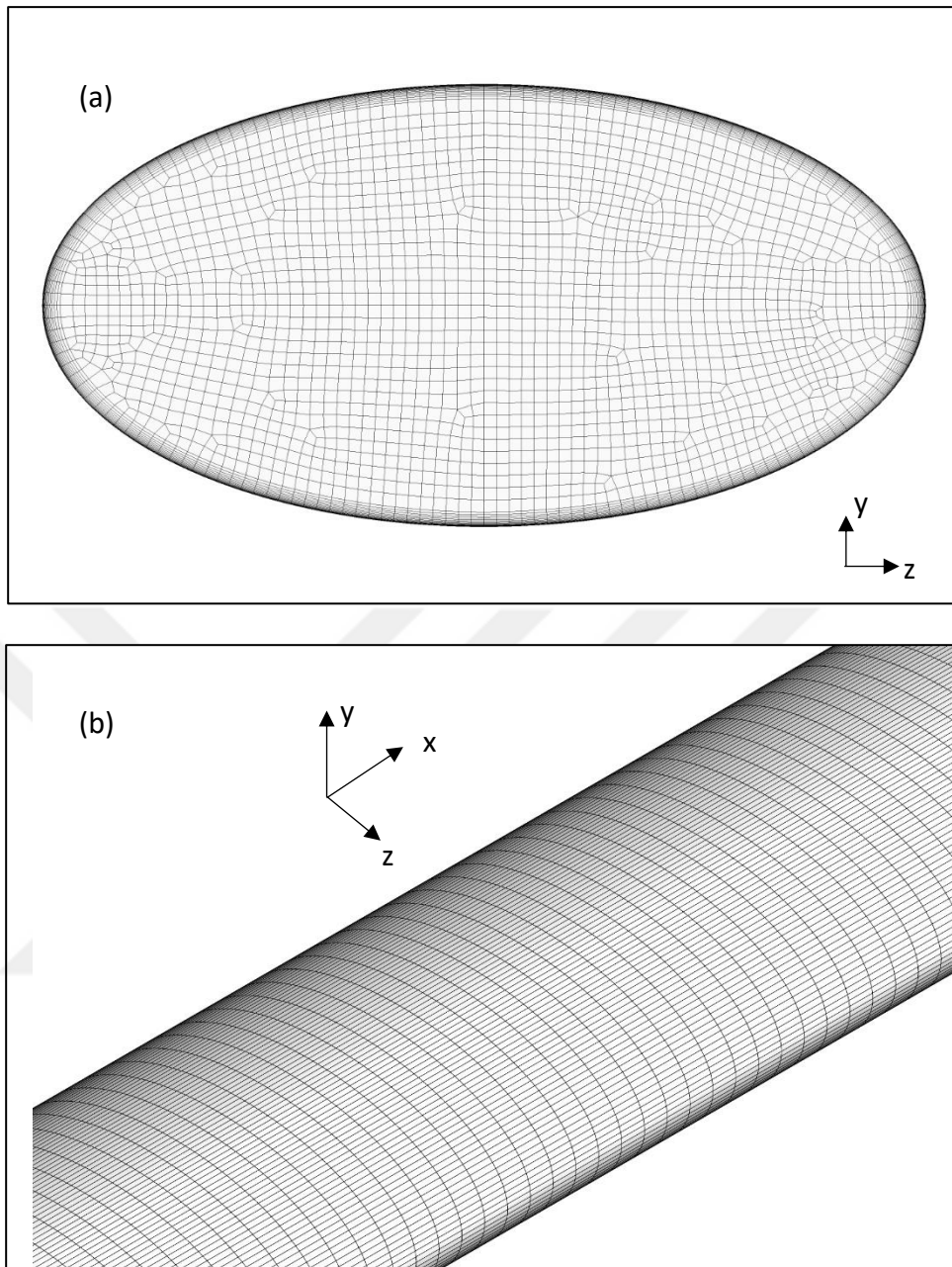
Figure 6. (a) Cross-Sectional View (b) Isometric View of the Mesh Elements

In numerical simulations, mesh independency is required to obtain accurate solutions. Mesh independency means that there is no change in the result of numerical simulation in spite of increasing number of mesh elements. The following methodology was performed to obtain results of mesh independent numerical simulations.

a. The different number in mesh cells were created for every model to obtain mesh independent results.

b. Every different mesh systems were used in ANSYS Fluent to obtain a solution at the highest Reynolds number. After the solutions, the figures of change in average Nusselt number with respect to increasing number of mesh elements were plotted. The number of mesh was selected after the change in Nusselt number was minimized. The selected number of mesh is quite enough to obtain highly accurate solution.

c. All the simulations were performed with selected number of mesh.

The change in average Nusselt number with respect to increasing number of mesh element is showed in Figure 7 for the simulations which Reynolds number is 100000 and a/b=2.00. The simulations were repeated until change in average Nusselt number was minimized. So optimum number of mesh element was found out.
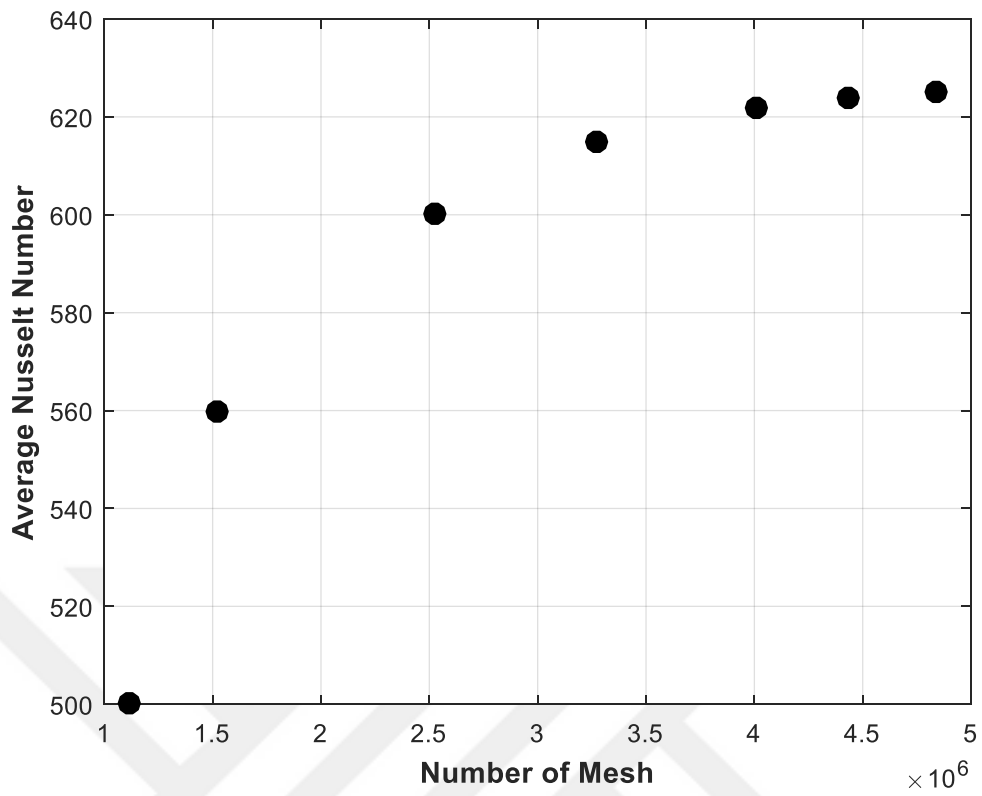
Figure 7. Change of Average Nusselt Number with Respect to Number of Mesh Element in the Simulation which is Reynolds Number in 100000 and a/b=2.00

6.   RESULTS OF NUMERICAL STUDIES

In this section, the numerical simulations in Reynolds Number between 10000 and 100000 were investigated for elliptic tube in various major-to-minor axis ratio. The results of five different elliptic tube which has varying major to minor axis ratios are 2.00, 2.25, 2.50, 2.75 and 3.00 were examined, respectively. Five different mesh independency analysis was performed at highest Reynolds number for every model.

After the end of simulations; parameters such as Nusselt number, friction factor, etc. were calculated and plotted as an appropriate form.

Mesh Independency

In numerical simulations, mesh independency is required to obtain accurate solutions. Mesh independency means that there is no change in the result of numerical simulation in spite of increasing number of mesh elements. Mesh independency simulations were carried out for Reynolds number in 100000. The simulations carried on until the change in Nusselt numbers were minimized with respect to increasing number of mesh element.

The change in average Nusselt number with respect to increasing number of mesh element is showed in Figure 8, Figure 9, Figure 10, Figure 11 and Figure 12. According to figures, the change in Nusselt number is minimized after 4 million, 4 million, 4 million, 4.5 million and 5 million mesh element for aspect ratios 2.00, 2.25, 2.50, 2.75 and 3.00, respectively. Therefore, these mesh elements are quite enough to obtain highly accurate results for all cases.
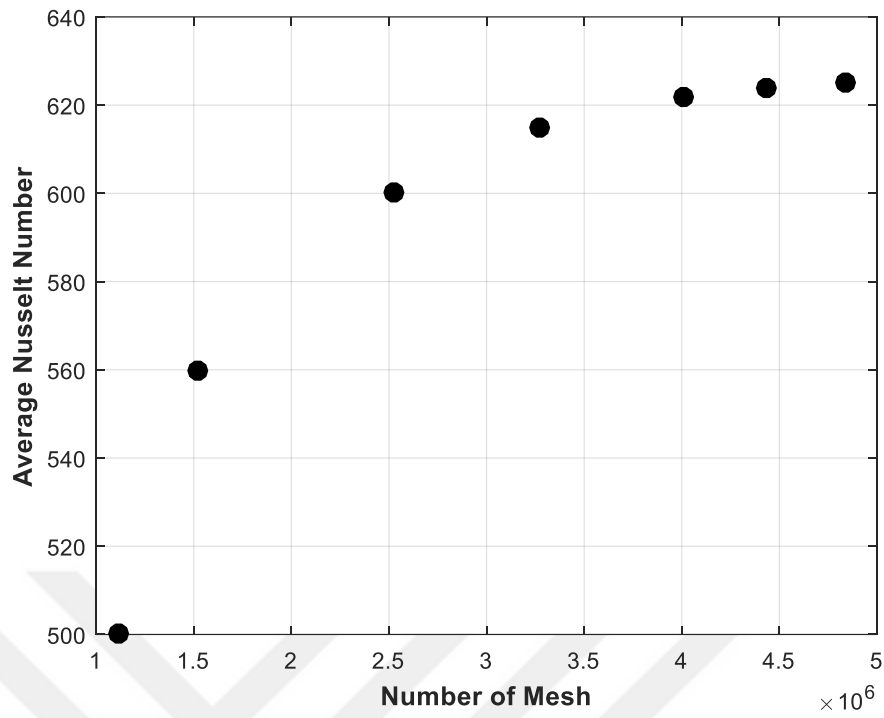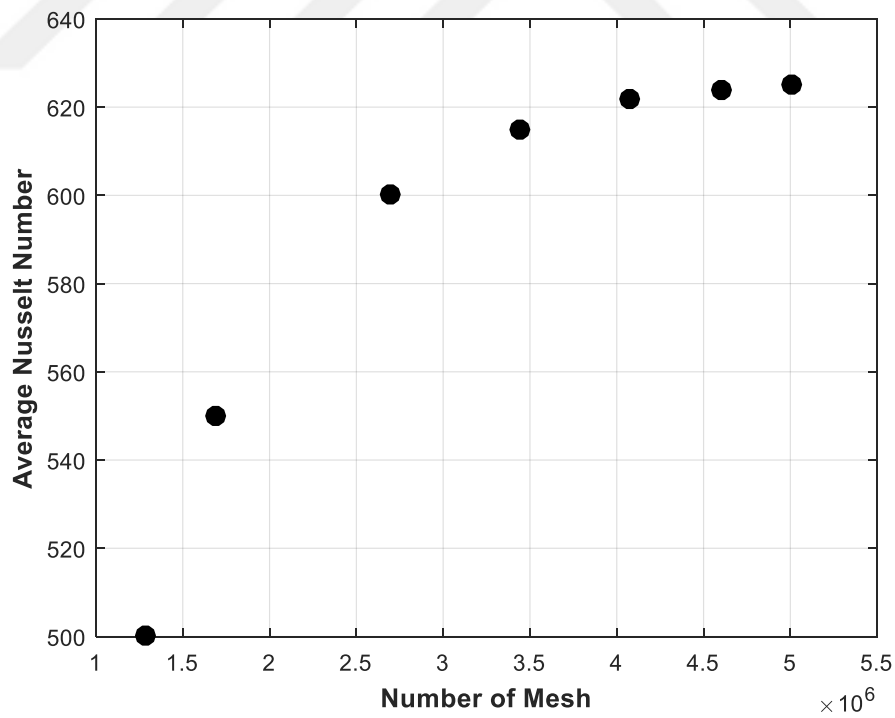
Figure 8. Change of Average Nusselt Number with Respect to Number of Mesh Element in the Simulation which is Reynolds Number in 100000 and a/b=2.00

Figure 9. Change of Average Nusselt Number with Respect to Number of Mesh Element in the Simulation which is Reynolds Number in 100000 and a/b=2.25
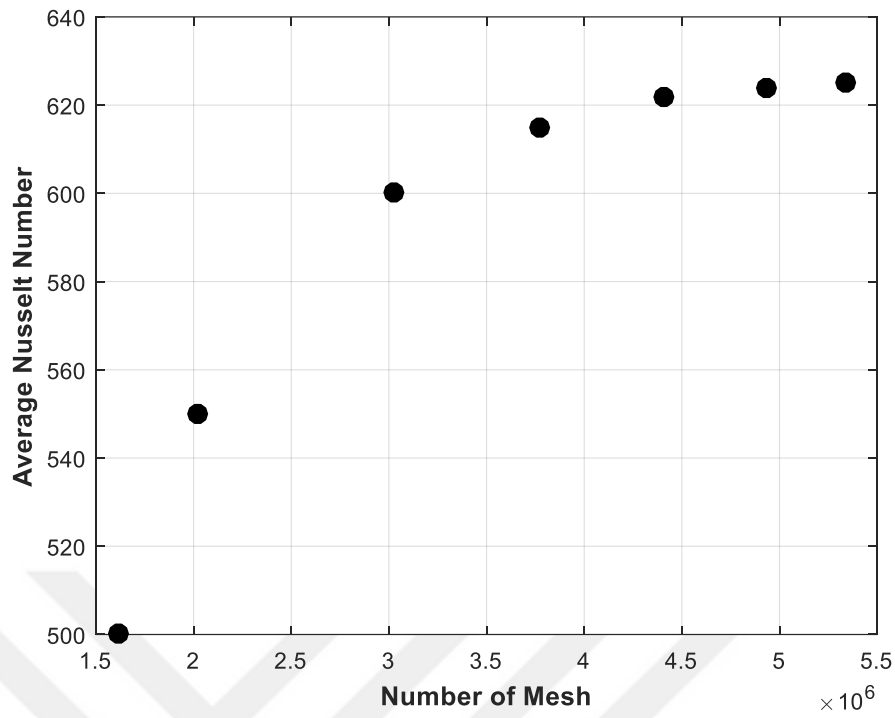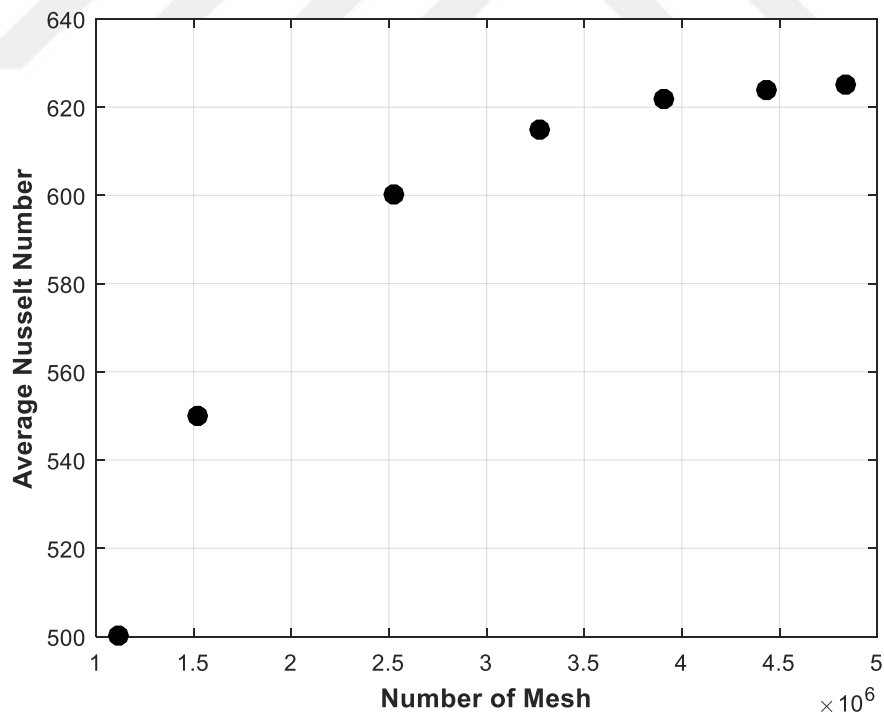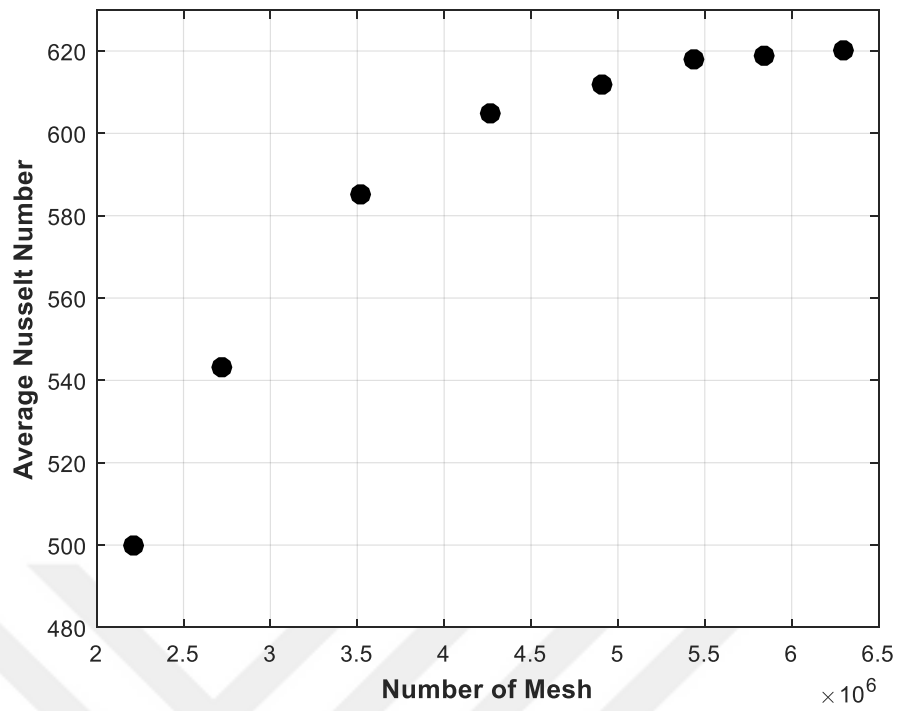
Figure 10. Change of Average Nusselt Number with Respect to Number of Mesh Element in the Simulation which is Reynolds Number in 100000 and a/b=2.50

Figure 11. Change of Average Nusselt Number with Respect to Number of Mesh Element in the Simulation which is Reynolds Number in 100000 and a/b=2.75

Figure 12. Change of Average Nusselt Number with Respect to Number of Mesh Element in the Simulation which is Reynolds Number in 100000 and a/b=3.00

6.1. Results of Simulations: Working Fluid is Water

Before the simulation, mesh optimization and mesh independency studies were carried out to determine the number of meshes used in simulations. With specified mesh, simulations were repeated and results were obtained. Local Nusselt number, local Darcy friction factor, average Nusselt number, average Darcy friction factor and velocity profiles were calculated and plotted as appropriate form. Average Nusselt number and average Darcy friction factor were compared with similar works in literature and they were expressed as appropriate Reynolds number form. Results are given separately for two different sections. Local Nusselt number, local Darcy friction factor, velocity profiles and dimensionless temperature profiles were given in the results of developing region part. Average Nusselt number and average Darcy friction factor were given in the results of fully developed region part.

6.1.1. Results of Hydrodynamically and Thermally Developing Region

In this part local Nusselt number, local Darcy friction factor, velocity profiles and dimensionless temperature profiles were examined.

Local Nusselt Number

Local Nusselt numbers were calculated for the Reynolds number of 10000, 20000, 60000 and 100000 on planes which are created for 0.050 m intervals from the beginning of the tube. The planes are represented in Figure 13.
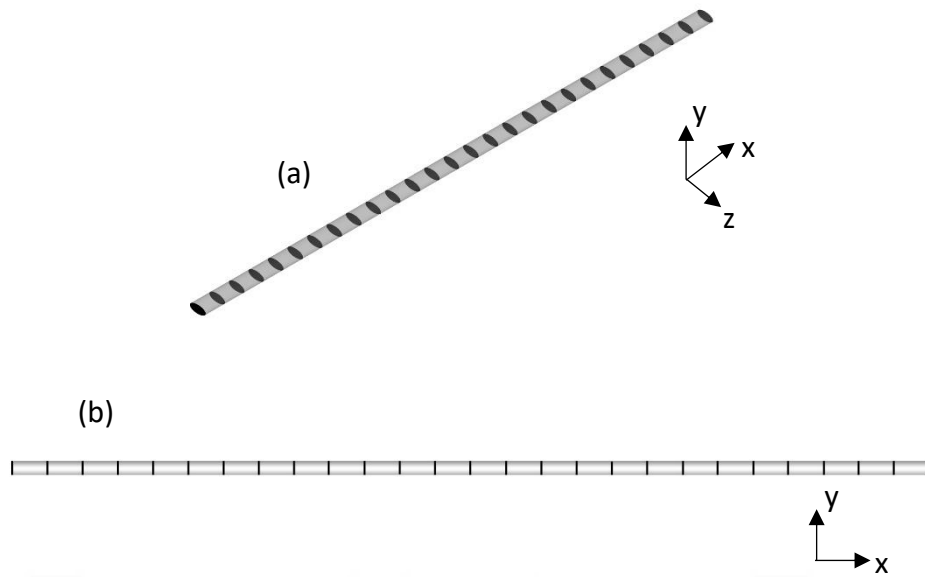
Figure 13. (a) Isometric View (b) Side View of the Planes

Local Nusselt number and local Darcy friction factor are calculated on that planes and the results of them are represented as XY-Plot form.
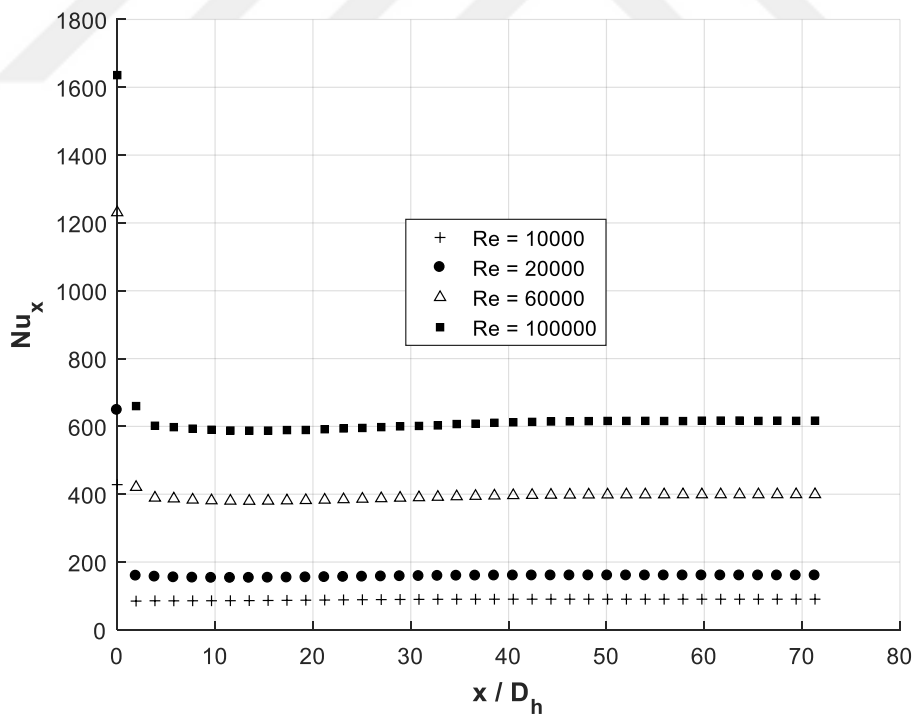

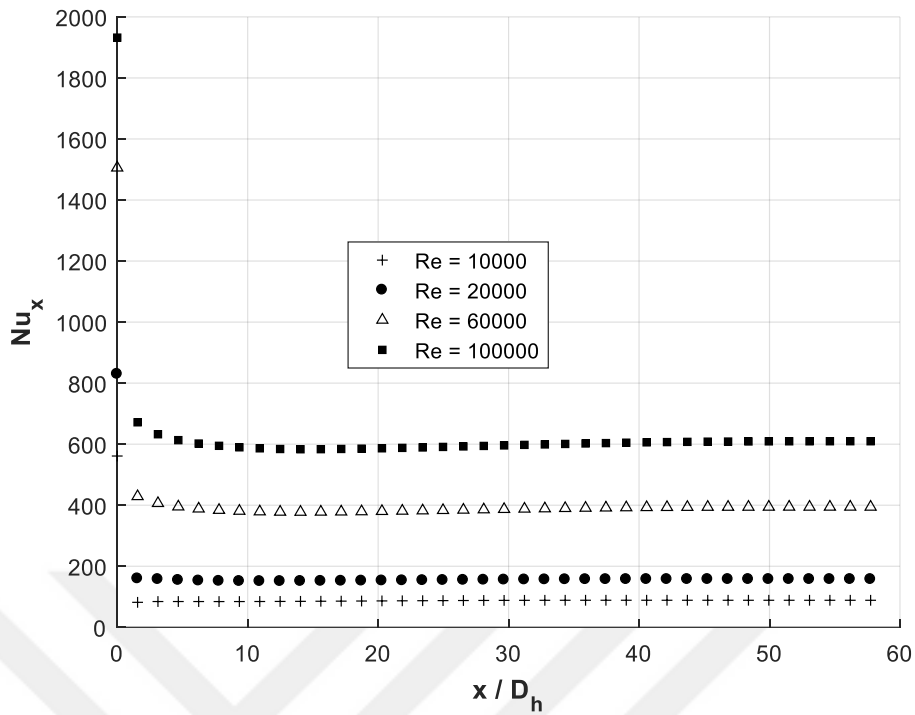*Figure 14. Change of Local Nusselt Number with respect to Created Planes in the Simulation which is a/b=2.00*

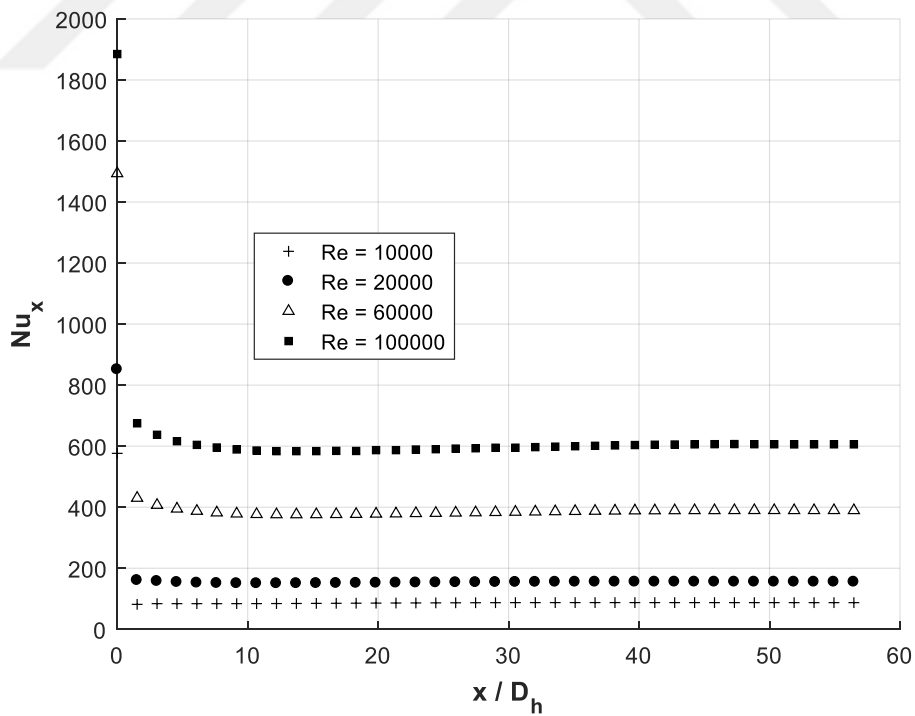*Figure 15. Change of Local Nusselt Number with respect to Created Planes in the Simulation which is a/b=2.25*

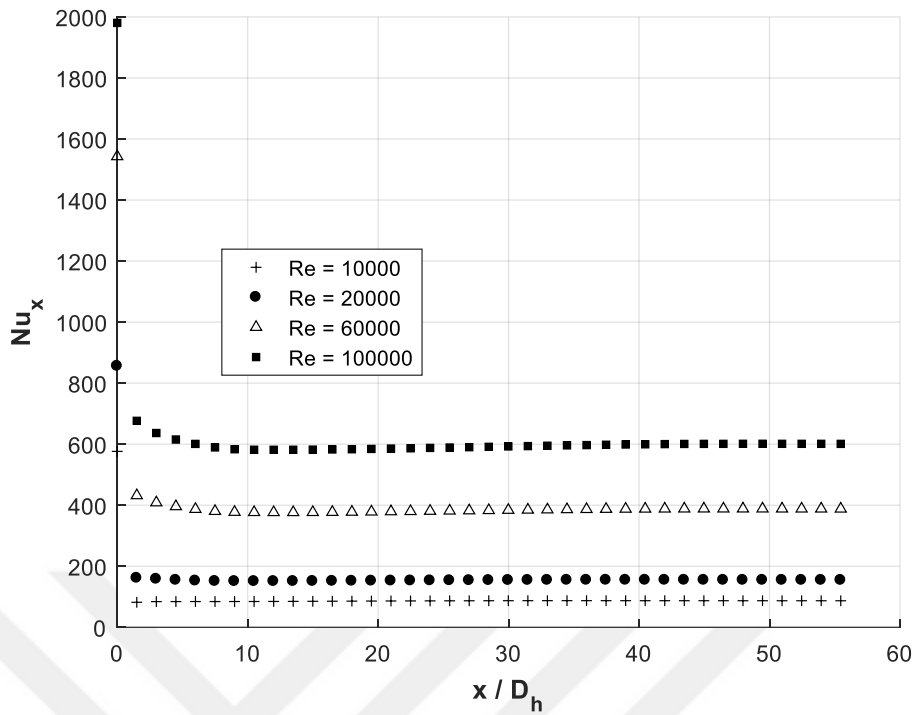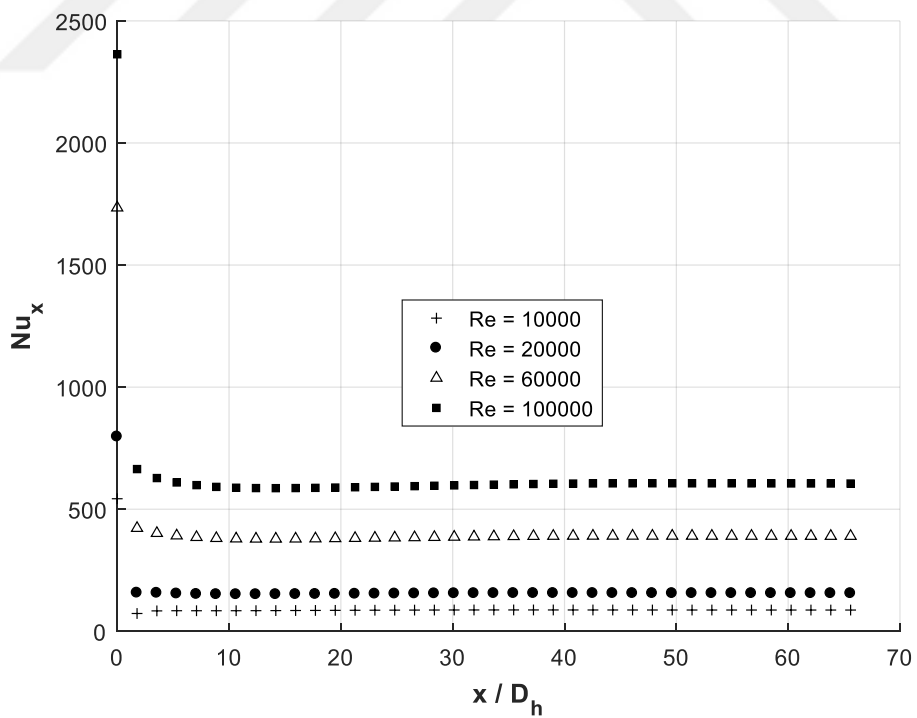*Figure 16. Change of Local Nusselt Number with respect to Created Planes in the Simulation which is a/b=2.50*

Figure 17. Change of Local Nusselt Number with respect to Created Planes in the Simulation which is a/b=2.75

Figure 18. Change of Local Nusselt Number with respect to Created Planes in the Simulation which is a/b=3.00

As seen in the Figure 14, Figure 15, Figure 16, Figure 17 and Figure 18 local Nusselt numbers in all cases are high as expected at the beginning of tube. Also it is observed that local Nusselt numbers in high Reynolds number are relatively high. Also, local Nusselt numbers take almost constant values after certain locations in all cases. So it means that, after this certain location, thermally fully-developed condition is provided in the tube. Approximately, thermally fully developed conditions are provided at $x/D_h = 20$ in Re=10000 and $x/D_h = 25$ in Re=100000.

Local Darcy Friction Factor

In this part, local Darcy friction factors were calculated for Reynolds number in 10000, 20000, 60000 and 100000 on planes which are created for 0.050 m intervals from the beginning of the tube.
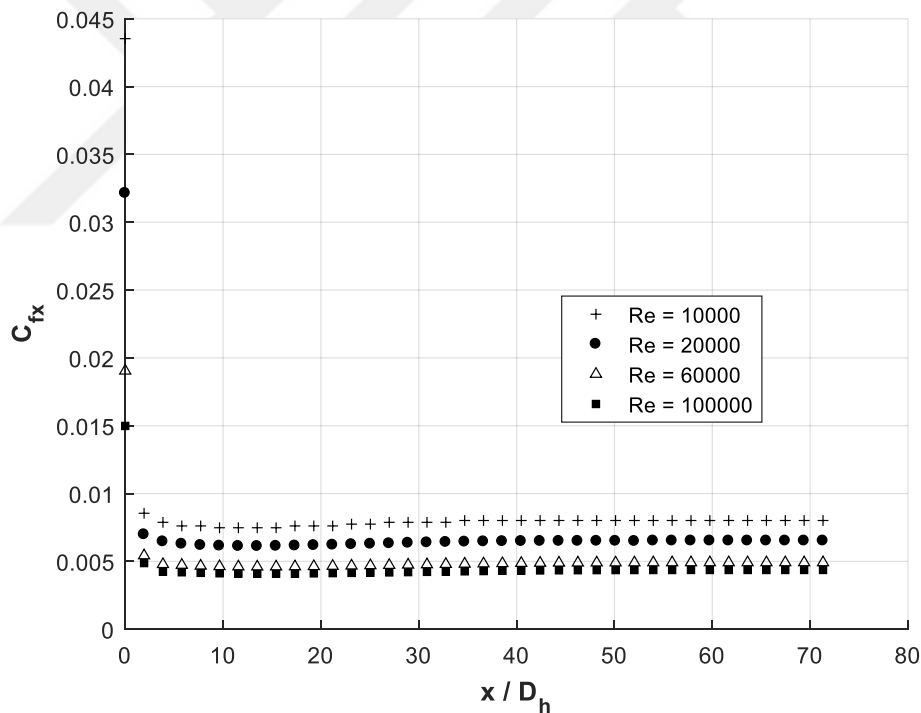

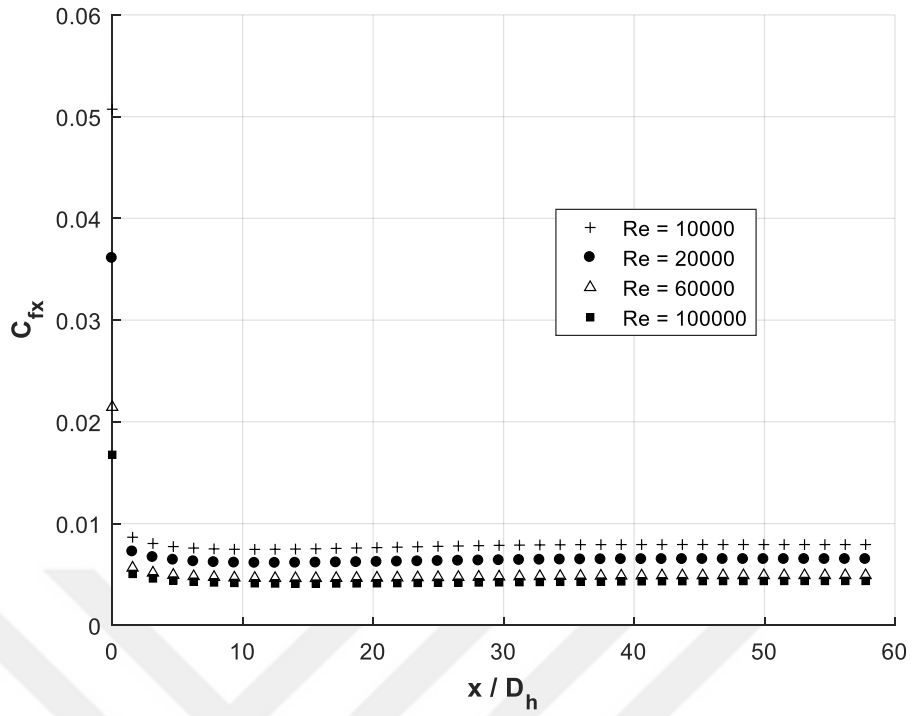*Figure 19. Change of Local Darcy Friction Factor with respect to Created Planes in the Simulation which is a/b=2.00*

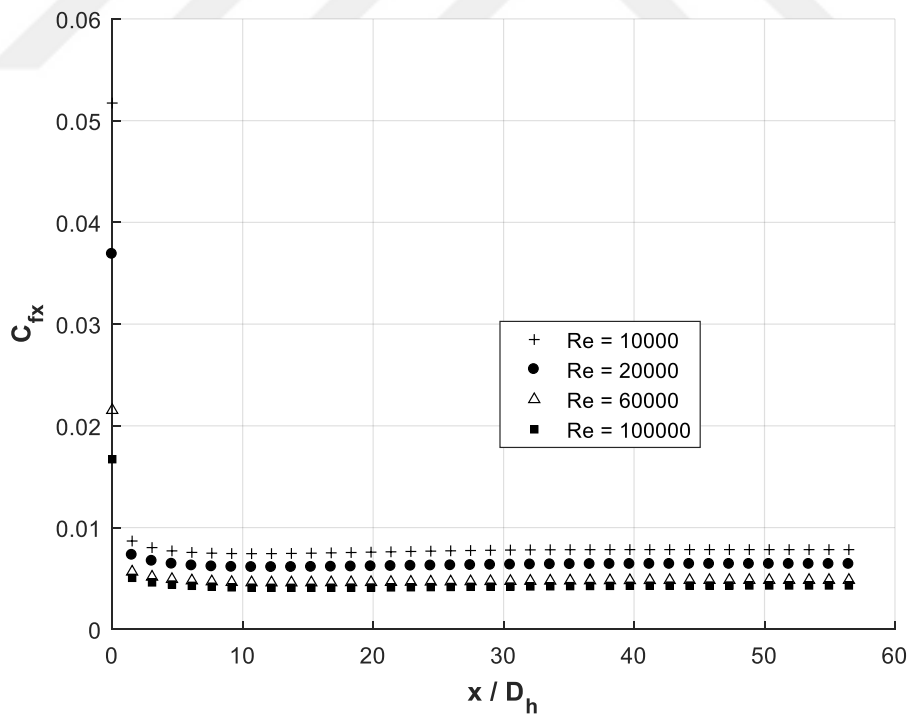*Figure 20. Change of Local Darcy Friction Factor with respect to Created Planes in the Simulation which is a/b=2.25*

Figure 21. Change of Local Darcy Friction Factor with respect to Created Planes in the Simulation which is a/b=2.50
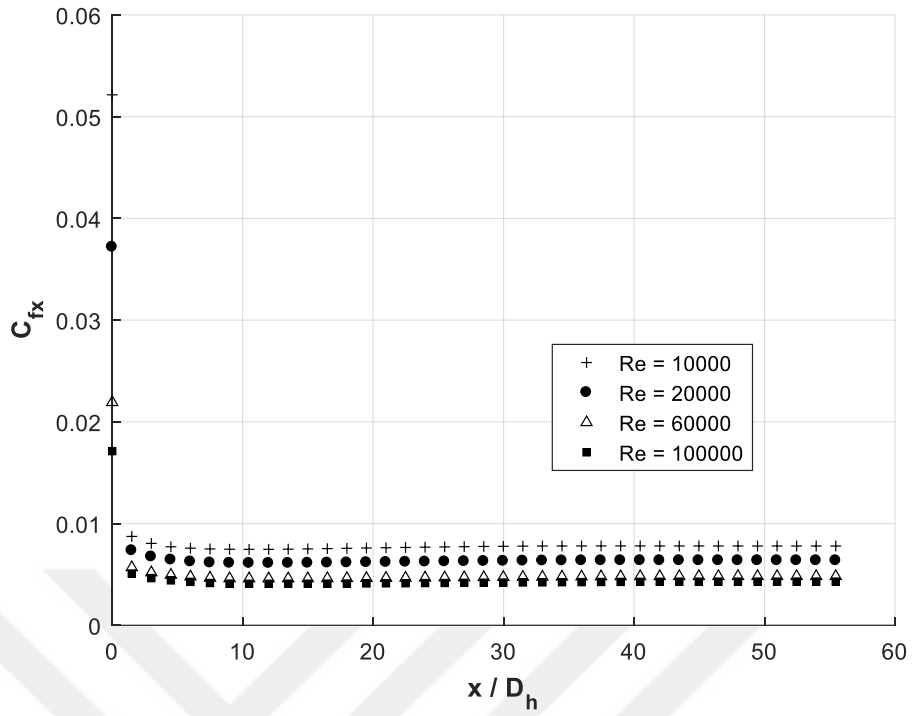
Figure 22. Change of Local Darcy Friction Factor with respect to Created Planes in the Simulation which is a/b=2.75
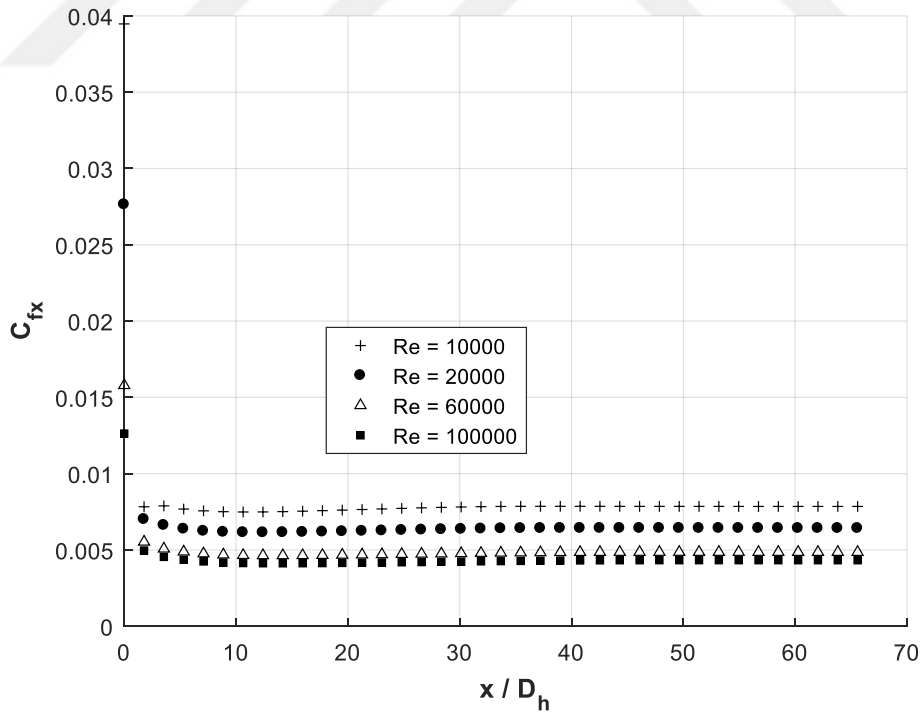

Figure 23. Change of Local Darcy Friction Factor with respect to Created Planes in the Simulation which is a/b=3.00

As seen in the Figure 19, Figure 20, Figure 21, Figure 22 and Figure 23 local Darcy friction factors in all cases are high as expected at the beginning of the tube. Also it is observed that local Darcy friction factors in high Reynolds Number are relatively low.

Also, local Darcy friction factors take almost constant values after certain locations in all cases. So it means that, after this certain location, hydrodynamically fully-developed condition is provided in the tube.

Velocity Profiles at Different Planes

Velocity profiles are examined in different planes along the tube. In that planes, x/D_h ratio is calculated as 10, 15, 20, 25 and 30. Velocity profiles are represented in Figure 24 - Figure 33 for Re=10000 and Re=100000 at that planes.
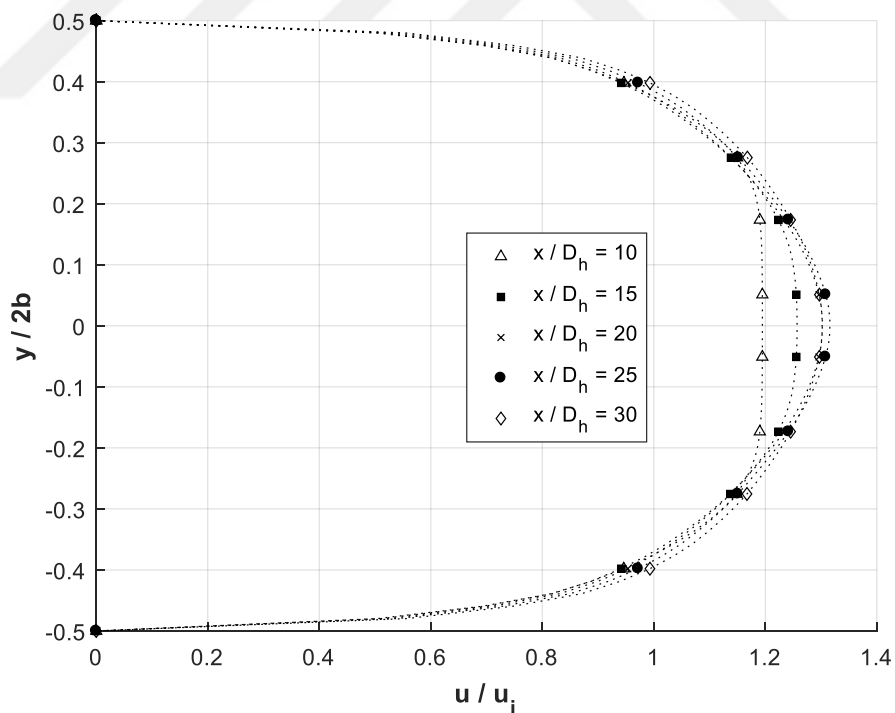

Figure 24. Change of Velocity Profile on Different Planes in the Simulation is which Reynolds Number in 10000 and a/b=2.00
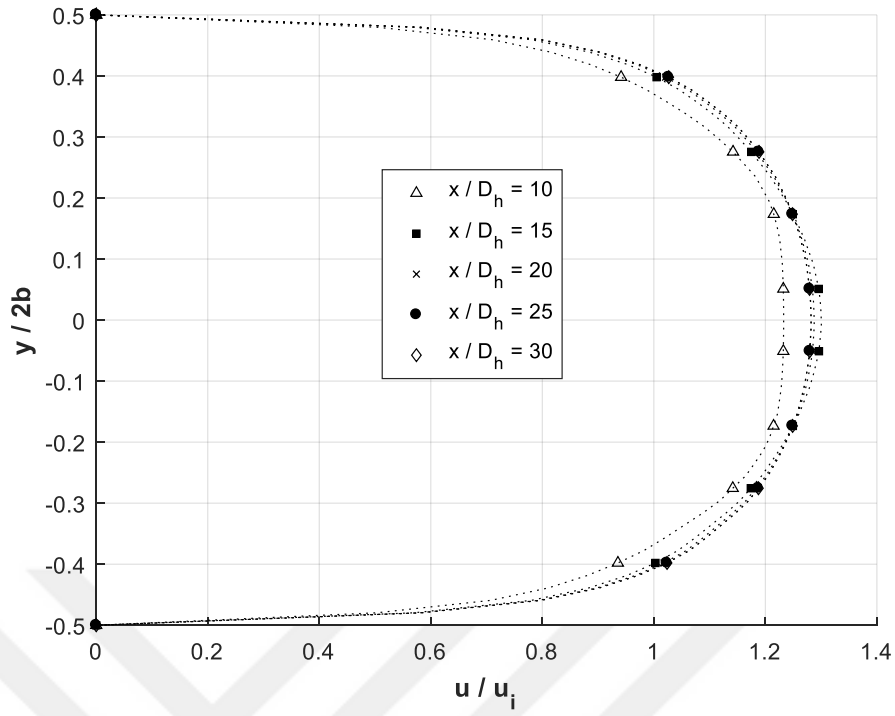
Figure 25. Change of Velocity Profile on Different Planes in the Simulation is which Reynolds Number in 10000 and a/b=2.25

Figure 26. Change of Velocity Profile on Different Planes in the Simulation is which Reynolds Number in 10000 and a/b=2.50

Figure 27. Change of Velocity Profile on Different Planes in the Simulation is which Reynolds Number in 10000 and a/b=2.75
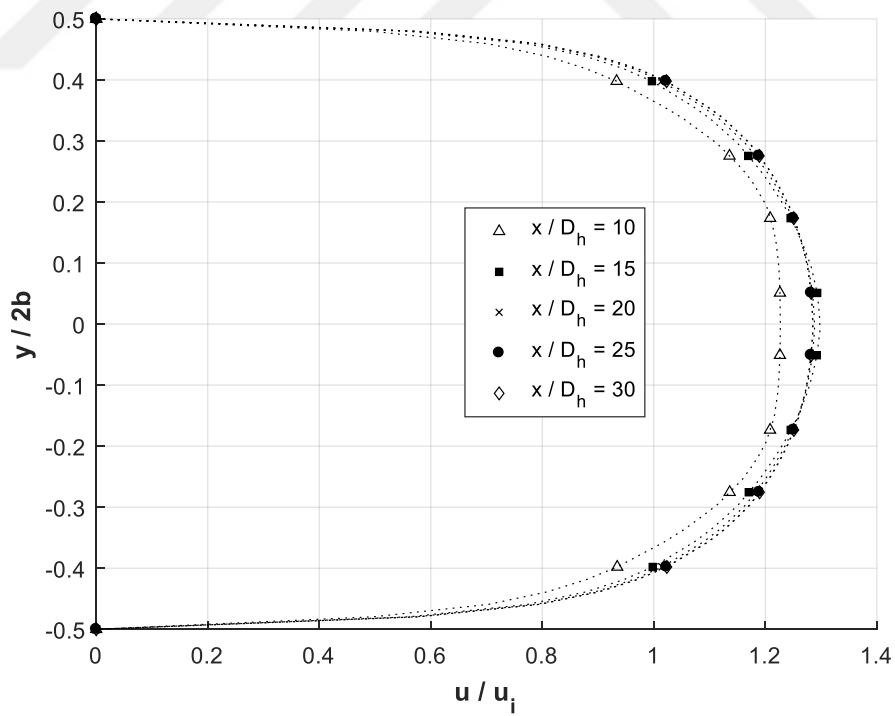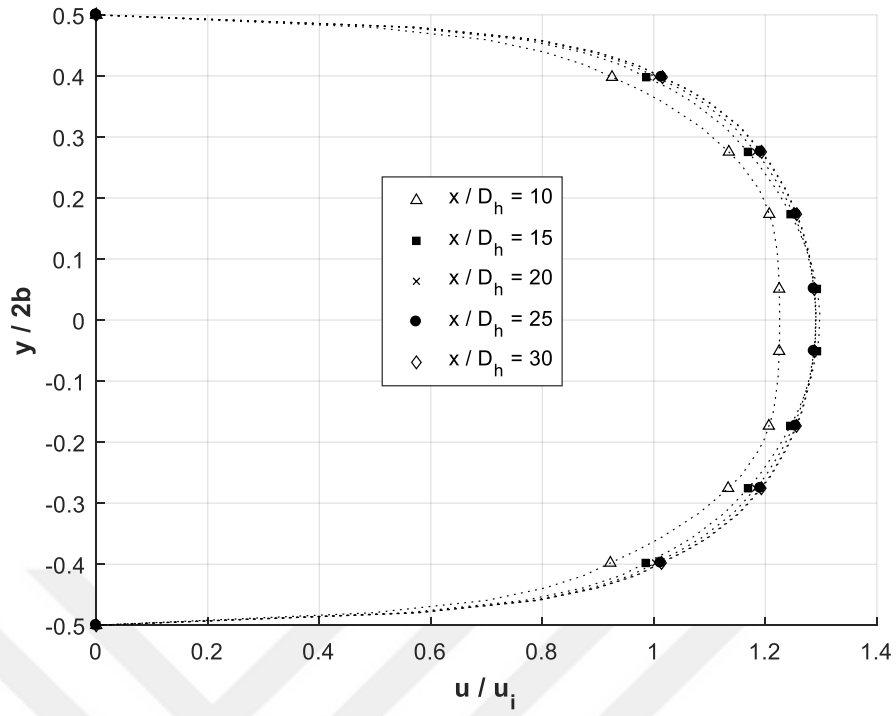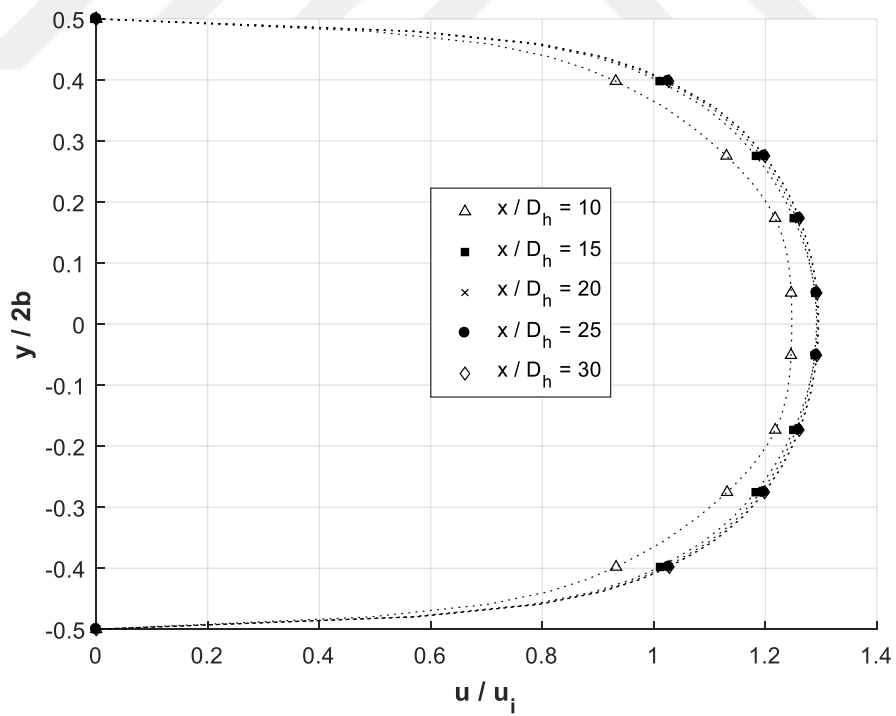

Figure 28. Change of Velocity Profile on Different Planes in the Simulation is which Reynolds Number in 10000 and a/b=3.00

Figure 29. Change of Velocity Profile on Different Planes in the Simulation which is Reynolds Number in 100000 and a/b=2.00

Figure 30. Change of Velocity Profile on Different Planes in the Simulation which is Reynolds Number in 100000 and a/b=2.25
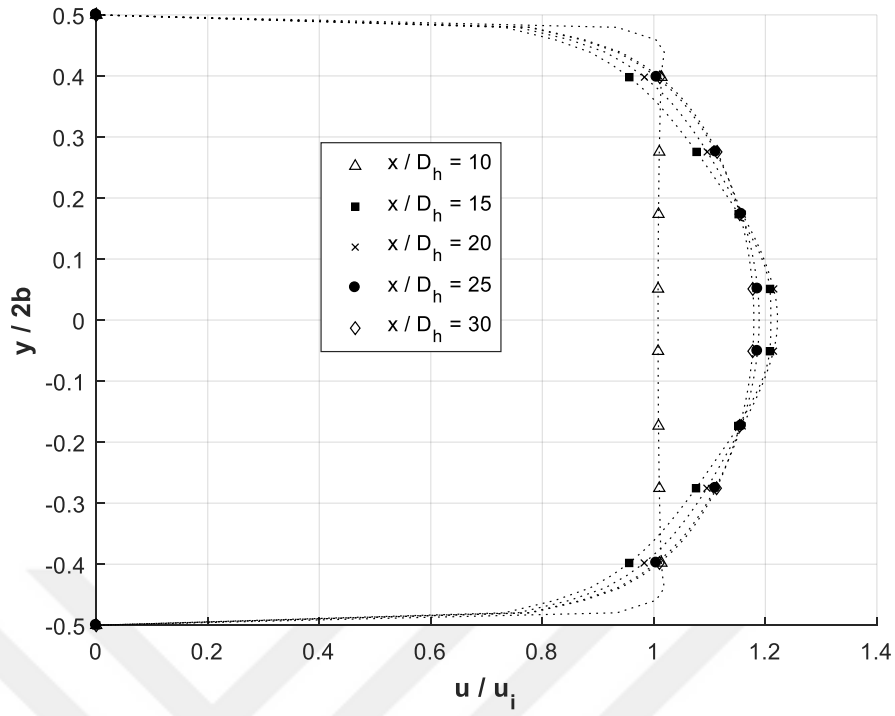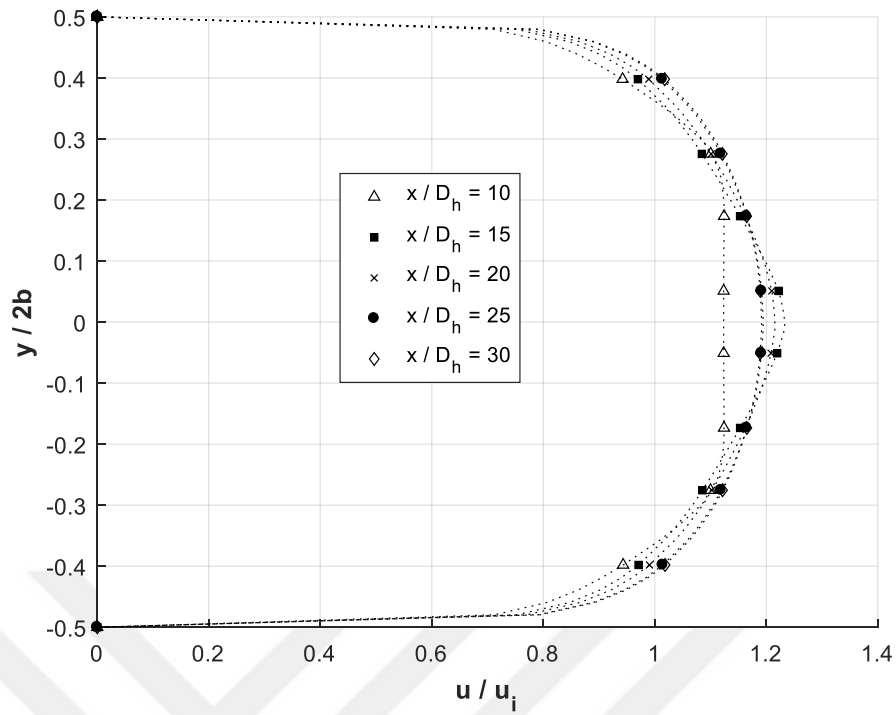
Figure 31. Change of Velocity Profile on Different Planes in the Simulation which is Reynolds Number in 100000 and a/b=2.50
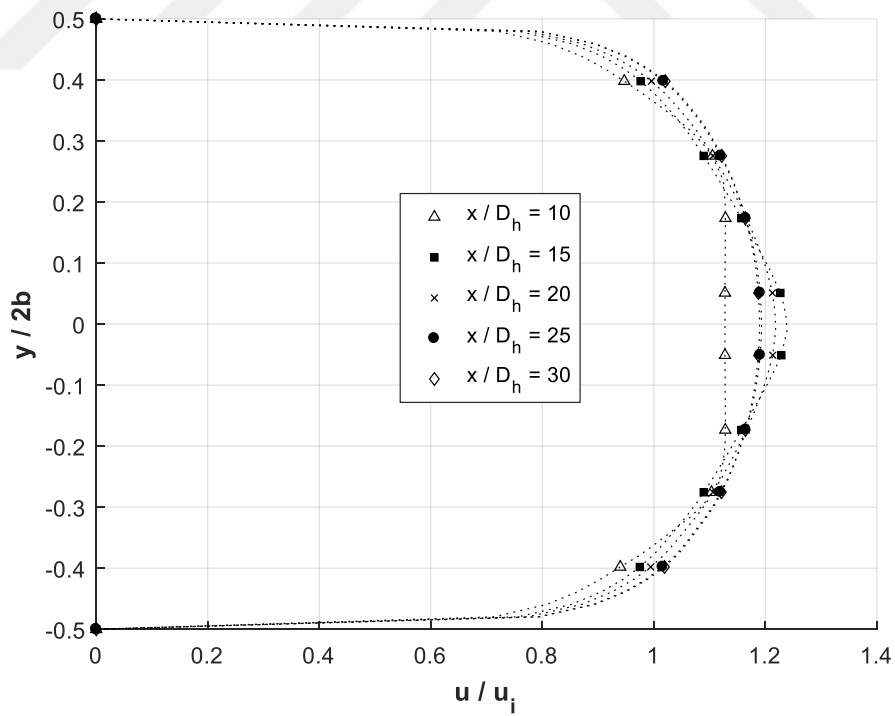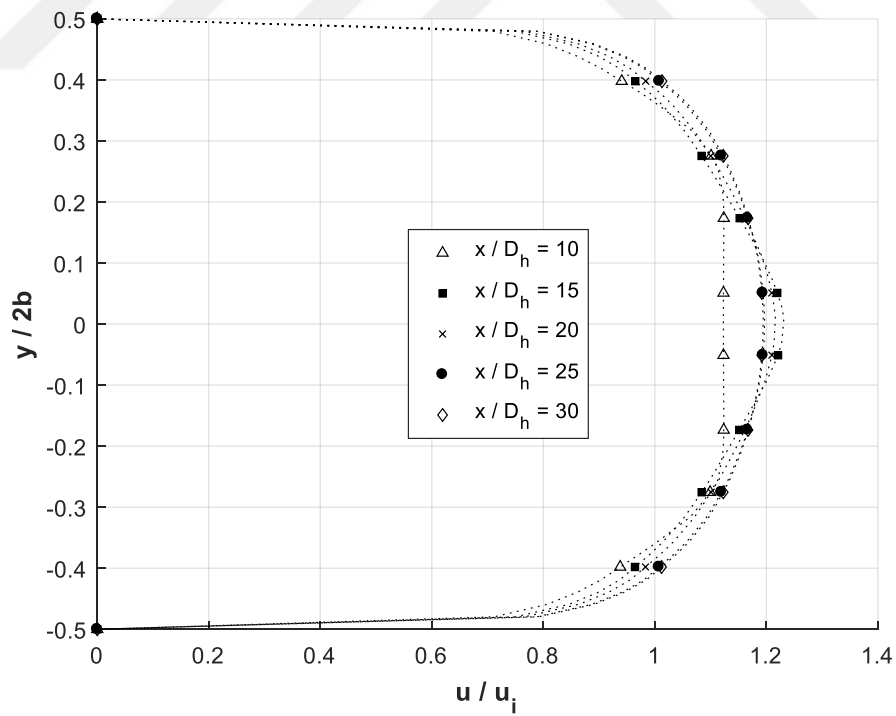

Figure 32. Change of Velocity Profile on Different Planes in the Simulation which is Reynolds Number in 100000 and a/b=2.75
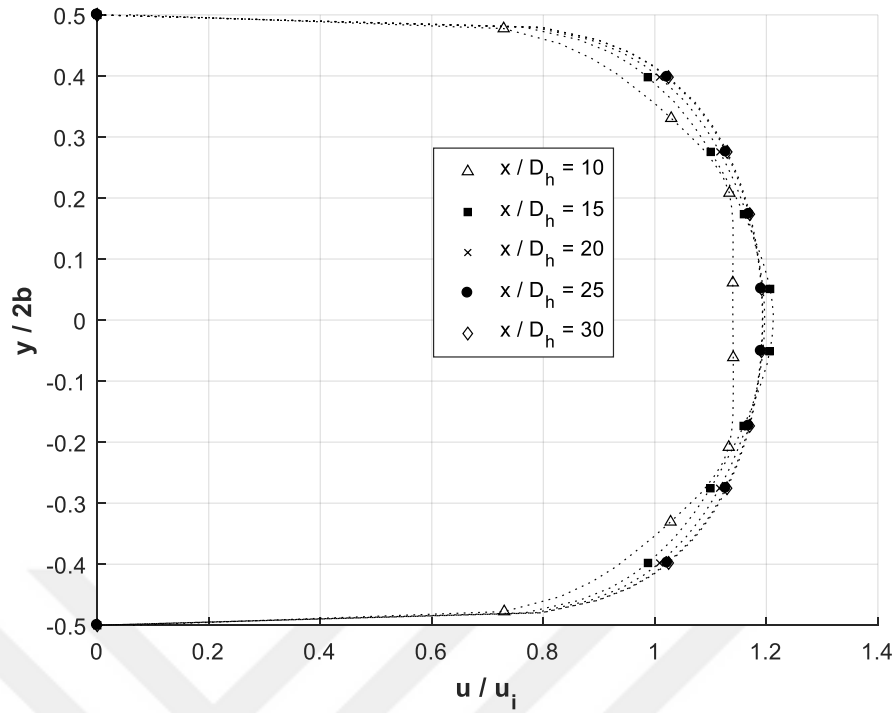
Figure 33. Change of Velocity Profile on Different Planes in the Simulation which is Reynolds Number in 100000 and a/b=3.00

As seen in the velocity profiles figures, velocity profiles do not change after certain locations. So it means that, after this certain location, hydrodynamically fully-developed condition is provided in the tube. Approximately, hydrodynamically fully-developed conditions are provided at $x/D_h = 15$ in Re=10000 and $x/D_h = 20$ in Re=100000. So, velocity develops faster in low Reynolds number.

Dimensionless Temperatures at Different Planes

Dimensionless temperatures are examined in different planes along the tube. In that planes, x/D_h ratio is calculated as 10, 20, 40, 45 and 50. Dimensionless temperatures are represented in Figure 34 - Figure 43for Re=10000 and Re=100000 at that planes.

Figure 34. Change of Dimensionless Temperature Profile on Different Planes in the Simulation is which Reynolds Number in 10000 and a/b=2.00
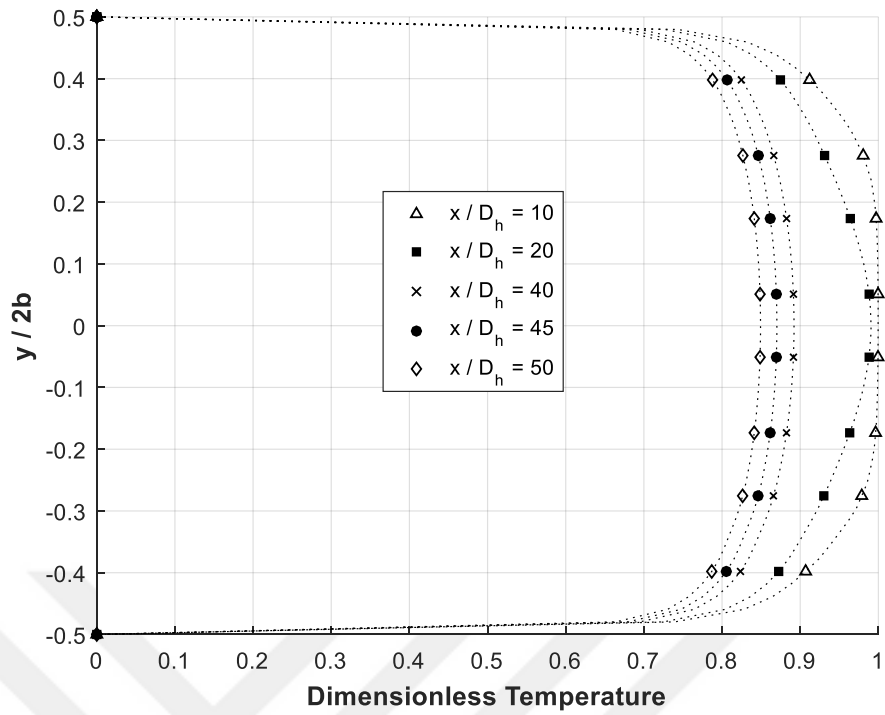
Figure 35. Change of Dimensionless Temperature Profile on Different Planes in the Simulation is which Reynolds Number in 10000 and a/b=2.25
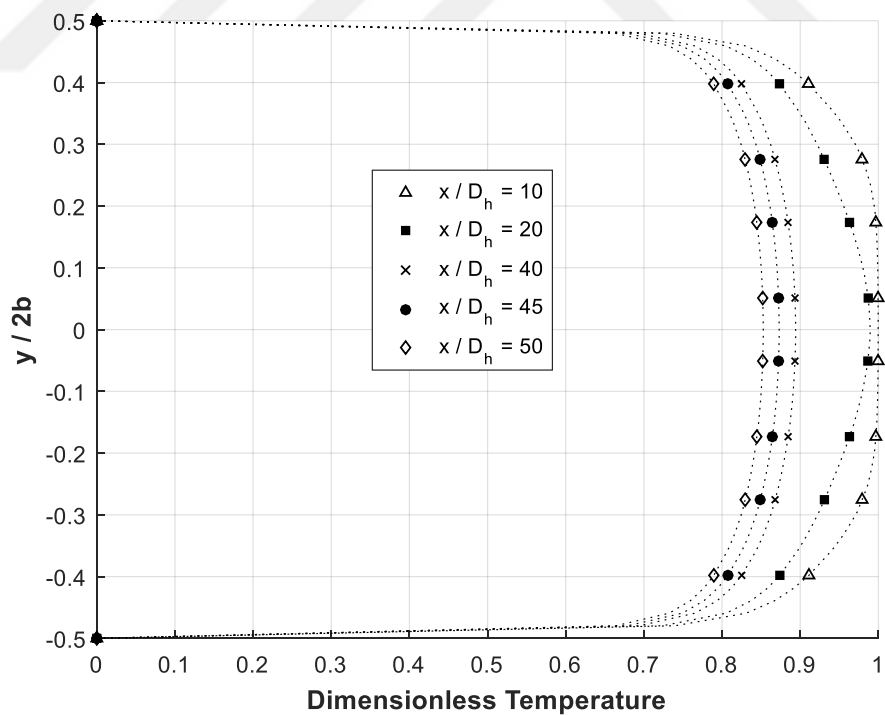
Figure 36. Change of Dimensionless Temperature Profile on Different Planes in the Simulation is which Reynolds Number in 10000 and a/b=2.50

70
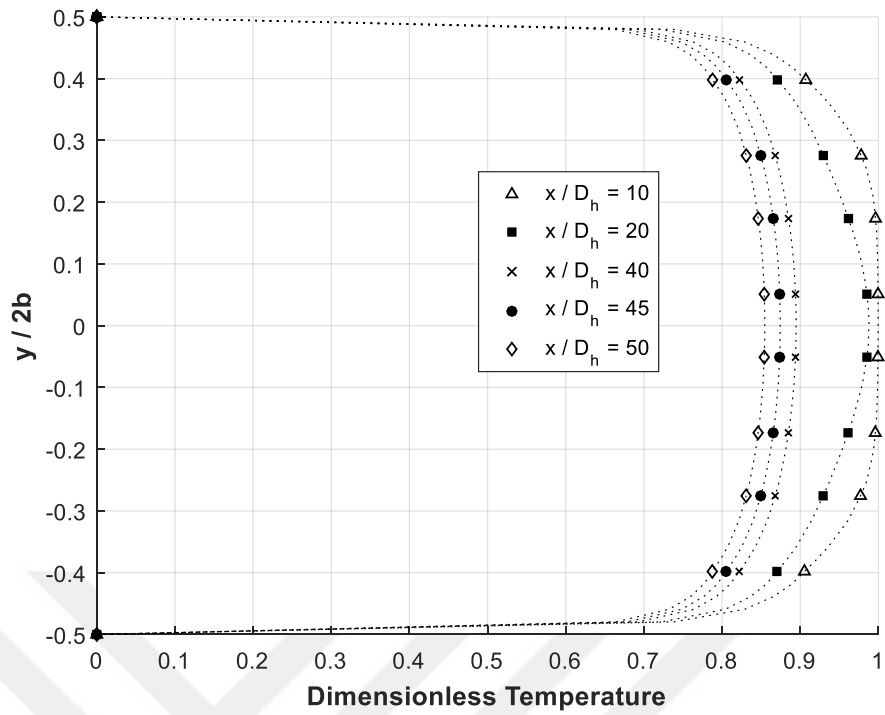
Figure 37. Change of Dimensionless Temperature Profile on Different Planes in the Simulation is which Reynolds Number in 10000 and a/b=2.75
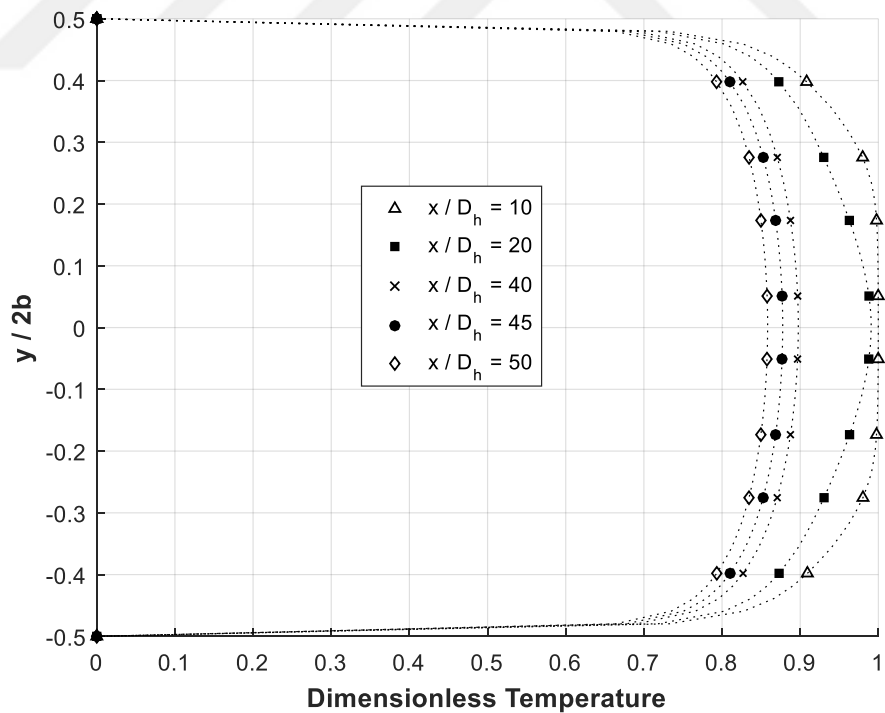
Figure 38. Change of Dimensionless Temperature Profile on Different Planes in the Simulation is which Reynolds Number in 10000 and a/b=3.00
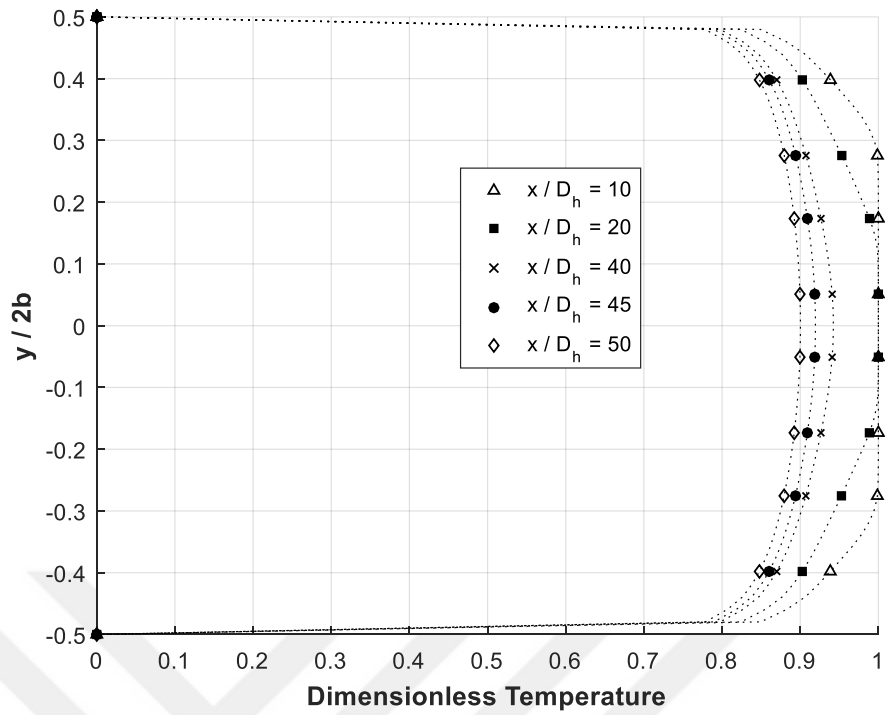
Figure 39. Change of Dimensionless Temperature Profile on Different Planes in the Simulation is which Reynolds Number in 100000 and a/b=2.00
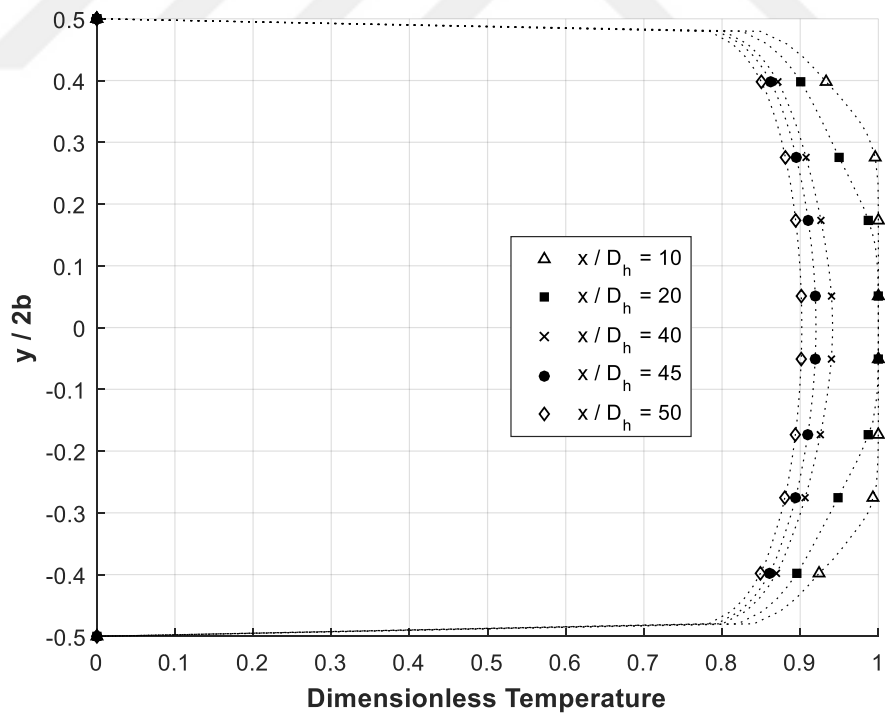
Figure 40. Change of Dimensionless Temperature Profile on Different Planes in the Simulation is which Reynolds Number in 100000 and a/b=2.25
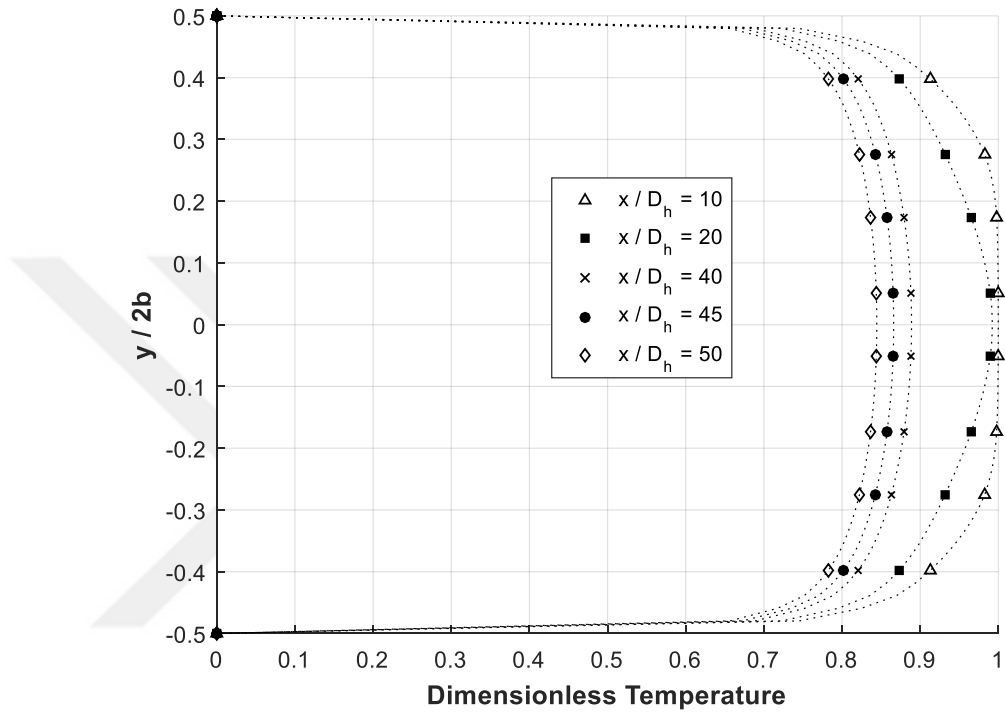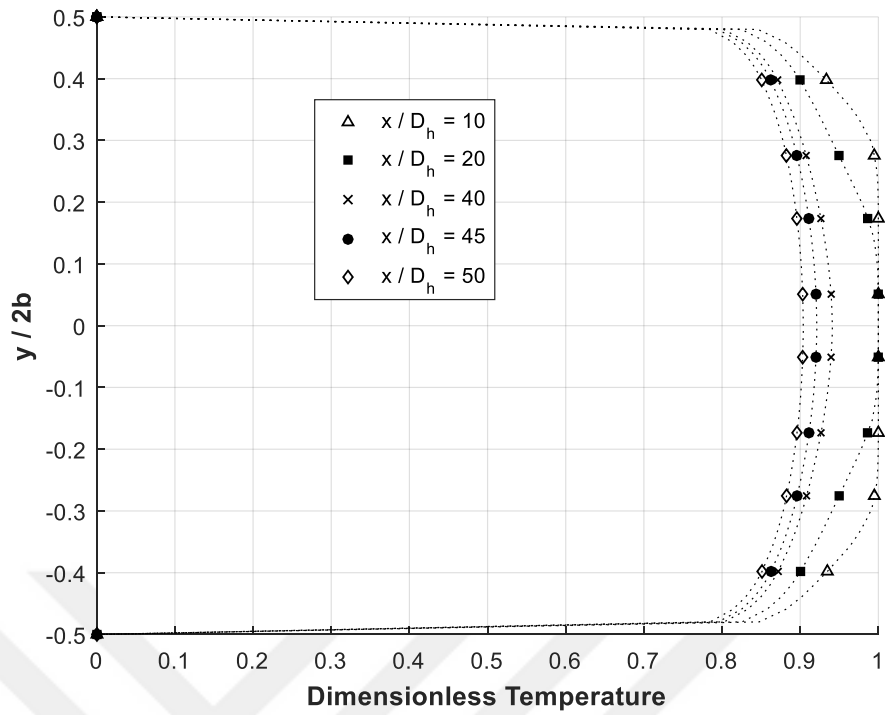
Figure 41. Change of Dimensionless Temperature Profile on Different Planes in the Simulation is which Reynolds Number in 100000 and a/b=2.50
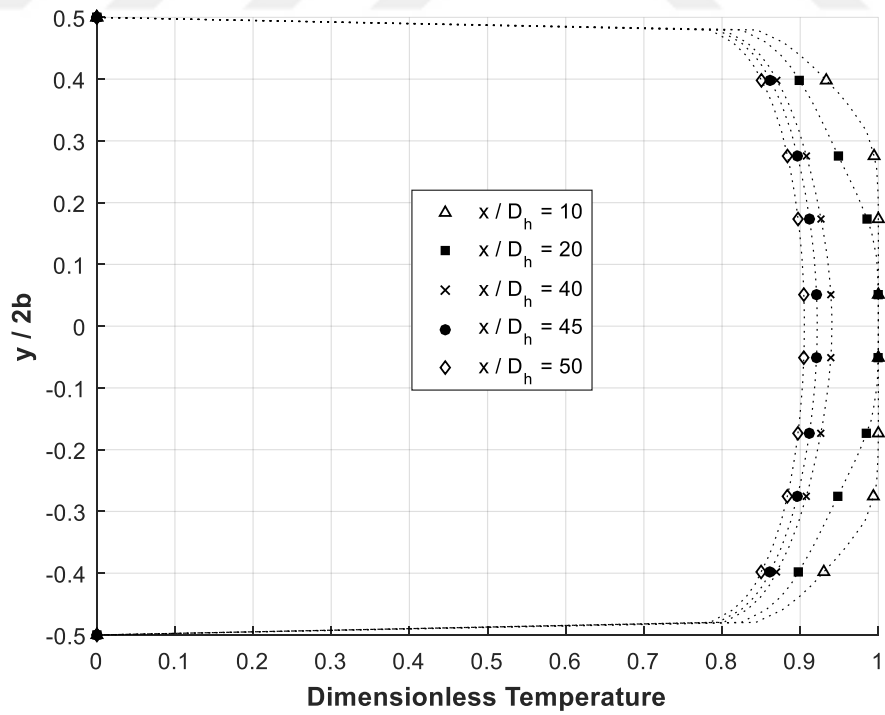
Figure 42. Change of Dimensionless Temperature Profile on Different Planes in the Simulation is which Reynolds Number in 100000 and a/b=2.75

73
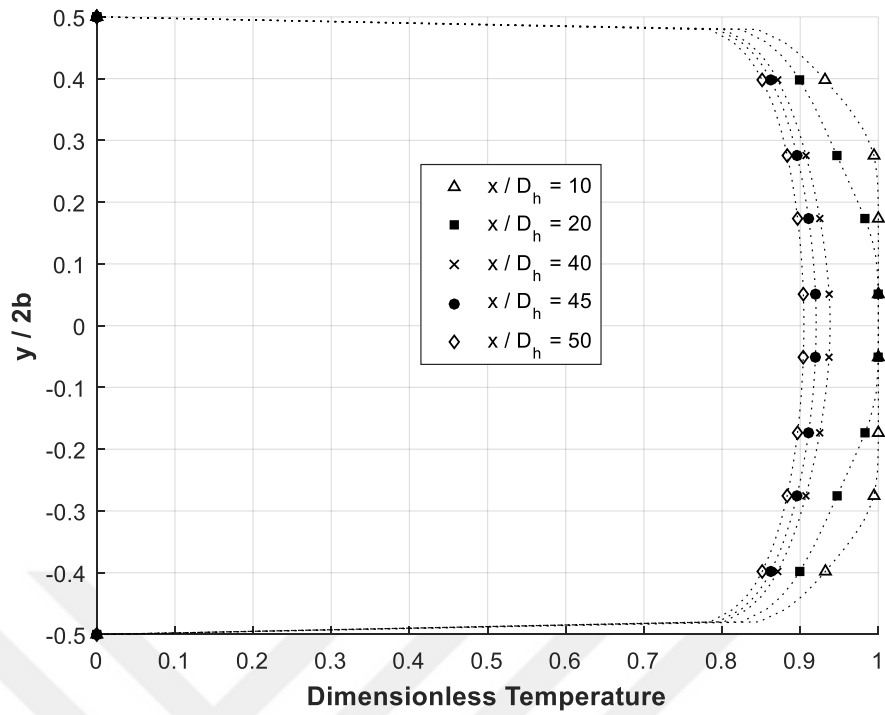
Figure 43. Change of Dimensionless Temperature Profile on Different Planes in the Simulation is which Reynolds Number in 100000 and a/b=3.00

According to the dimensionless temperature definition, it is expected that the dimensionless temperature values in the entrance region should be close to one. In addition, it is expected that the dimensionless temperature values decrease as the fluid moves along the channel.

6.1.2. Results of Hydrodynamically and Thermally Fully Developed Region

In this part average Nusselt number and average Darcy friction factor were examined.

Average Nusselt Number

The plots of average Nusselt number with respect to Reynolds number are showed in Figure 44 - Figure 48. Also they were compared with Dittus-Boelter and Gnielinski correlation which are most commonly used in literature.

$$\overline{Nu_D} = \frac{(f/8)(Re_D - 1000)Pr}{1 + 12.7(f/8)^{1/2}(Pr^{2/3} - 1)} \qquad \text{Gnielinski} \qquad 6.1$$

$$\overline{Nu_D} = 0.023 Re_D^{0.8} Pr^{0.4} \qquad \text{Dittus-Boelter} \qquad 6.2$$
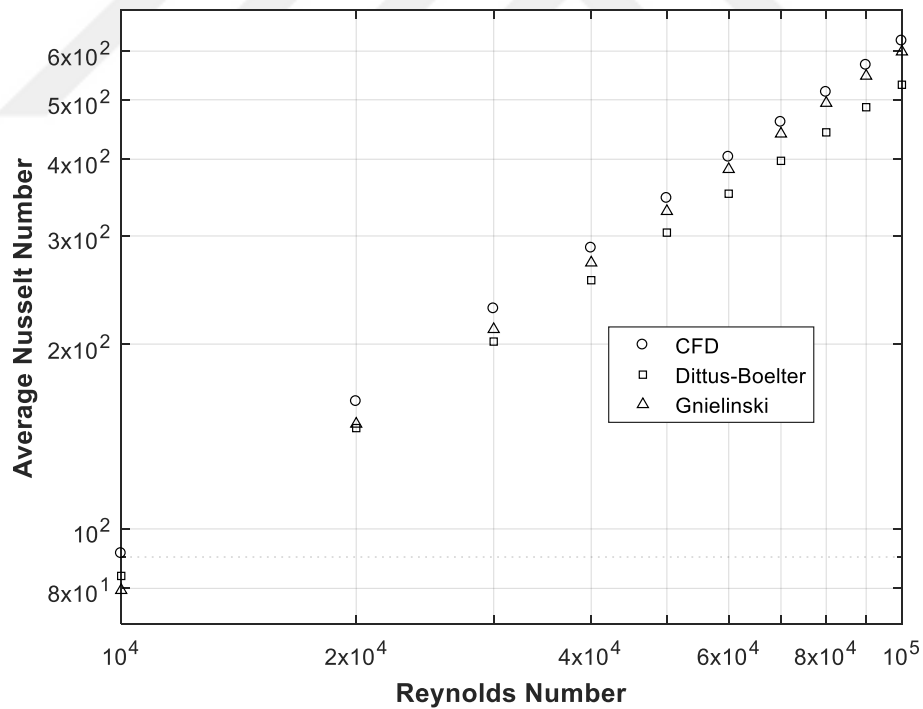
Figure 44. Change of Average Nusselt Number with respect to Reynolds Number in the Simulation which is a/b=2.00
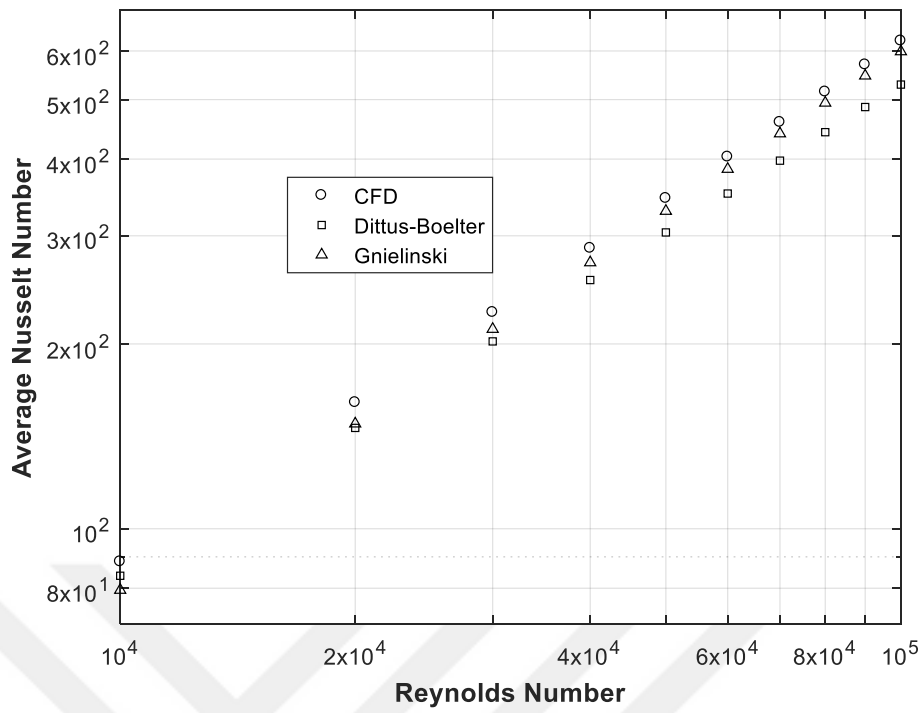
Figure 45. Change of Average Nusselt Number with respect to Reynolds Number in the Simulation which is a/b=2.25

Figure 46. Change of Average Nusselt Number with respect to Reynolds Number in the Simulation which is a/b=2.50

76
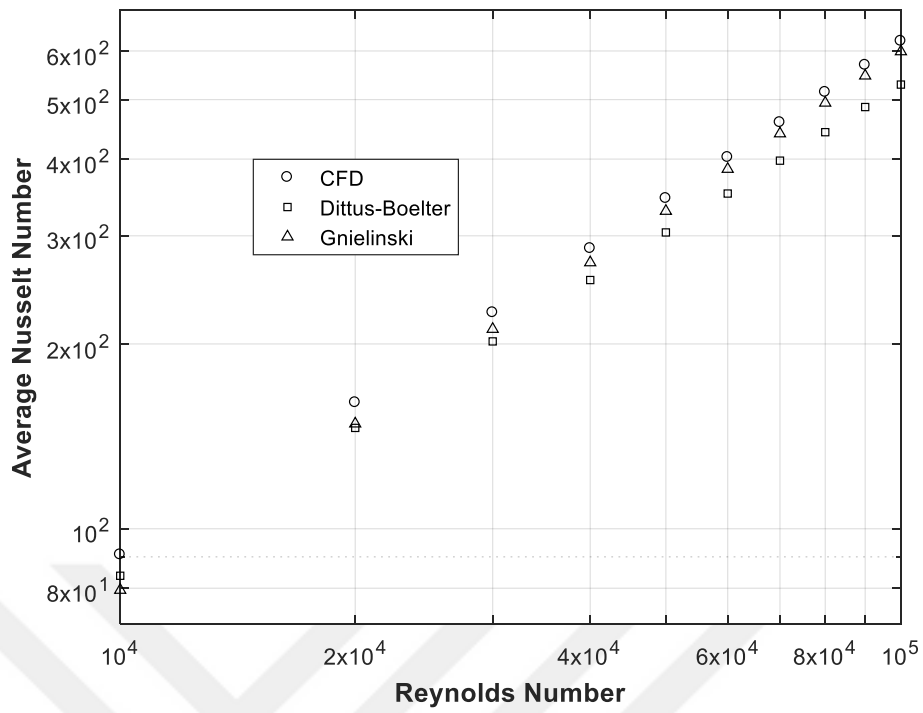
Figure 47. Change of Average Nusselt Number with respect to Reynolds Number in the Simulation which is a/b=2.75

Figure 48. Change of Average Nusselt Number with respect to Reynolds Number in the Simulation which is a/b=3.00

77

The figures were plotted as logarithmic form. As seen in the Figure 44 - Figure 48, when Reynolds number increases, average Nusselt number increases. It is noticed that the results are similar when it is compared with the correlations in literature.

When Reynolds number increases, flow becomes more turbulent. As a result of this, high heat transfer coefficient and high thermal performance is obtained.

Table 3. Comparison of Average Nusselt Number with Correlations

		CFD	Dittus-Boelter	Gnielinski
	Re=20000	161.3	146.0	148.2
a / b = 2.00	Re=60000	403.2	351.5	385.2
	Re=100000	623.4	529.0	598.7
	Re=20000	160.5	146.0	148.2
a / b = 2.25	Re=60000	403.2	351.5	385.2
	Re=100000	623.2	529.0	598.7
	Re=20000	159.7	146.0	148.2
a / b = 2.50	Re=60000	401.4	351.5	385.2
	Re=100000	623.7	529.0	598.7
	Re=20000	160.4	146.0	148.2
a / b = 2.75	Re=60000	402.6	351.5	385.2
	Re=100000	622.5	529.0	598.7
	Re=20000	160.2	146.0	148.2
a / b = 3.00	Re=60000	400.0	351.5	385.2
	Re=100000	620.7	529.0	598.7

The results of CFD are compared with correlations available in literature, and there is a good agreement with average deviation 6% with Gnielinski and 12% with Dittus-Boelter.

<u>Average Darcy Friction Factor</u>

Average Darcy friction factors with respect to Reynolds number are shown in Figure 49 - Figure 53. Also they were compared with Petukhov correlation which is most commonly used in literature.

$$f = (0.790 \ln Re_D - 1.64)^{-2} \qquad\qquad \text{Petukhov} \qquad\qquad 6.3$$

Figure 49. Change of Average Darcy Friction Factor with respect to Reynolds Number in the Simulation which is a/b=2.00
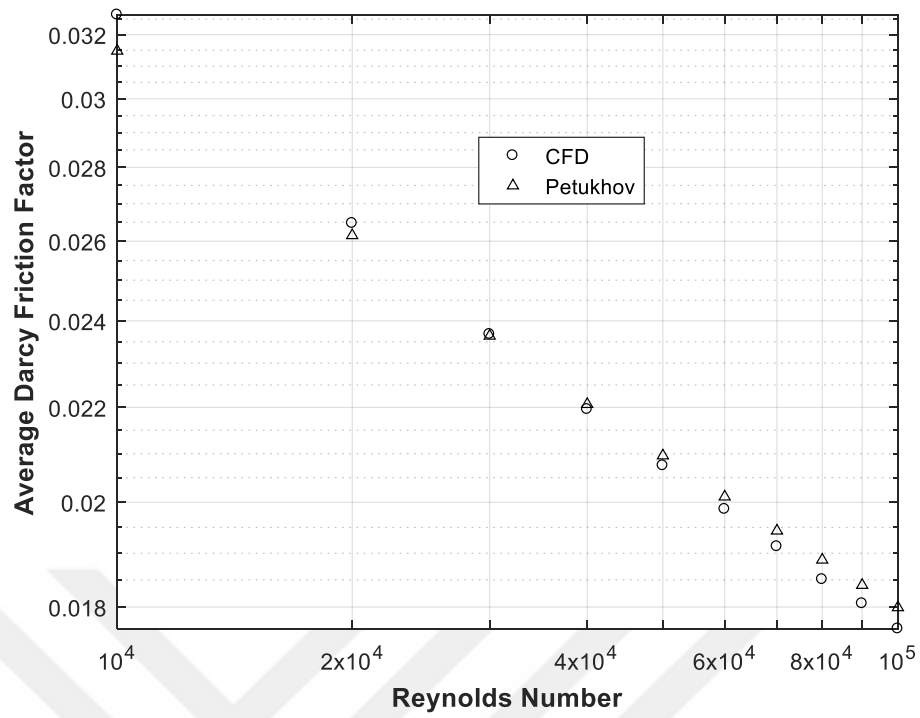
Figure 50. Change of Average Darcy Friction Factor with respect to Reynolds Number in the Simulation which is a/b=2.25
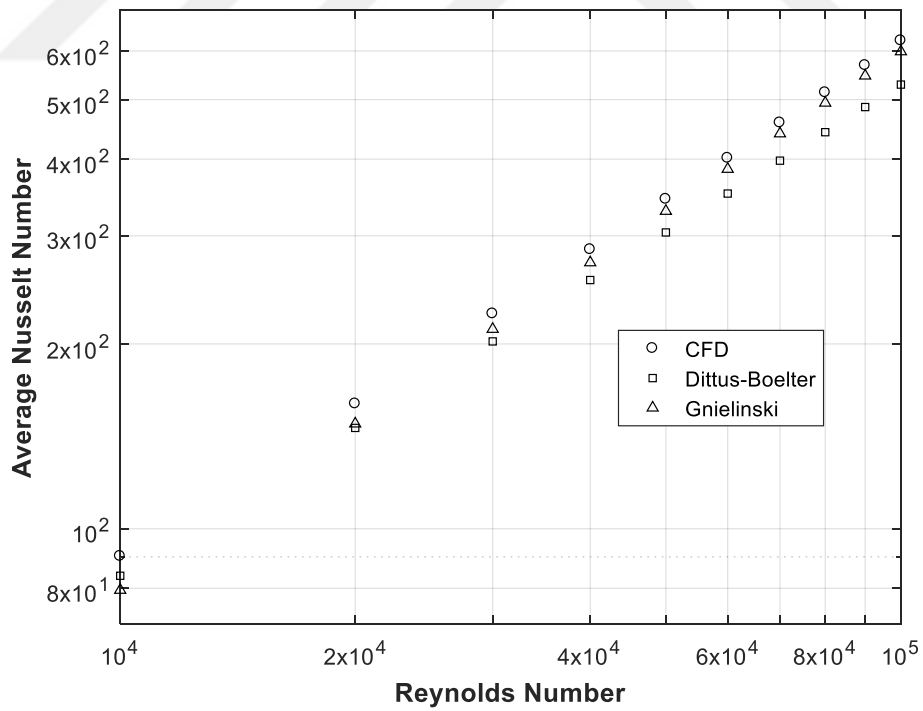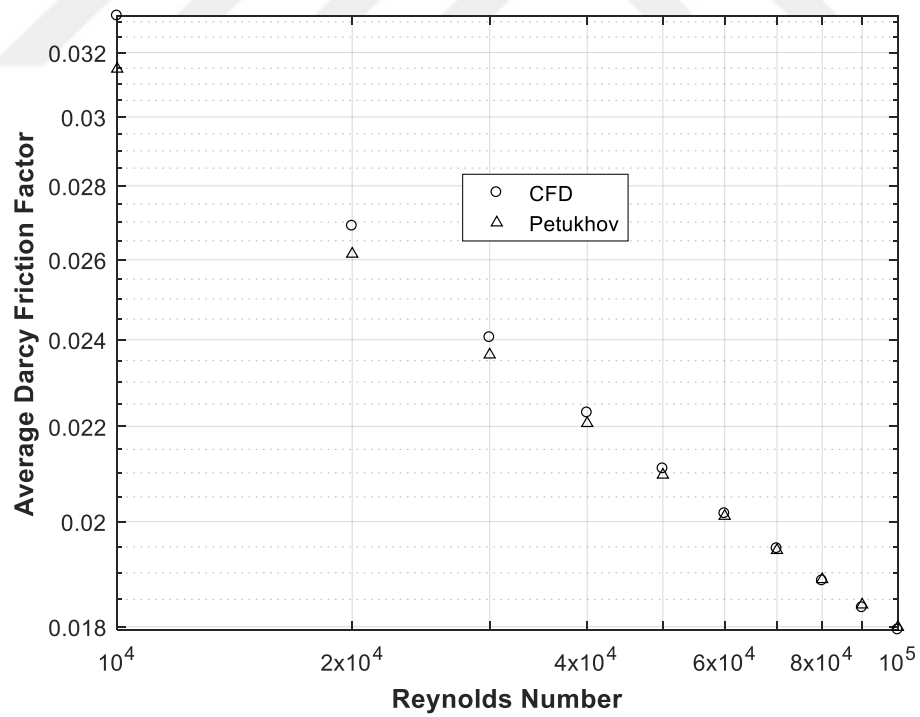

Figure 51. Change of Average Darcy Friction Factor with respect to Reynolds Number in the Simulation which is a/b=2.50
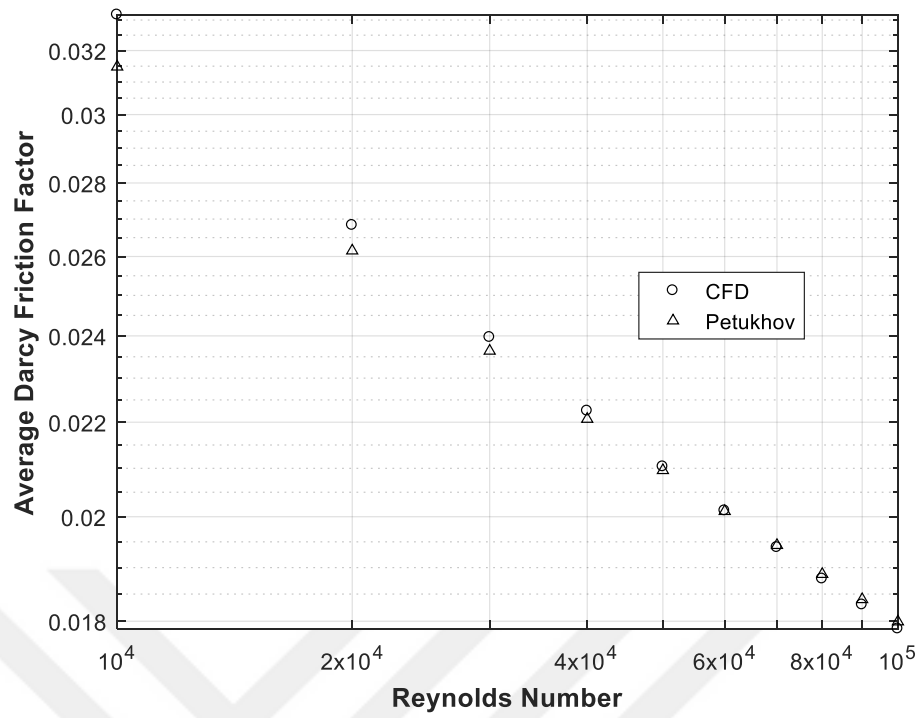
Figure 52. Change of Average Darcy Friction Factor with respect to Reynolds Number in the Simulation which is a/b=2.75
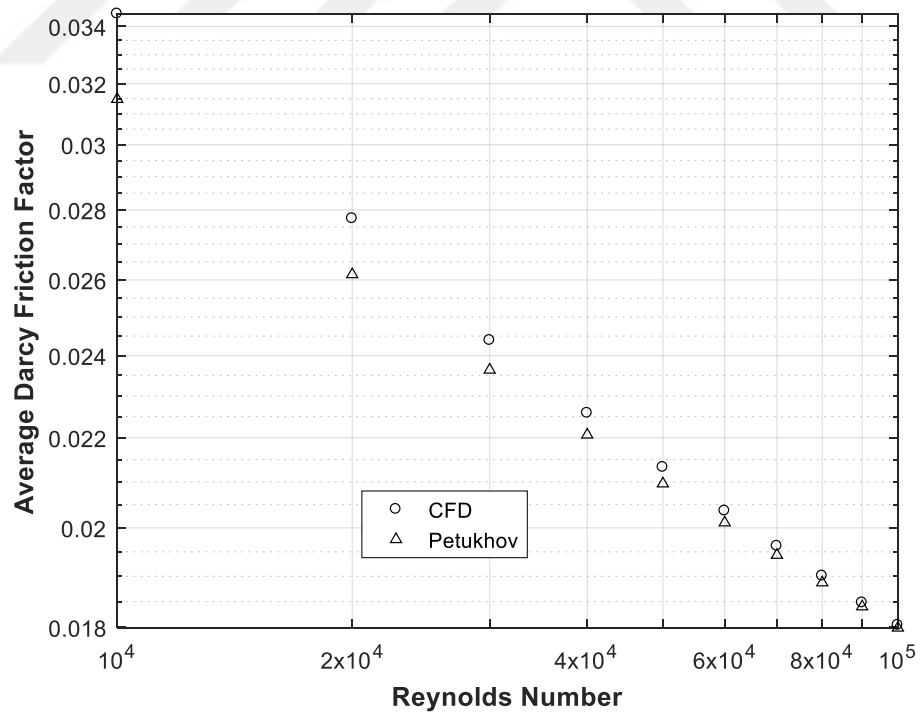
Figure 53. Change of Average Darcy Friction Factor with respect to Reynolds Number in the Simulation which is a/b=3.00
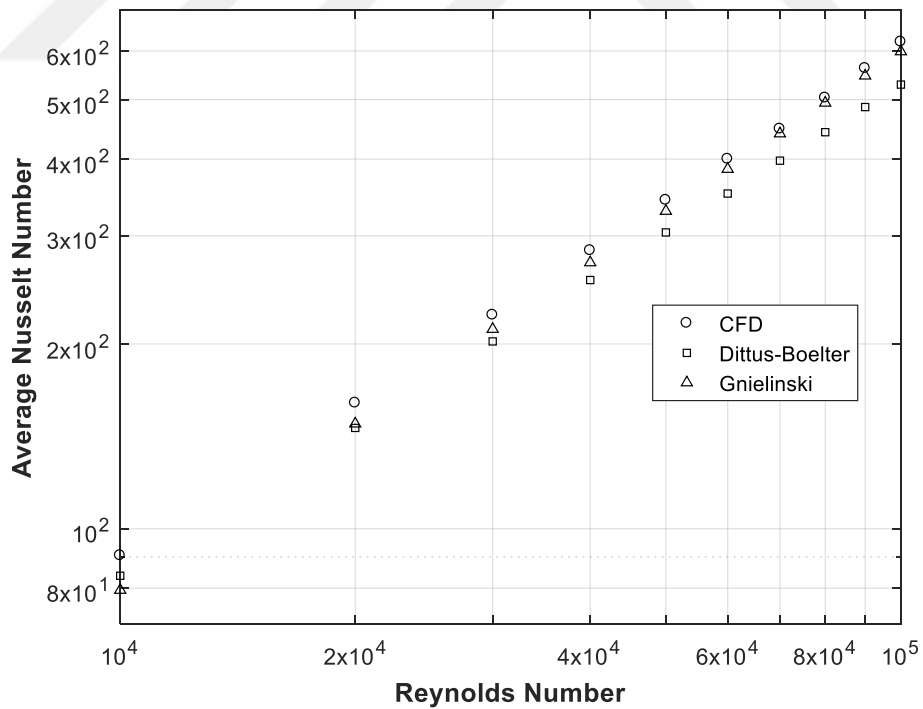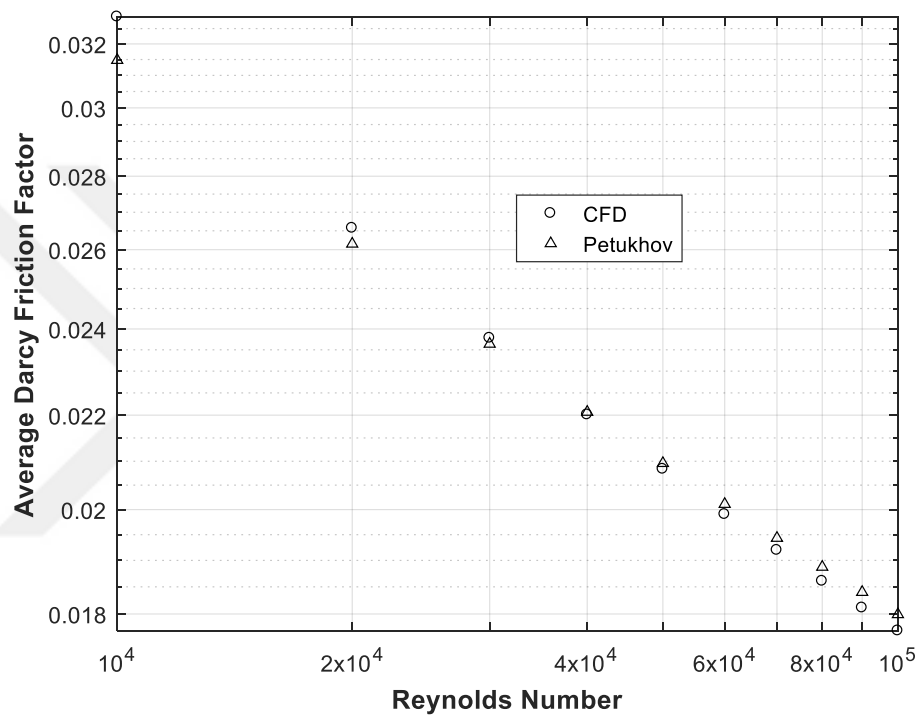
The figures were plotted as logarithmic form. As seen in the Figure 49 - Figure 53, when Reynolds number increases, average Darcy friction factor decreases. It is noticed that the results are similar when it is compared with Petukhov correlation in literature.

Table 4. Comparison of Average Darcy Friction Factor with Correlation

		CFD	Petukhov
	Re=20000	0.0266	0.0262
a / b = 2.00	Re=60000	0.0199	0.0201
	Re=100000	0.0177	0.0180
	Re=20000	0.0265	0.0262
a / b = 2.25	Re=60000	0.0199	0.0201
	Re=100000	0.0176	0.0180
	Re=20000	0.0269	0.0262
a / b = 2.50	Re=60000	0.0202	0.0201
	Re=100000	0.0179	0.0180
	Re=20000	0.0268	0.0262
a / b = 2.75	Re=60000	0.0201	0.0201
	Re=100000	0.0179	0.0180
	Re=20000	0.0277	0.0262
a / b = 3.00	Re=60000	0.0204	0.0201
	Re=100000	0.0180	0.0180

The results of CFD are compared with correlation available in literature, and there is a good agreement with average deviation 2%

According to results of simulations, the correlations for average Nusselt number and average Darcy friction factor are developed by using MATLAB curve fitting toolbox. Correlations in the form of $Nu = a_1 \times Re^{b_1}$ and $f = a_2 \times Re^{b_2}$ are developed for average Nusselt numbers and average friction factors in all models.

Table 5. Correlation Constants for Water Cases

a / b	a_1	b_1	a_2	b_2
2.00	0.039	0.840	0.397	-0.272
2.25	0.036	0.847	0.389	-0.270
2.50	0.035	0.849	0.395	-0.270
2.75	0.037	0.845	0.398	-0.271
3.00	0.037	0.843	0.471	-0.285

6.2. Results of Simulations: Working Fluid is Al_2O_3+Water

Before the simulation, mesh optimization and mesh independency studies were carried out to determine the number of meshes used in simulations. With specified mesh, simulations were repeated and results were obtained. Local Nusselt number, local Darcy friction factor, average Nusselt number, average Darcy friction factor and velocity profiles were calculated and plotted as appropriate form. Average Nusselt number and average Darcy friction factor were compared with similar works in literature and they were expressed as appropriate Reynolds number form. Results are given separately for two different sections. Local Nusselt number, local Darcy friction factor, velocity profiles and dimensionless temperature profiles were given in the results of developing region part. Average Nusselt number and average Darcy friction factor were given in the results of fully developed region part.

6.2.1. Results of Hydrodynamically and Thermally Developing Region

In this part local Nusselt number, local Darcy friction factor, velocity profiles and dimensionless temperature profiles were examined.

<u>Local Nusselt Number</u>

Local Nusselt numbers were calculated for the Reynolds number of 10000, 20000, 60000 and 100000 on planes which are created for 0.050 m intervals from the beginning of the tube. The planes are represented in Figure 54.

Figure 54. (a) Isometric View (b) Side View of the Planes

Local Nusselt number and local Darcy friction factor are calculated on that planes and the results of them are represented as XY-Plot form.
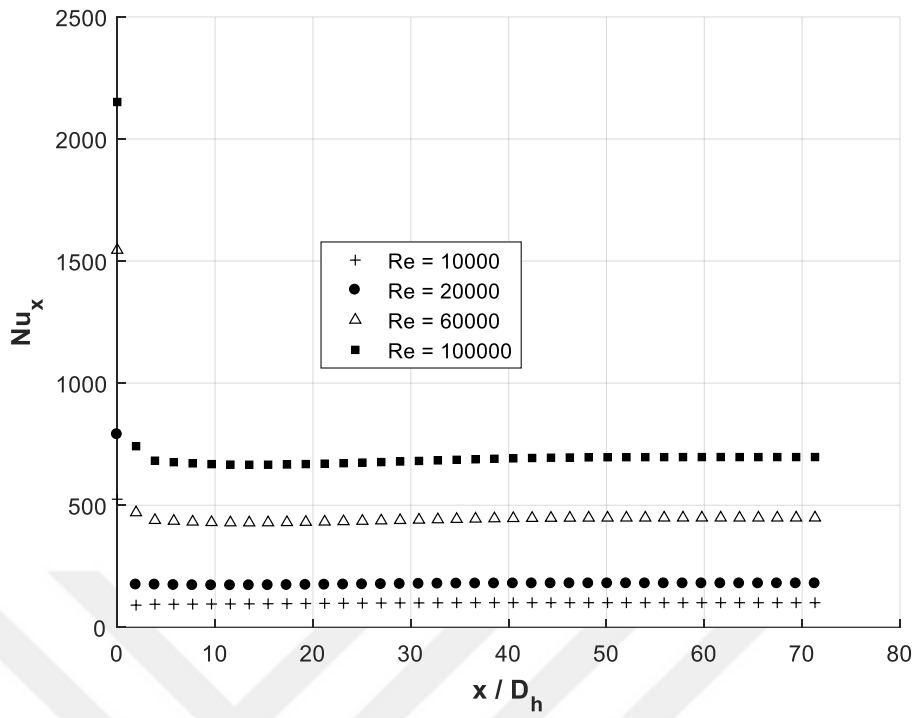
Figure 55. Change of Local Nusselt Number with respect to Created Planes in the Simulation which is a/b=2.00
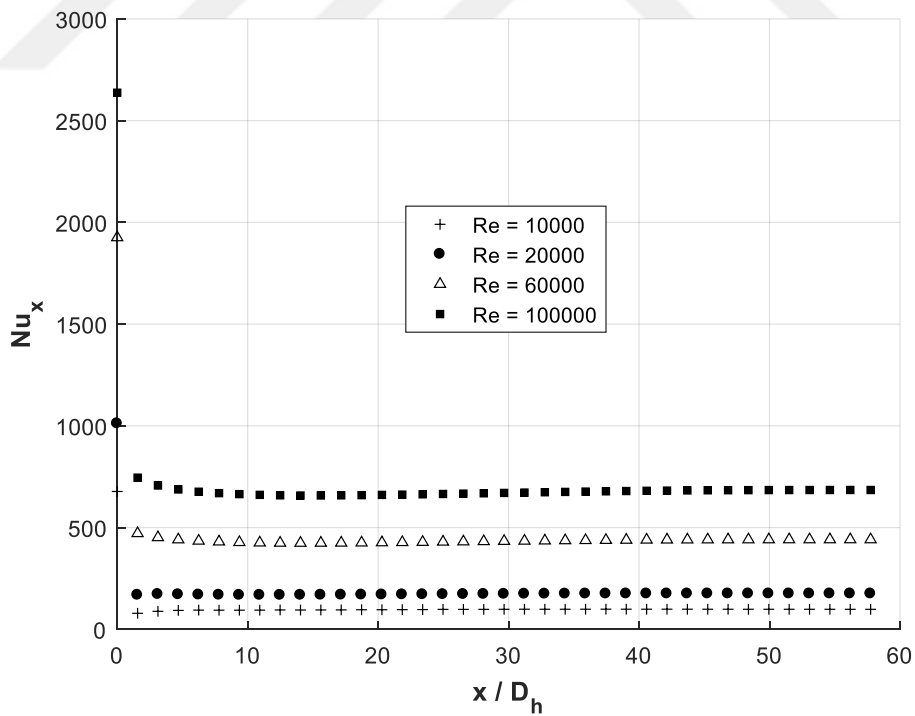
Figure 56. Change of Local Nusselt Number with respect to Created Planes in the Simulation which is a/b=2.25
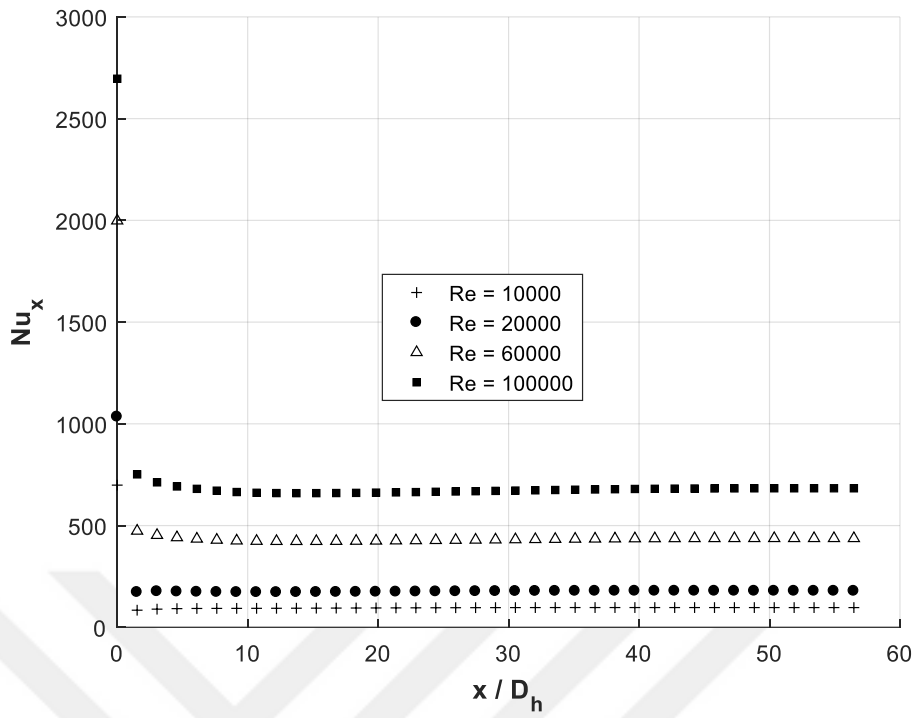
Figure 57. Change of Local Nusselt Number with respect to Created Planes in the Simulation which is a/b=2.50
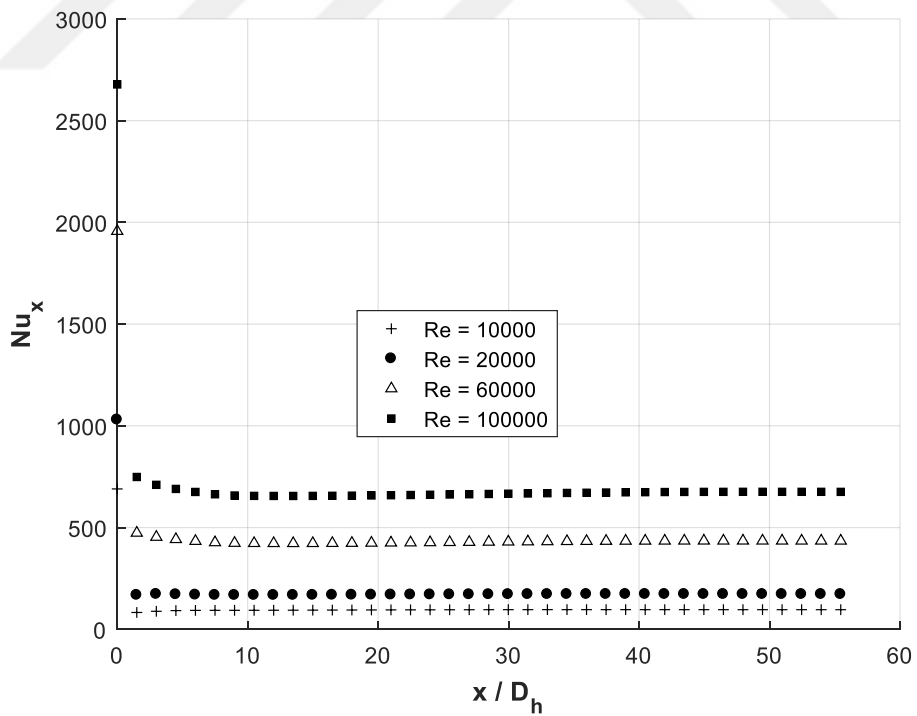
Figure 58. Change of Local Nusselt Number with respect to Created Planes in the Simulation which is a/b=2.75
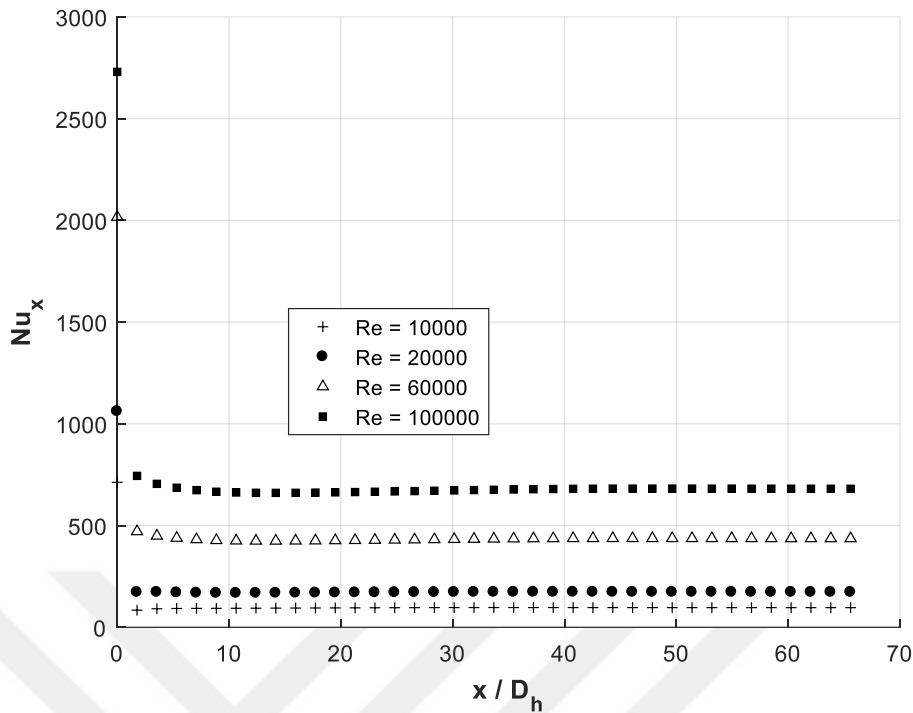
Figure 59. Change of Local Nusselt Number with respect to Created Planes in the Simulation which is a/b=3.00

As seen in the Figure 55, Figure 56, Figure 57, Figure 58 and Figure 59 local Nusselt numbers in all cases are high as expected at the beginning of tube. Also it is observed that local Nusselt number in high Reynolds number is relatively high. Also, local Nusselt numbers take almost constant values after certain locations in all cases. So it means that, after this certain location, thermally fully-developed condition is provided in the tube. Approximately, thermally fully developed conditions are provided at $x/D_h = 25$ in Re=10000 and $x/D_h = 30$ in Re=100000.

Local Darcy Friction Factor

In this part, local Darcy friction factors were calculated for Reynolds number in 10000, 20000, 60000 and 100000 on planes which are created for 0.050 m intervals from the beginning of the tube.
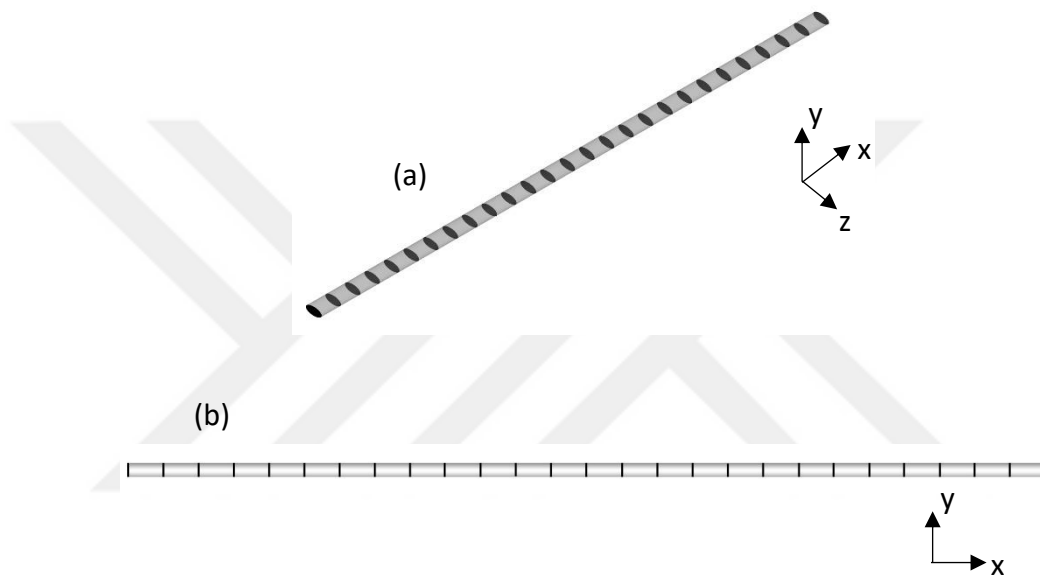
87
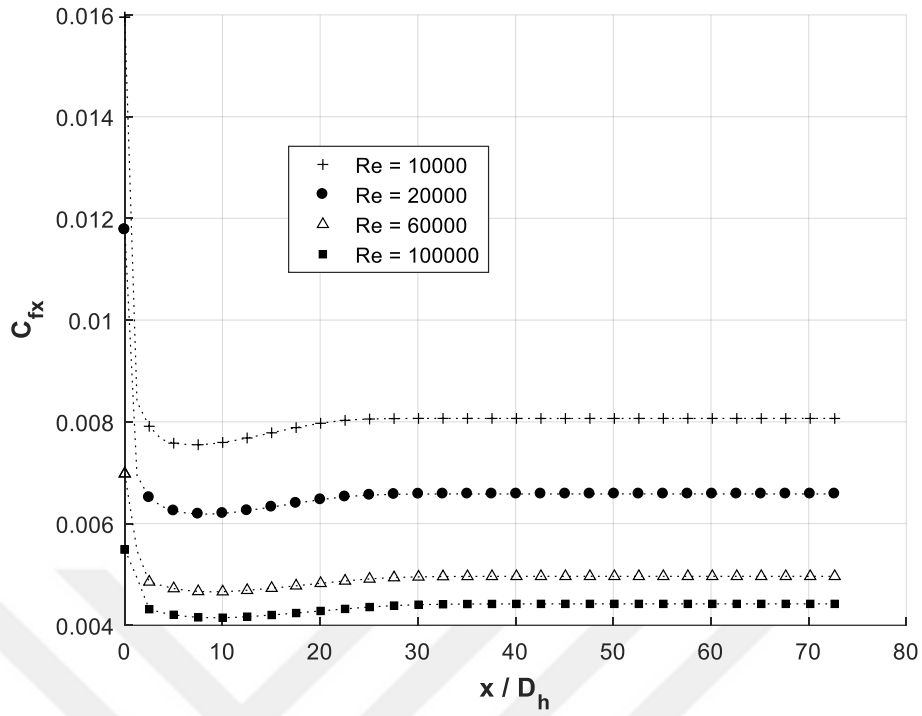
Figure 60. Change of Local Darcy Friction Factor with respect to Created Planes in the Simulation which is a/b=2.00
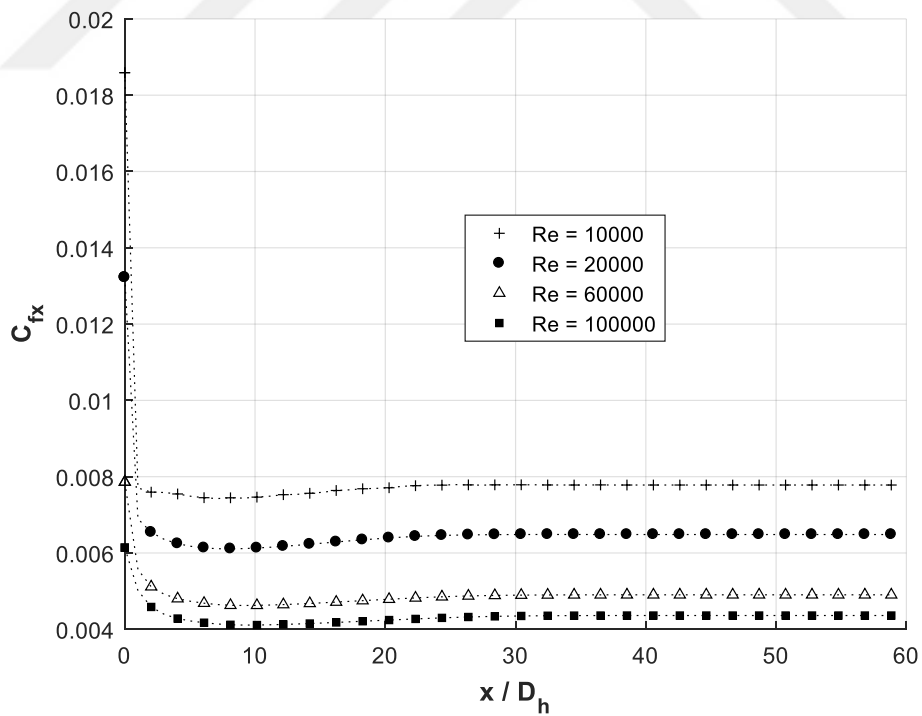
Figure 61. Change of Local Darcy Friction Factor with respect to Created Planes in the Simulation which is a/b=2.25
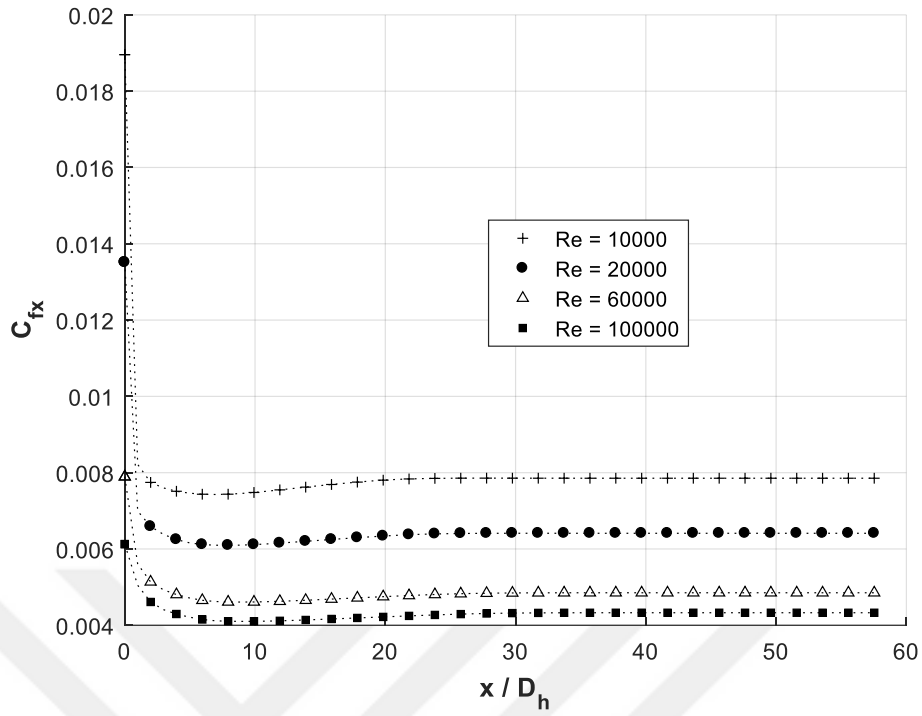
Figure 62. Change of Local Darcy Friction Factor with respect to Created Planes in the Simulation which is a/b=2.50
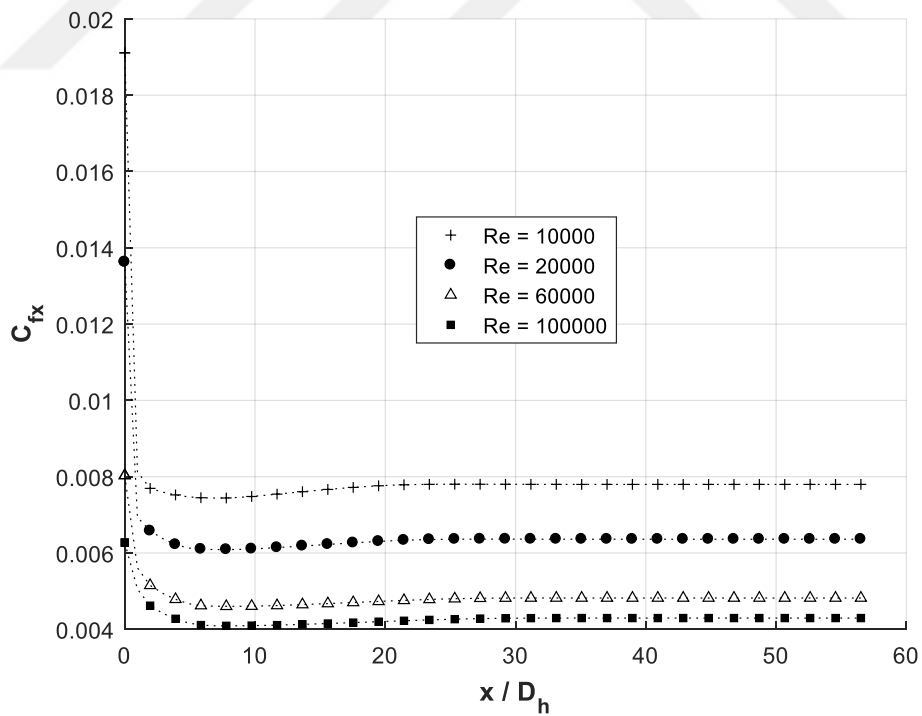
Figure 63. Change of Local Darcy Friction Factor with respect to Created Planes in the Simulation which is a/b=2.75
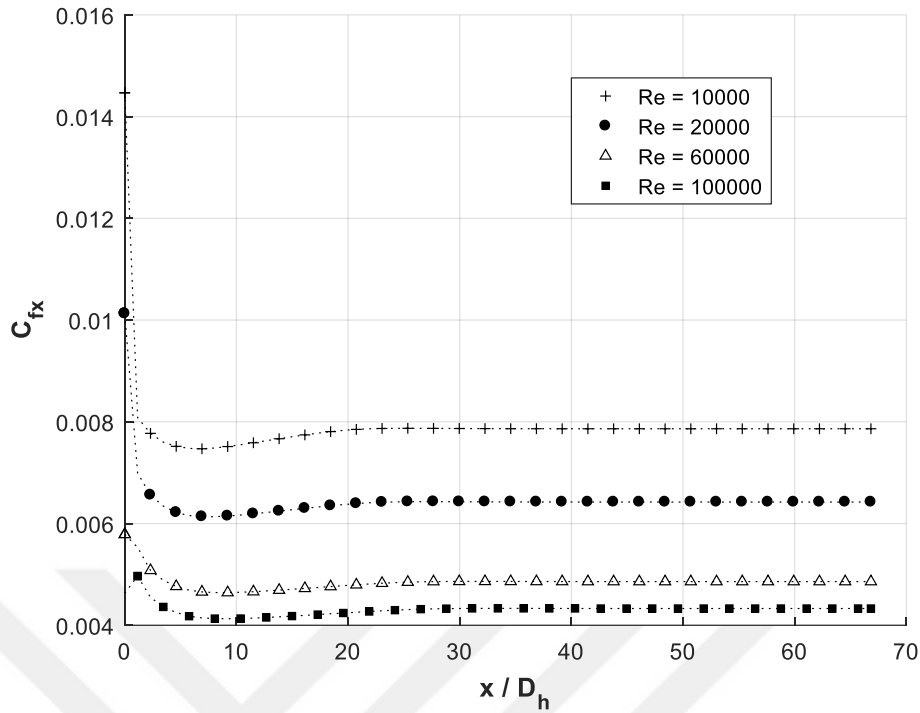
Figure 64. Change of Local Darcy Friction Factor with respect to Created Planes in the Simulation which is a/b=3.00

As seen in the Figure 60, Figure 61, Figure 62, Figure 63 and Figure 64 local Darcy friction factors in all cases are high as expected at the beginning of the tube. Also it is observed that local Darcy friction factors in high Reynolds Number are relatively low.

Also, local Darcy friction factors take almost constant values after certain locations in all cases. So it means that, after this certain location, hydrodynamically fully-developed condition is provided in the tube.

Velocity Profiles at Different Planes

Velocity profiles are examined in different planes along the tube. In that planes, x/D_h ratio is calculated as 10, 15, 20, 25 and 30. Velocity profiles are represented in Figure 65 - Figure 74for Re=10000 and Re=100000 at that planes.

90
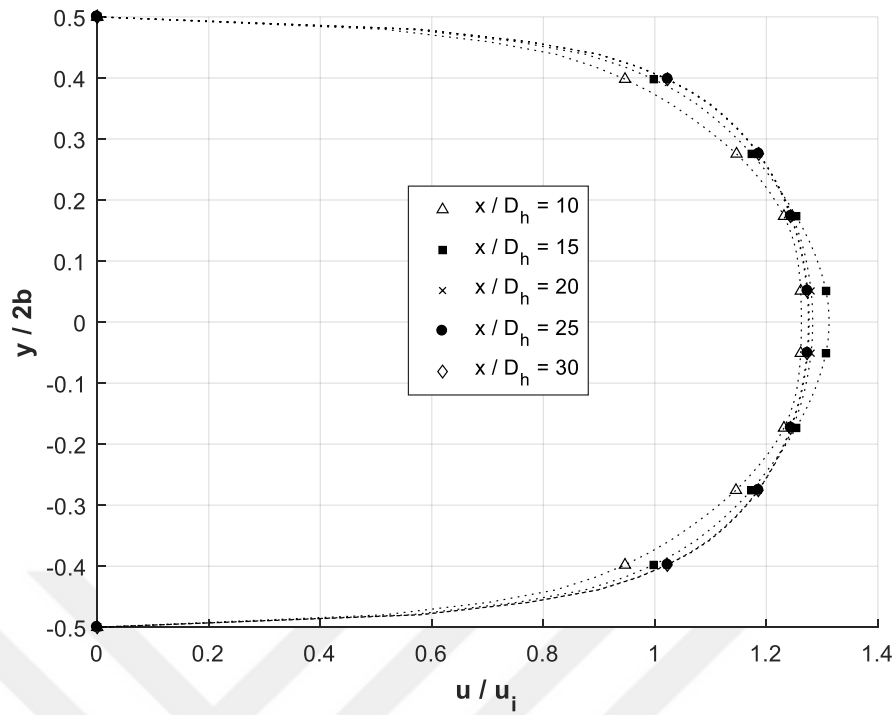
Figure 65. Change of Velocity Profile on Different Planes in the Simulation is which Reynolds Number in 10000 and a/b=2.00

Figure 66. Change of Velocity Profile on Different Planes in the Simulation is which Reynolds Number in 10000 and a/b=2.25

91
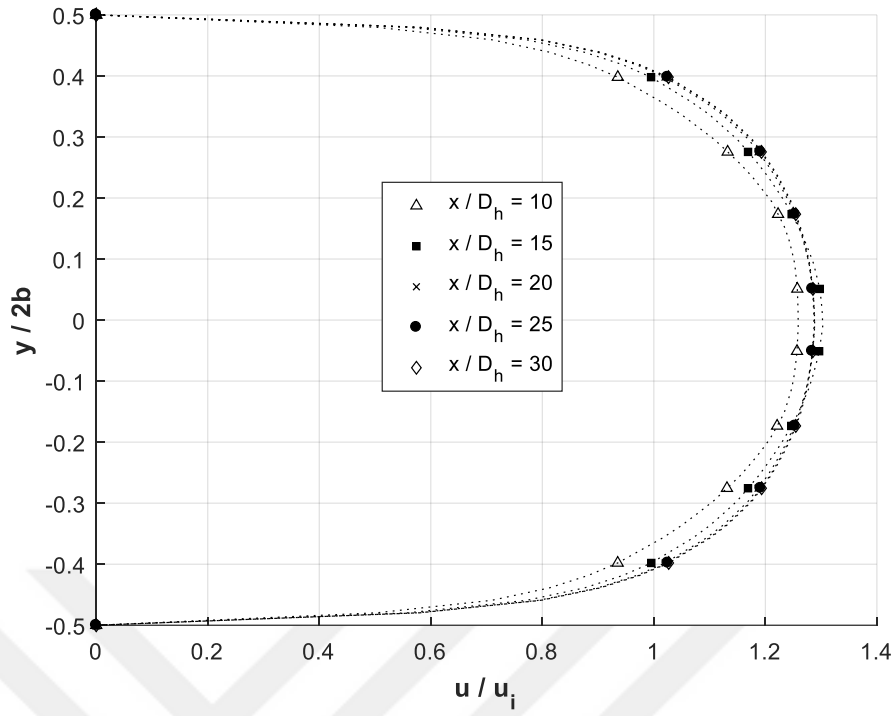
Figure 67. Change of Velocity Profile on Different Planes in the Simulation is which Reynolds Number in 10000 and a/b=2.50

Figure 68. Change of Velocity Profile on Different Planes in the Simulation is which Reynolds Number in 10000 and a/b=2.75
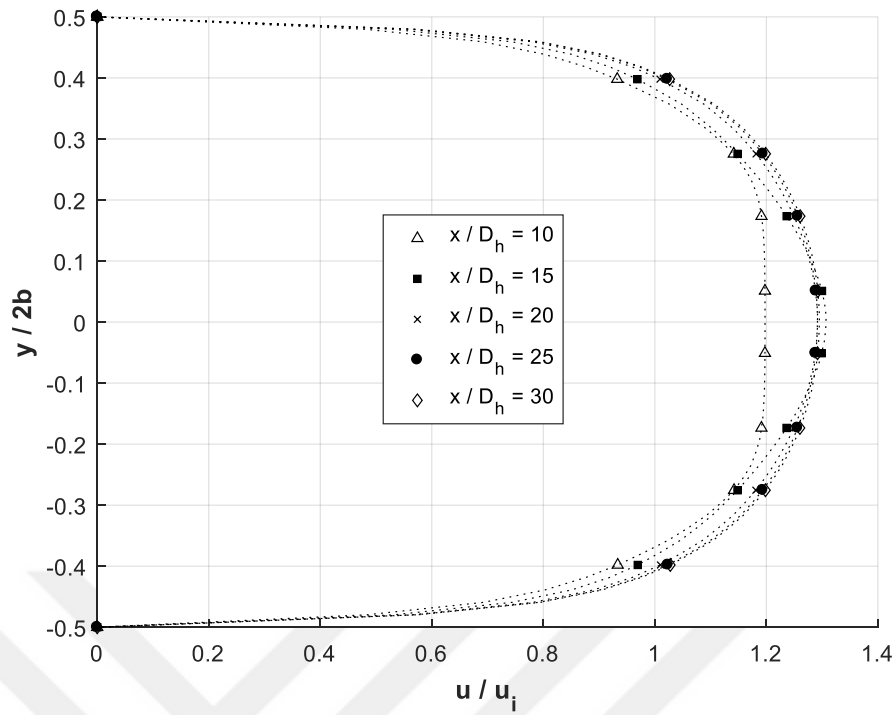
Figure 69. Change of Velocity Profile on Different Planes in the Simulation is which Reynolds Number in 10000 and a/b=3.00
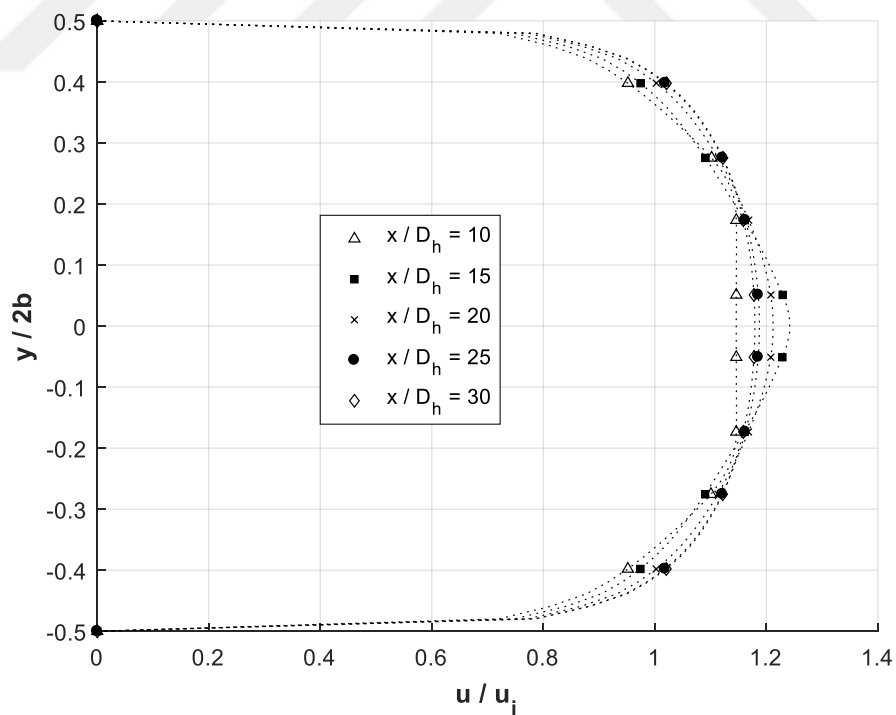
Figure 70. Change of Velocity Profile on Different Planes in the Simulation which is Reynolds Number in 100000 and a/b=2.00

93
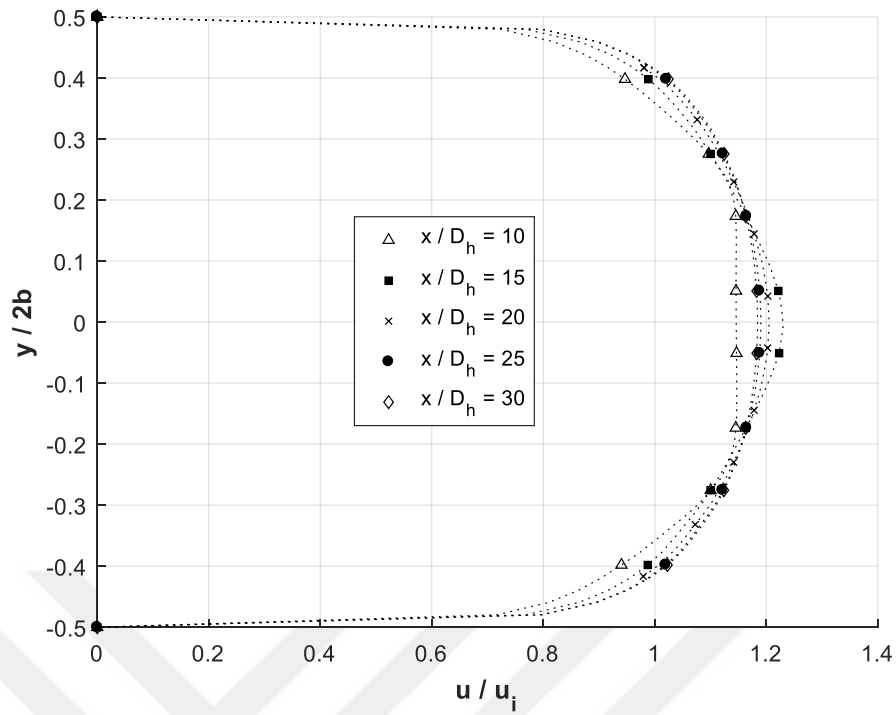
Figure 71. Change of Velocity Profile on Different Planes in the Simulation which is Reynolds Number in 100000 and a/b=2.25
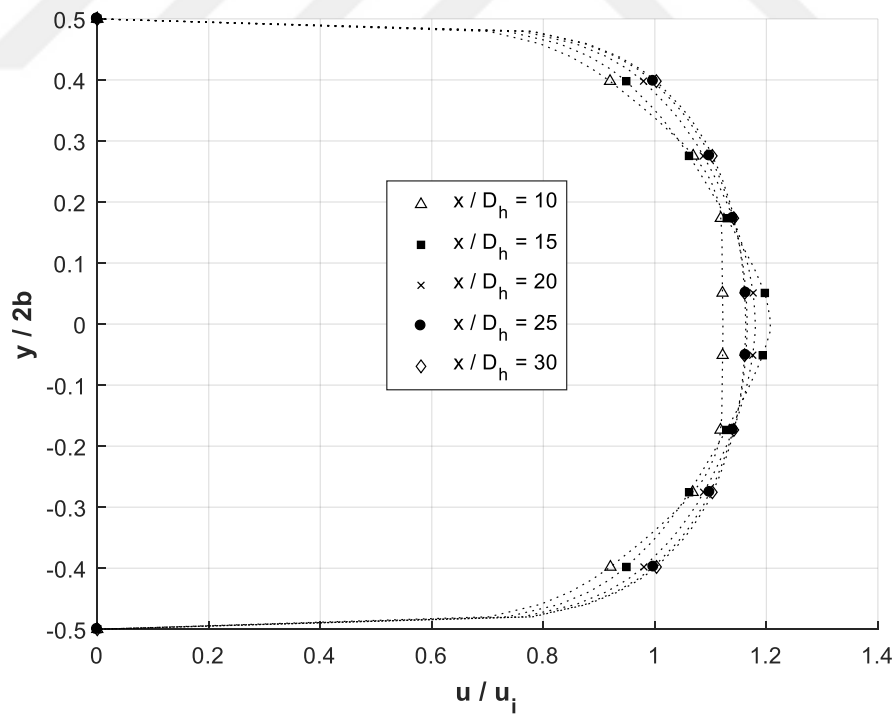
Figure 72. Change of Velocity Profile on Different Planes in the Simulation which is Reynolds Number in 100000 and a/b=2.50

94
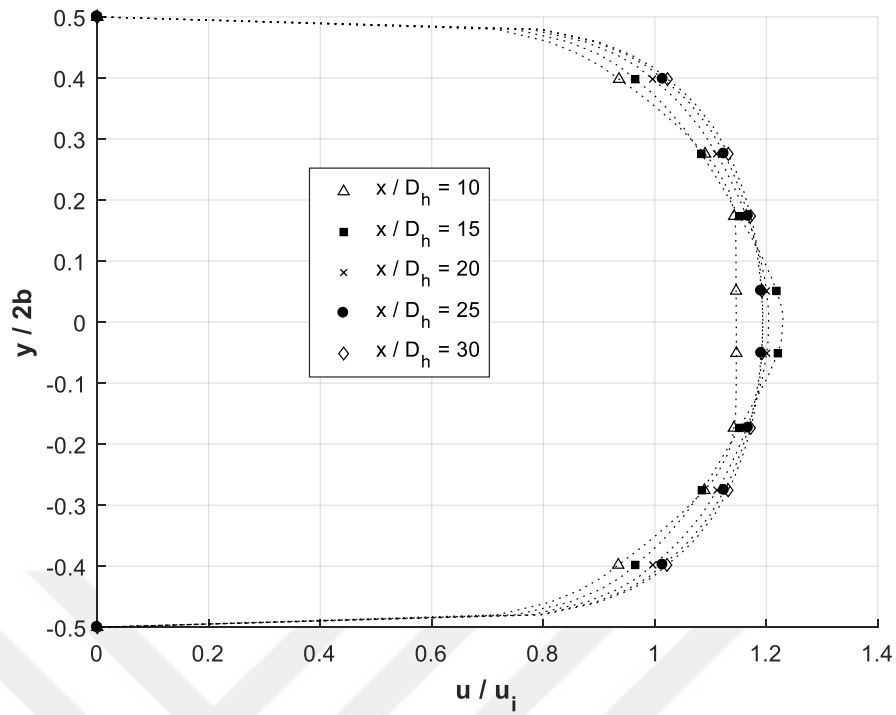
Figure 73. Change of Velocity Profile on Different Planes in the Simulation which is Reynolds Number in 100000 and a/b=2.75
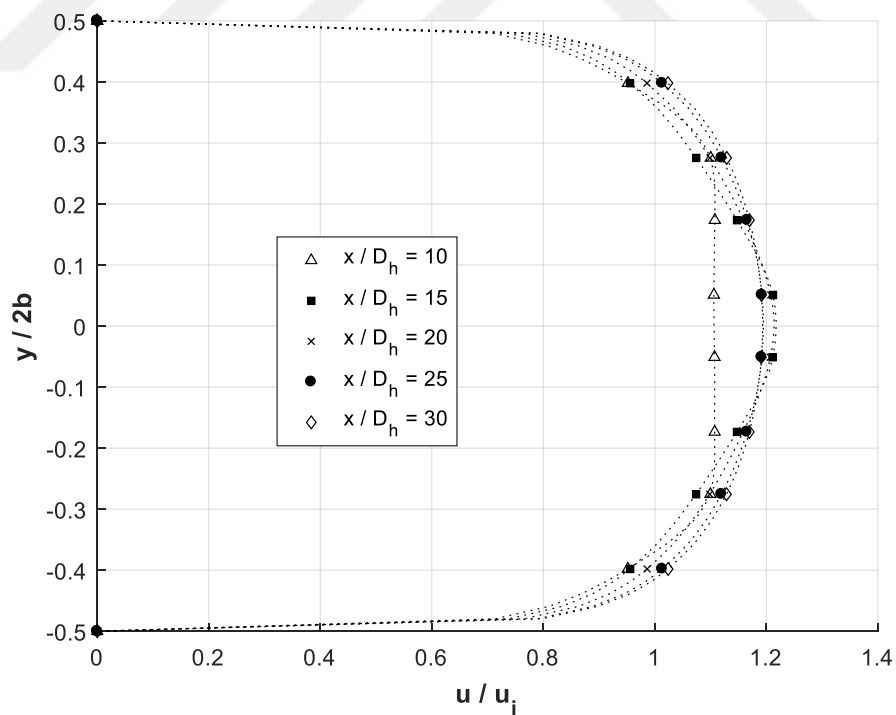
Figure 74. Change of Velocity Profile on Different Planes in the Simulation which is Reynolds Number in 100000 and a/b=3.00

As seen in the velocity profiles figures, velocity profiles do not change after certain locations. So it means that, after this certain location, hydrodynamically fully-developed condition is provided in the tube. Approximately, hydrodynamically fully-developed conditions are provided at $x/D_h = 20$ in Re=10000 and $x/D_h = 25$ in Re=100000. So, velocity develops faster in low Reynolds number.

Dimensionless Temperatures at Different Planes

Dimensionless temperatures are examined in different planes along the tube. In that planes, x/D_h ratio is calculated as 10, 20, 40, 45 and 50. Dimensionless temperatures are represented in Figure 75 - Figure 84 for Re=10000 and Re=100000 at that planes.
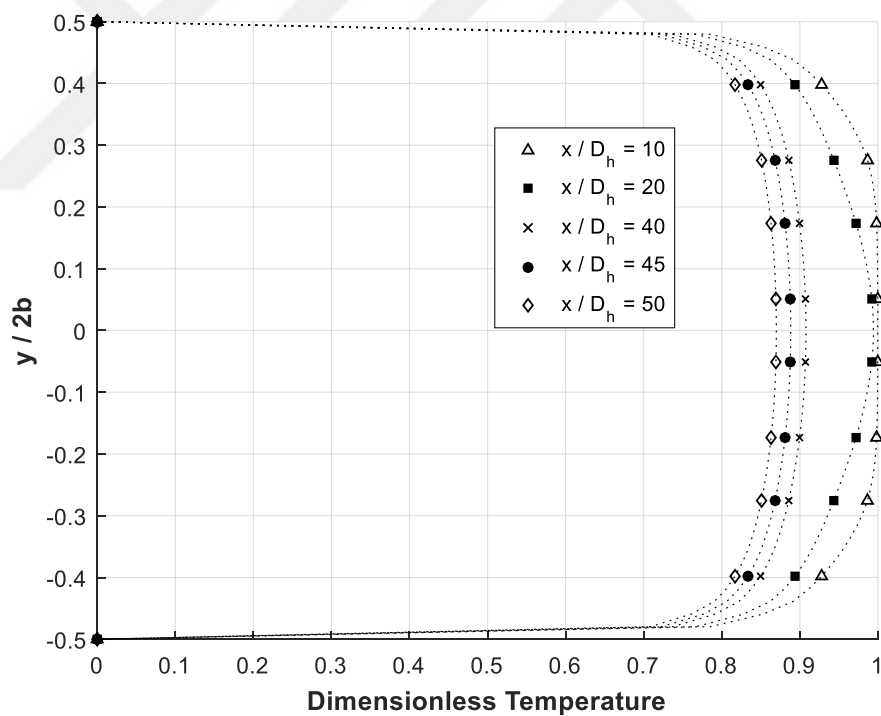
Figure 75. Change of Dimensionless Temperature Profile on Different Planes in the Simulation is which Reynolds Number in 10000 and a/b=2.00

96
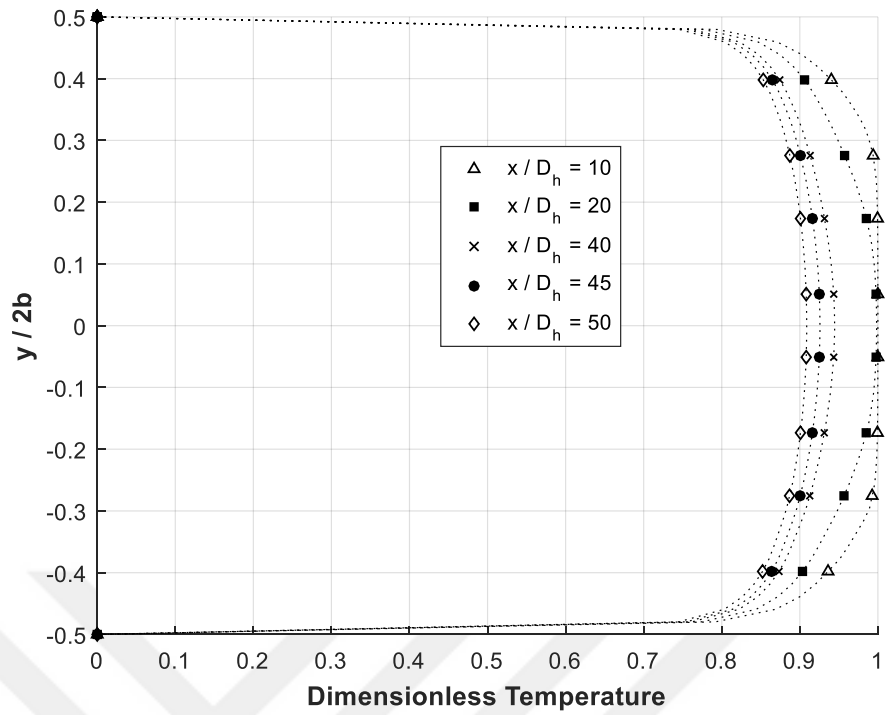
Figure 76. Change of Dimensionless Temperature Profile on Different Planes in the Simulation is which Reynolds Number in 10000 and a/b=2.25
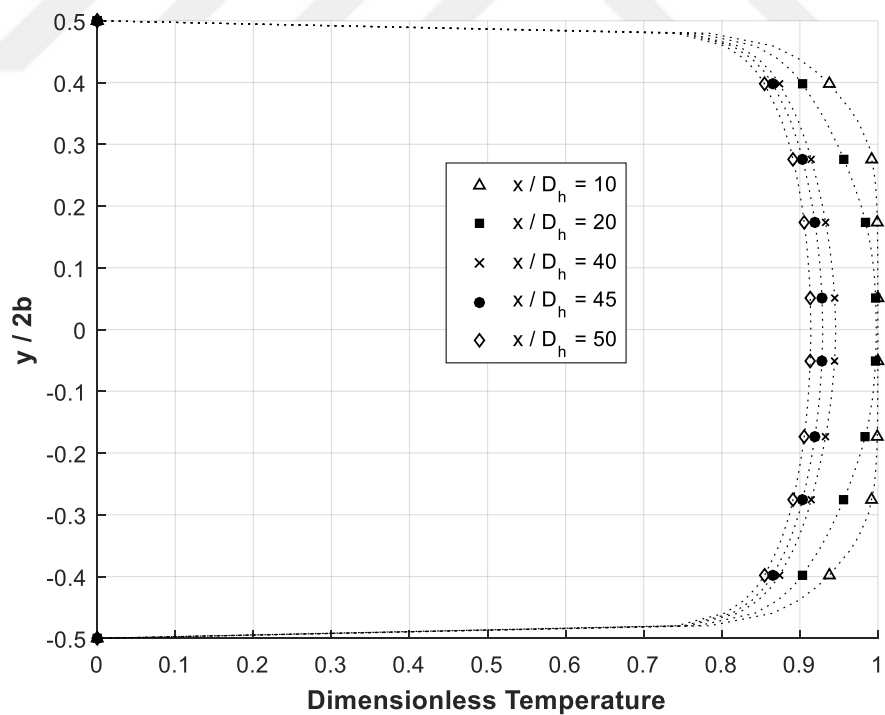
Figure 77. Change of Dimensionless Temperature Profile on Different Planes in the Simulation is which Reynolds Number in 10000 and a/b=2.50
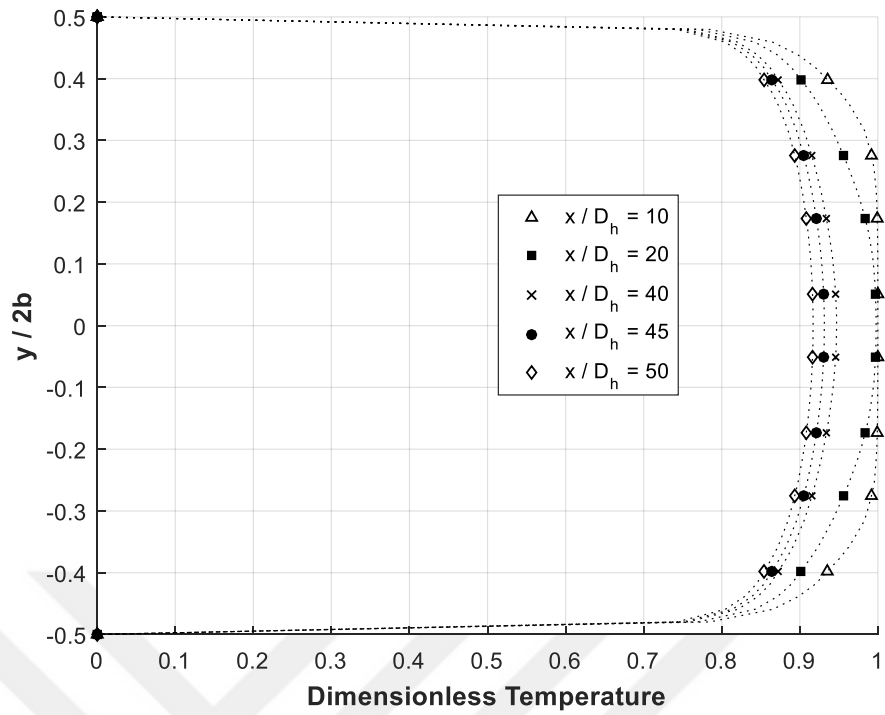
Figure 78. Change of Dimensionless Temperature Profile on Different Planes in the Simulation is which Reynolds Number in 10000 and a/b=2.75
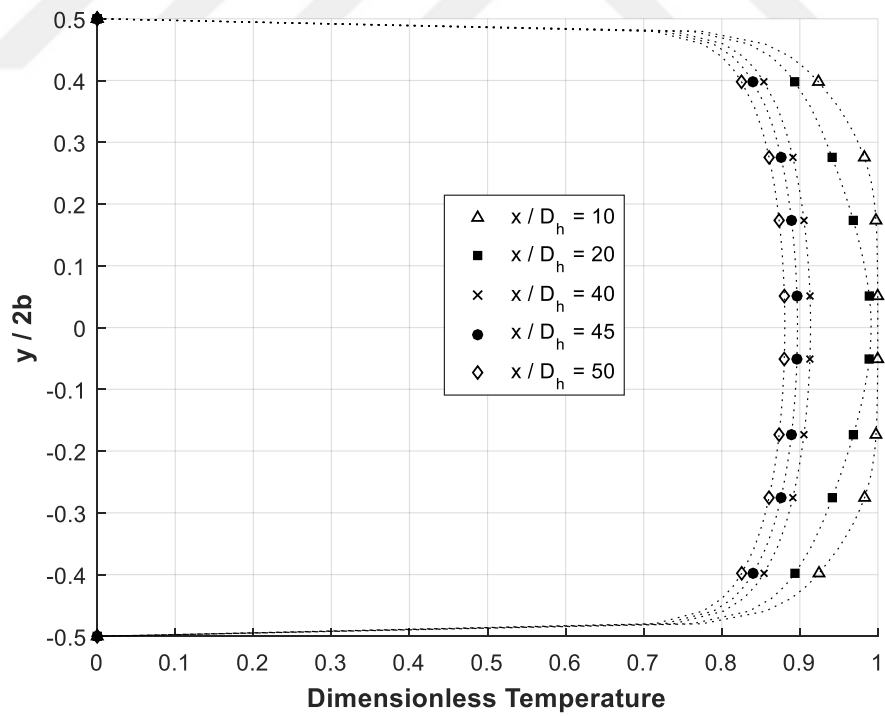
Figure 79. Change of Dimensionless Temperature Profile on Different Planes in the Simulation is which Reynolds Number in 10000 and a/b=3.00
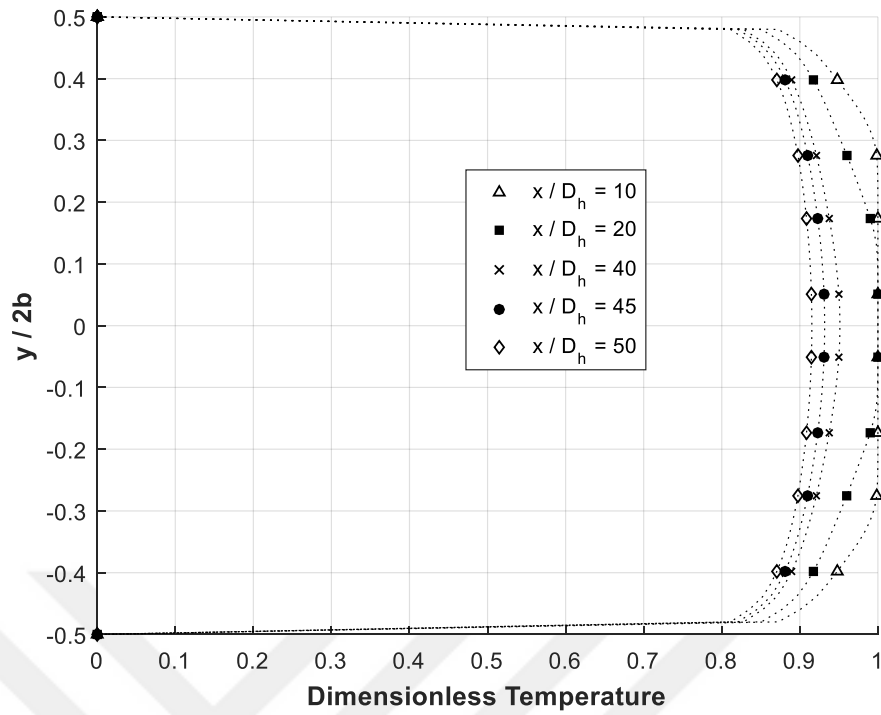
*Figure 80. Change of Dimensionless Temperature Profile on Different Planes in the Simulation is which Reynolds Number in 100000 and a/b=2.00*
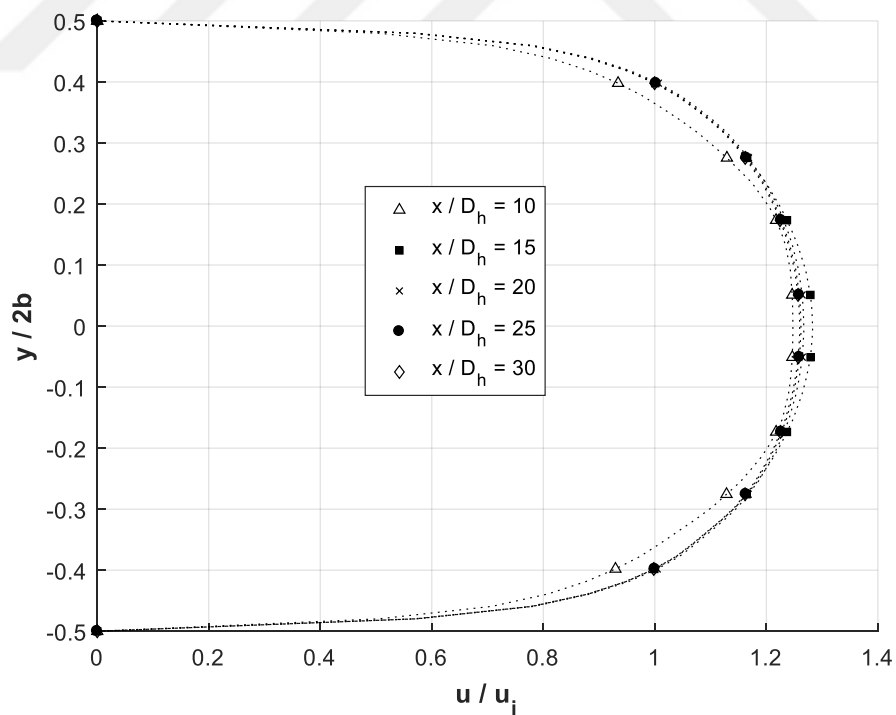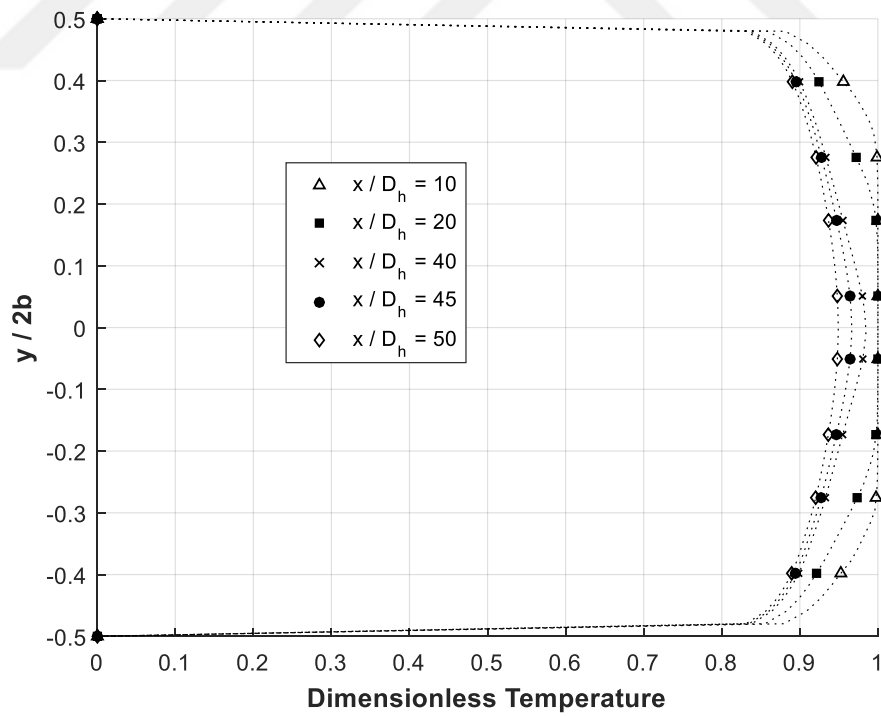

Figure 81. Change of Dimensionless Temperature Profile on Different Planes in the Simulation is which Reynolds Number in 100000 and a/b=2.25
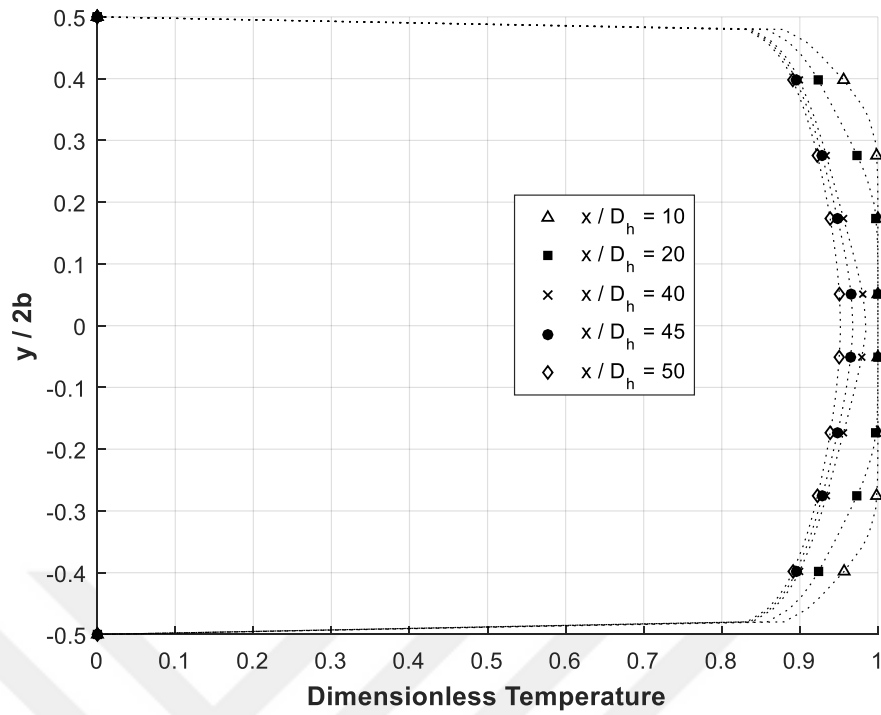
Figure 82. Change of Dimensionless Temperature Profile on Different Planes in the Simulation is which Reynolds Number in 100000 and a/b=2.50

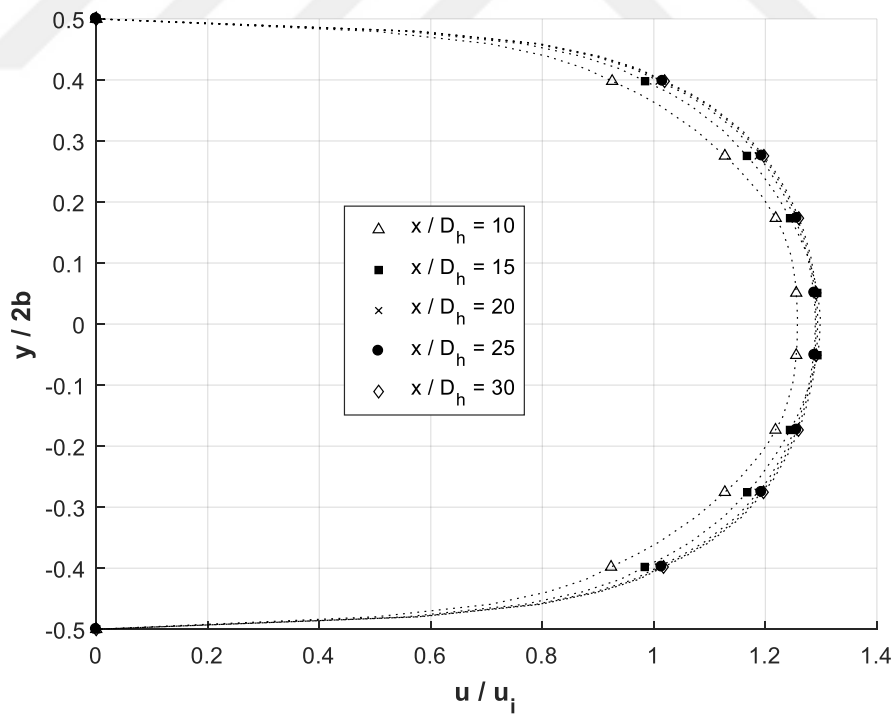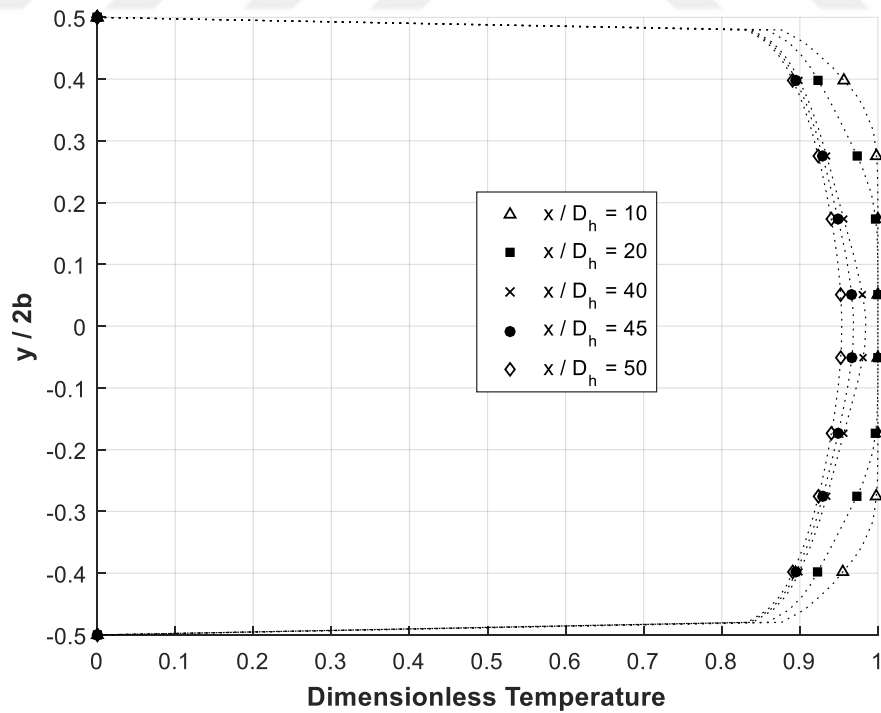*Figure 83. Change of Dimensionless Temperature Profile on Different Planes in the Simulation is which Reynolds Number in 100000 and a/b=2.75*
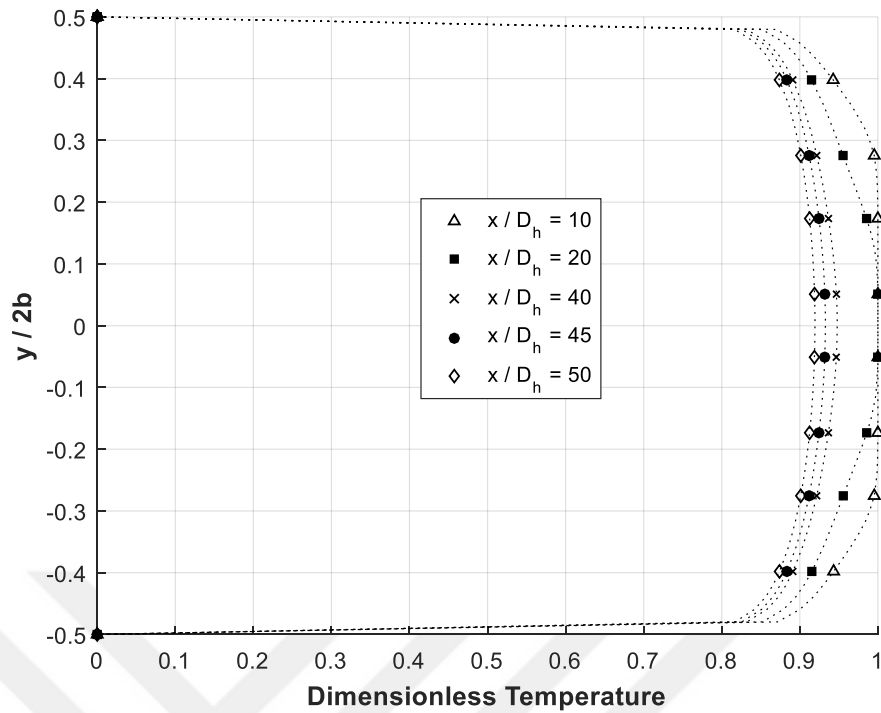
Figure 84. Change of Dimensionless Temperature Profile on Different Planes in the Simulation is which Reynolds Number in 100000 and a/b=3.00

According to the dimensionless temperature definition, it is expected that the dimensionless temperature values in the entrance region should be close to one. In addition, it is expected that the dimensionless temperature values decrease as the fluid moves along the channel.

6.2.2. Results of Hydrodynamically and Thermally Fully Developed Region

In this part average Nusselt numbers and average Darcy friction factors were examined.

<u>Average Nusselt Number</u>

The plots of average Nusselt number with respect to Reynolds number are showed in Figure 85 - Figure 89. Also they were compared with Maiga and Velagapudi et al. correlations which are more suitable than Dittus-Boelter and Gnielinski correlations for nanofluids. [3]

$$\overline{Nu_{nf}} = 0.085 Re_{nf}^{0.71} \text{Pr}_{nf}^{0.35} \qquad \text{Maiga et al.} \qquad 6.1$$

$$\overline{Nu_{nf}} = 0.0256 Re_{nf}^{0.8} \text{Pr}_{nf}^{0.4} \qquad \text{Velagapudi et al.} \qquad 6.2$$
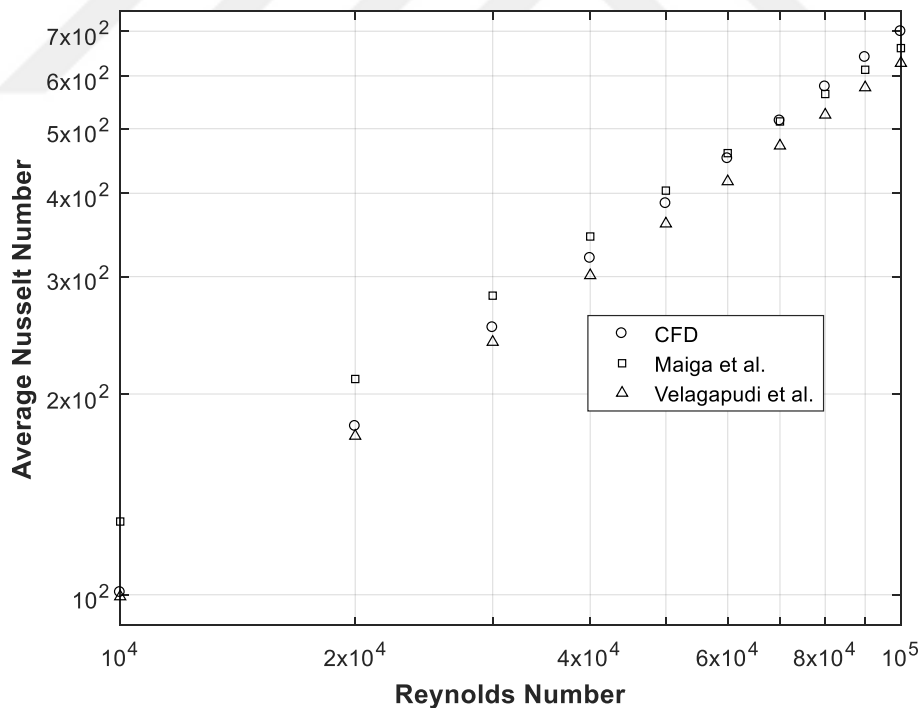
Figure 85. Change of Average Nusselt Number with respect to Reynolds Number in the Simulation which is a/b=2.00
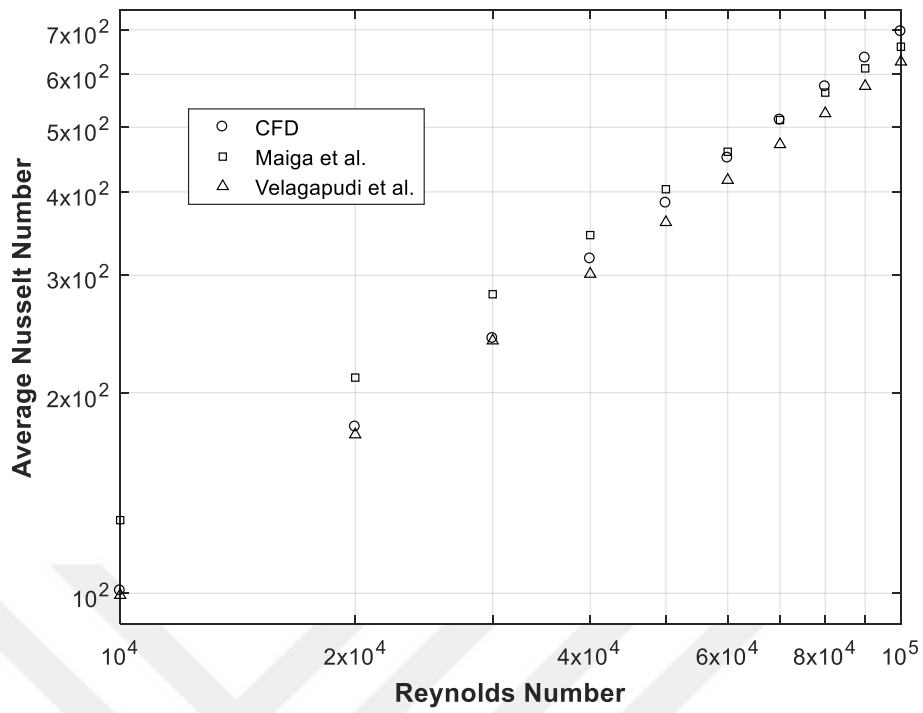
Figure 86. Change of Average Nusselt Number with respect to Reynolds Number in the Simulation which is a/b=2.25
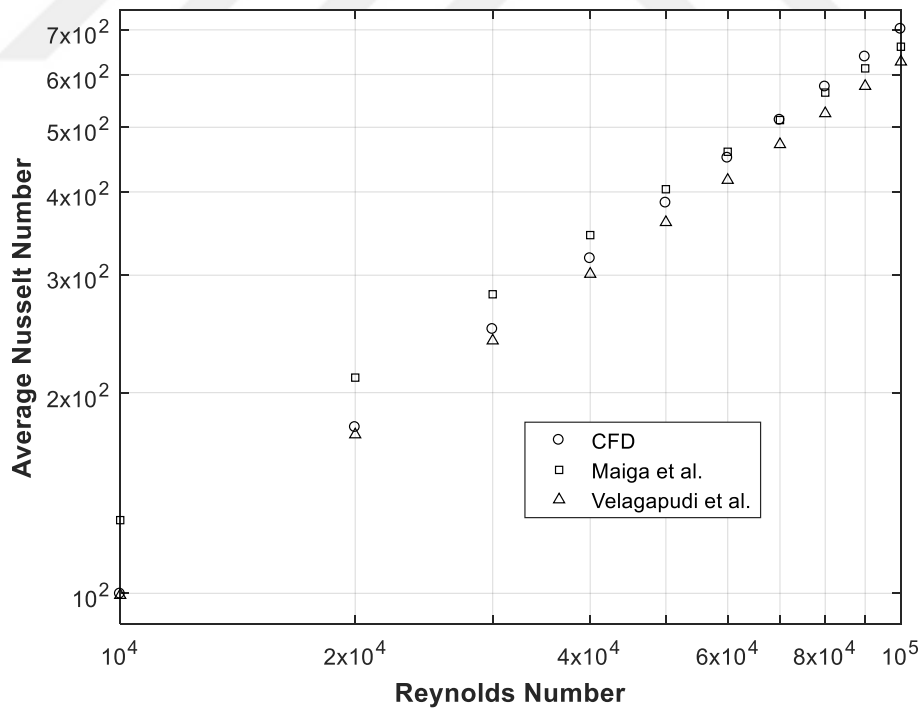
Figure 87. Change of Average Nusselt Number with respect to Reynolds Number in the Simulation which is a/b=2.50
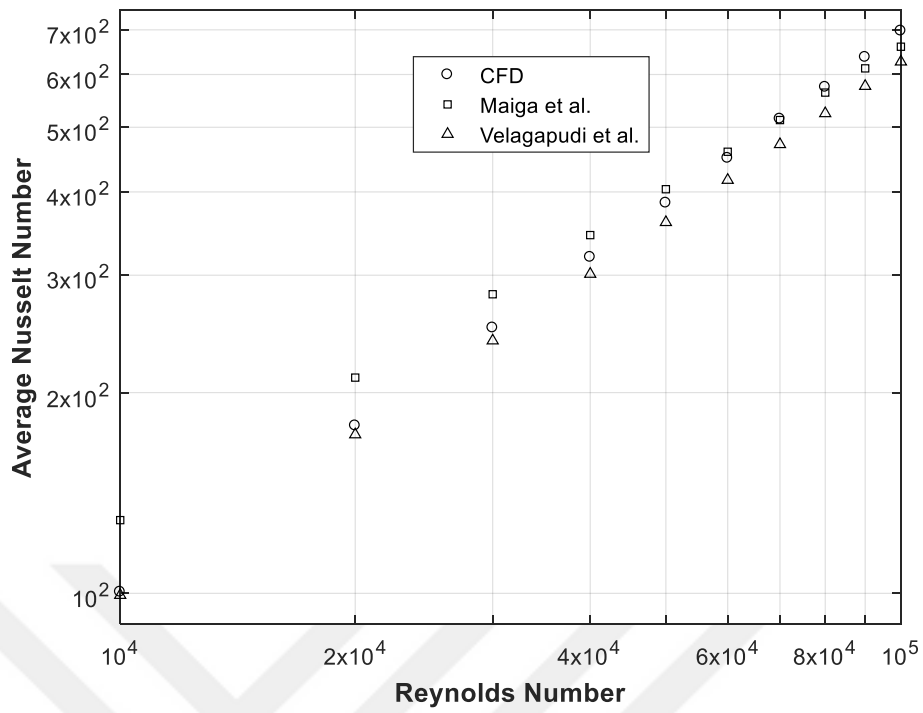
Figure 88. Change of Average Nusselt Number with respect to Reynolds Number in the Simulation which is a/b=2.75
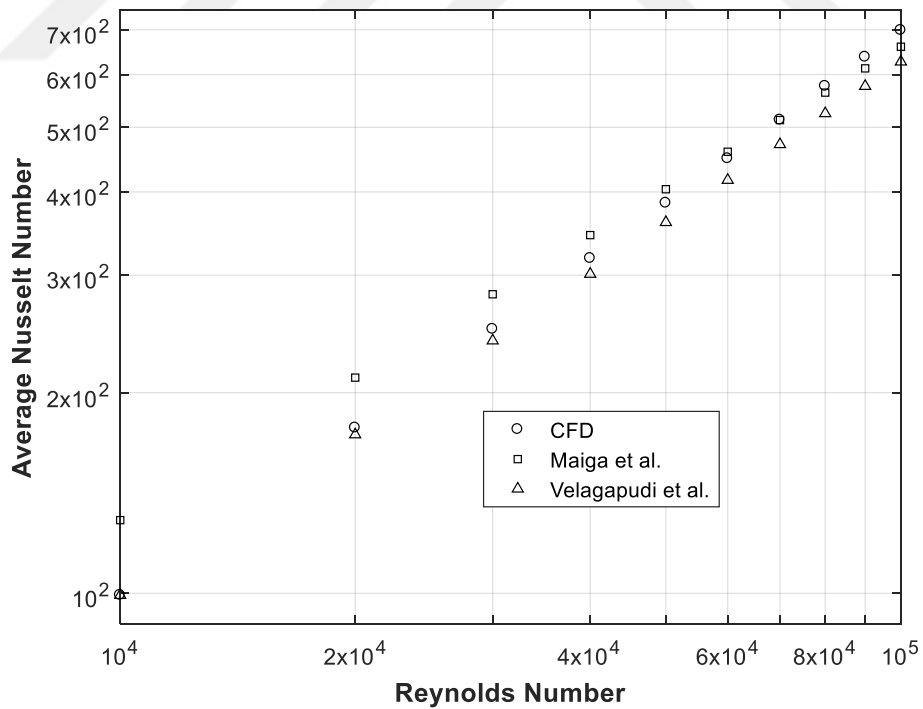
Figure 89. Change of Average Nusselt Number with respect to Reynolds Number in the Simulation which is a/b=3.00

104

The figures were plotted as logarithmic form. As seen in the Figure 85 - Figure 89, when Reynolds number increases, average Nusselt number increases. It is noticed that the results are similar when it is compared with the correlations in literature.

When Reynolds number increases, flow becomes more turbulent. As a result of this, high heat transfer coefficient and high thermal performance is obtained.

Table 6. Comparison of Average Nusselt Number with Correlations

		CFD	Maiga	Velagapudi
a / b = 2.00	Re=20000	178.9	210.6	173.0
	Re=60000	450.9	459.5	416.6
	Re=100000	699.2	660.3	626.9
a / b = 2.25	Re=20000	177.6	210.6	173.0
	Re=60000	449.6	459.5	416.6
	Re=100000	695.9	660.3	626.9
a / b = 2.50	Re=20000	177.3	210.6	173.0
	Re=60000	449.5	459.5	416.6
	Re=100000	701.6	660.3	626.9
a / b = 2.75	Re=20000	178.3	210.6	173.0
	Re=60000	449.3	459.5	416.6
	Re=100000	697.3	660.3	626.9
a / b = 3.00	Re=20000	177.0	210.6	173.0
	Re=60000	448.7	459.5	416.6
	Re=100000	698.9	660.3	626.9

The results of CFD are compared with correlations available in literature, and there is a good agreement with average deviation 8% with Maiga and 7% with Velagapudi.

Average Darcy Friction Factor

Average Darcy friction factors with respect to Reynolds number are shown in Figure 90 - Figure 94. Also they were compared with Petukhov correlation which is most commonly used in literature.

$$f = (0.790 \ln Re_D - 1.64)^{-2} \qquad \text{Petukhov} \qquad 6.3$$
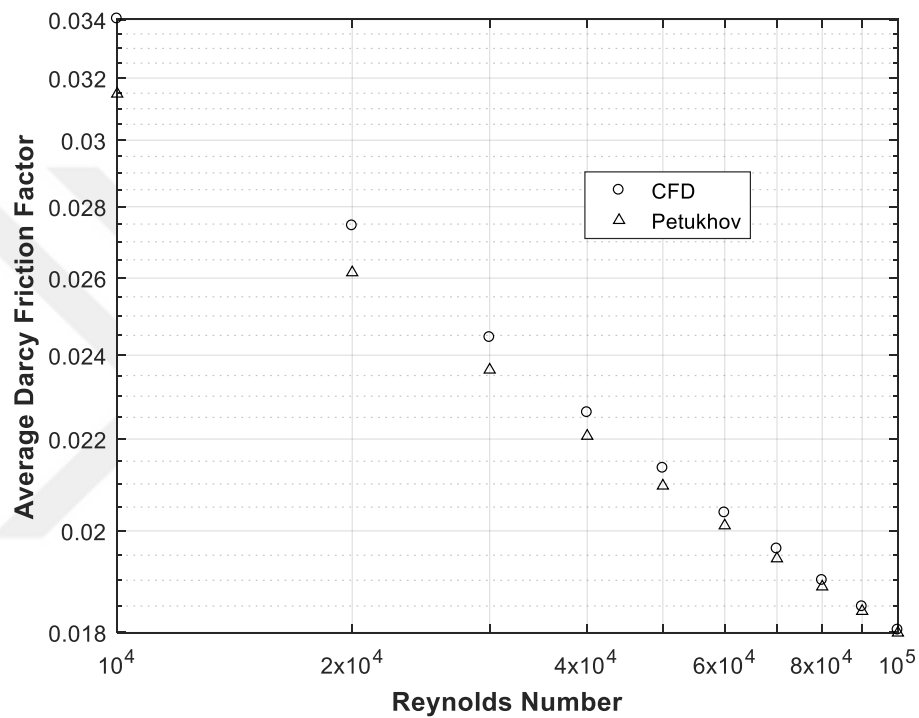
Figure 90. Change of Average Darcy Friction Factor with respect to Reynolds Number in the Simulation which is a/b=2.00
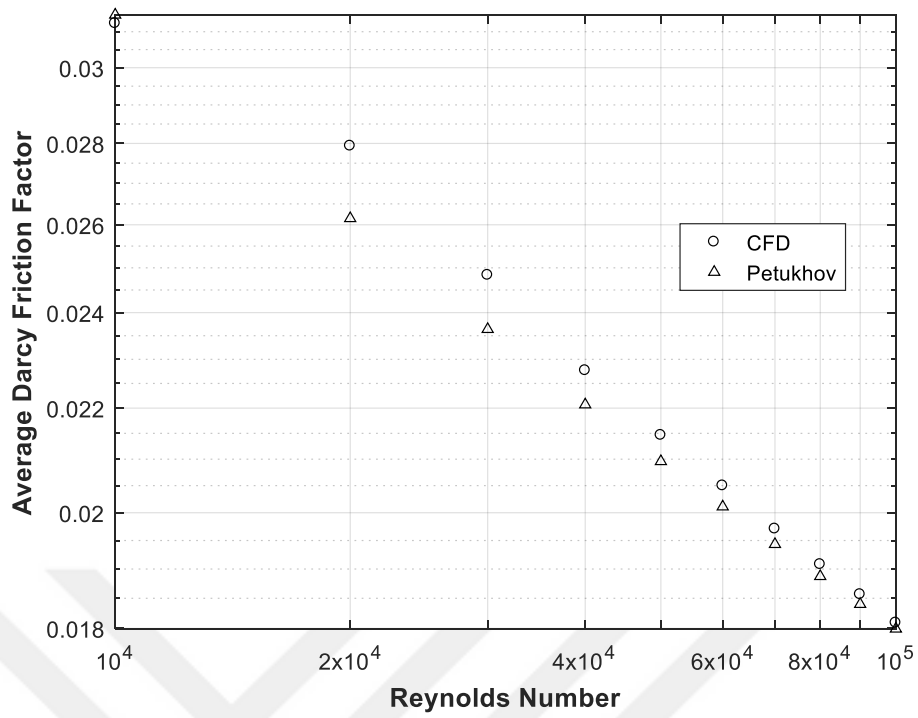
Figure 91. Change of Average Darcy Friction Factor with respect to Reynolds Number in the Simulation which is a/b=2.25
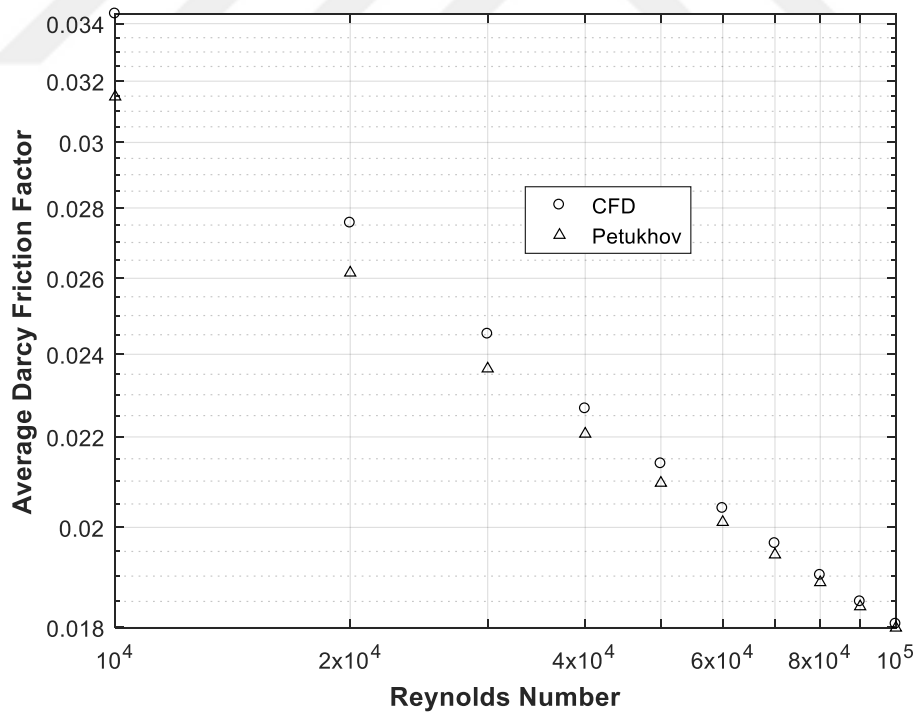
Figure 92. Change of Average Darcy Friction Factor with respect to Reynolds Number in the Simulation which is a/b=2.50
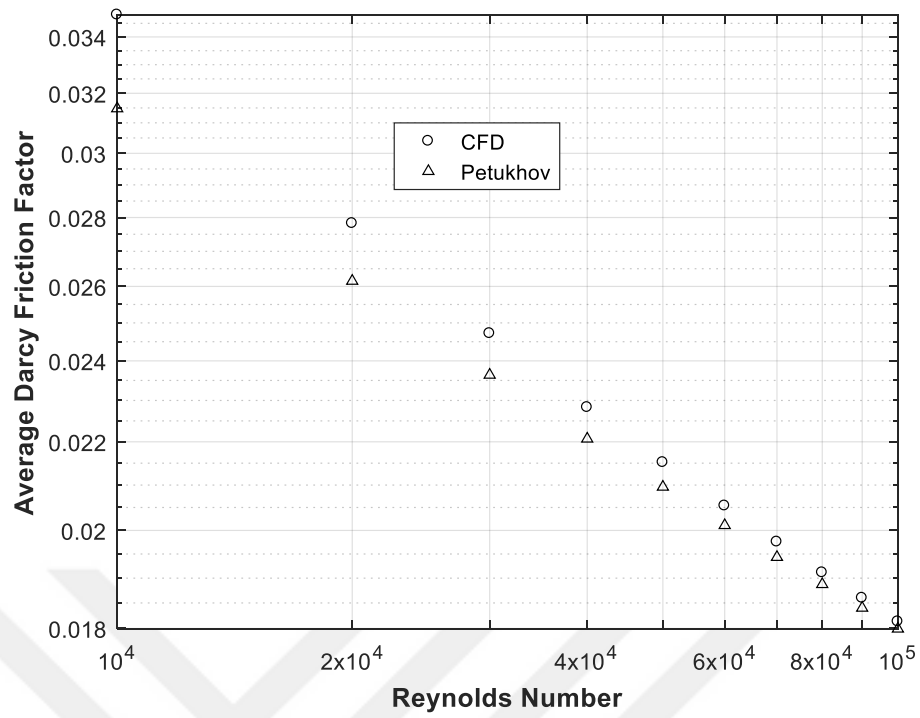
Figure 93. Change of Average Darcy Friction Factor with respect to Reynolds Number in the Simulation which is a/b=2.75
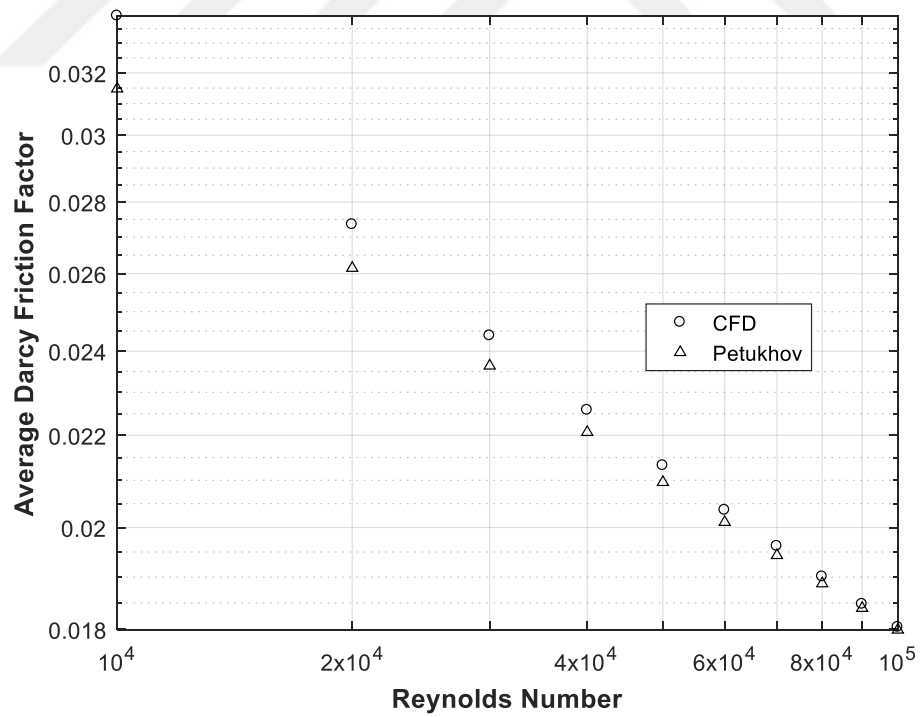
Figure 94. Change of Average Darcy Friction Factor with respect to Reynolds Number in the Simulation which is a/b=3.00

The figures were plotted as logarithmic form. As seen in the Figure 90 - Figure 94, when Reynolds number increases, average Darcy friction factor decreases. It is noticed that the results are similar when it is compared with Petukhov correlation in literature.

Table 7. Comparison of Average Darcy Friction Factor with Correlation

		CFD	Petukhov
	Re=20000	0.0275	0.0262
a / b = 2.00	Re=60000	0.0204	0.0201
	Re=100000	0.0180	0.0180
	Re=20000	0.0279	0.0262
a / b = 2.25	Re=60000	0.0205	0.0201
	Re=100000	0.0181	0.0180
	Re=20000	0.0276	0.0262
a / b = 2.50	Re=60000	0.0204	0.0201
	Re=100000	0.0181	0.0180
	Re=20000	0.0278	0.0262
a / b = 2.75	Re=60000	0.0205	0.0201
	Re=100000	0.0181	0.0180
	Re=20000	0.0274	0.0262
a / b = 3.00	Re=60000	0.0204	0.0201
	Re=100000	0.0180	0.0180

The results of CFD are compared with correlation available in literature, and there is a good agreement with average deviation 3%

According to results of simulations, the correlations for average Nusselt number and average Darcy friction factor are developed by using MATLAB curve fitting toolbox. Correlations in the form of $Nu = a_1 \times Re^{b_1}$ and $f = a_2 \times Re^{b_2}$ are developed for average Nusselt numbers and average friction factors in all models.

Table 8. Correlation Constants for Nanofluid Cases

a / b	a_1	b_1	a_2	b_2
2.00	0.039	0.850	0.437	-0.278
2.25	0.036	0.856	0.402	-0.244
2.50	0.036	0.857	0.457	-0.282
2.75	0.039	0.849	0.480	-0.286
3.00	0.036	0.855	0.431	-0.277

6.3.   Comparison of Geometric Shape of the Tubes

In this part of study, 5 different elliptic tube model is which major to minor axis ratios are 2.00, 2.25, 2.50, 2.75 and 3.00 were compared to determine which model is better in terms of heat transfer applications. To do this, average Nusselt numbers, average Darcy friction factors were examined for both water and nanofluid cases. In addition, the points where the flow is thermally and hydrodynamically fully developed are specified.

Average Nusselt Numbers

Average Nusselt numbers are given at specific Reynolds numbers for both water and nanofluid cases in the Table 3 and Table 6, respectively. As seen in the tables, average Nusselt numbers do not change with major to minor axis ratio significantly. In addition, average Nusselt numbers are higher in nanofluid cases as expected.

Average Friction Factors

Average Darcy friction factor is given at specific Reynolds numbers for both water and nanofluid cases in the Table *4* and Table *7*. As seen in the tables, average Darcy friction factors do not change with major to minor axis ratio significantly. Average friction factors in nanofluid cases are higher.

Hydrodynamic and Thermal Entrance

Hydrodynamic and thermal entrance lengths over hydraulic diameters is given at specific Reynolds numbers for both water and nanofluid cases. According to the results, hydrodynamic and thermal entrance lengths over hydraulic diameters ($x_{fd,h}/D_h \ and \ x_{fd,t}/D_h$) do not change with major to minor axis ratio significantly. The point where the fluid becomes hydrodynamically and thermally developed is farther away in nanofluid cases because of effect of viscosity.

Correlations between Re-Nu and Re-f for all models

The correlation for average Nusselt number and average Friction factor coefficient for five different elliptic channel in the range of $10000 \leq Re \leq 100000$ are tabulated in Table 5 and Table 8 for both water and nanofluid cases, respectively. According to the results, a_1, b_1, a_2, b_2 do not change with major to minor axis ratio significantly.

6.4.   Comparison of Water and Nanofluid

In this chapter, average Nusselt number and average Darcy friction factor parameters compared for base water and nanofluid with Al_2O_3 in order to understand the effect of use of nanofluid on heat transfer and pressure drop. To comparison, average Nusselt number with respect to Reynolds number for different a/b ratios is showed in Table 9. Due to small change in average Nusselt numbers with respect to a/b ratios, only a/b=2.00 ratio figure was plotted. As seen in the Figure 95 and Table 9, average Nusselt number is increased by using nanofluid. So heat transfer is enhanced significantly. To comparison, average Darcy friction factor with respect to Reynolds number for different a/b ratios is showed in Table 10. Due to small change in average Darcy friction factor according to different a/b ratios, only a/b=2.00 ratio figure was plotted. As seen in the Figure 96 and Table 10, average Darcy friction factor is increased by using nanofluid. So more pump power is required to obtain same Reynolds number in the tube.

Table 9. Average Nusselt Numbers at specified Reynolds Numbers for different a/b ratios and Base Water and Nanofluid

a/b Ratios	Reynolds Number 20000		Reynolds Number 60000		Reynolds Number 100000	
	Water	Nanofluid	Water	Nanofluid	Water	Nanofluid
2.00	161.3	179.3	403.3	450.9	623.4	700.4
2.25	160.6	177.5	403.3	449.1	623.2	696.6
2.50	159.8	177.4	401.6	448.7	623.8	700.0
2.75	160.5	178.4	402.6	450.2	622.5	698.3
3.00	160.2	177.2	400.0	448.8	620.8	699.5
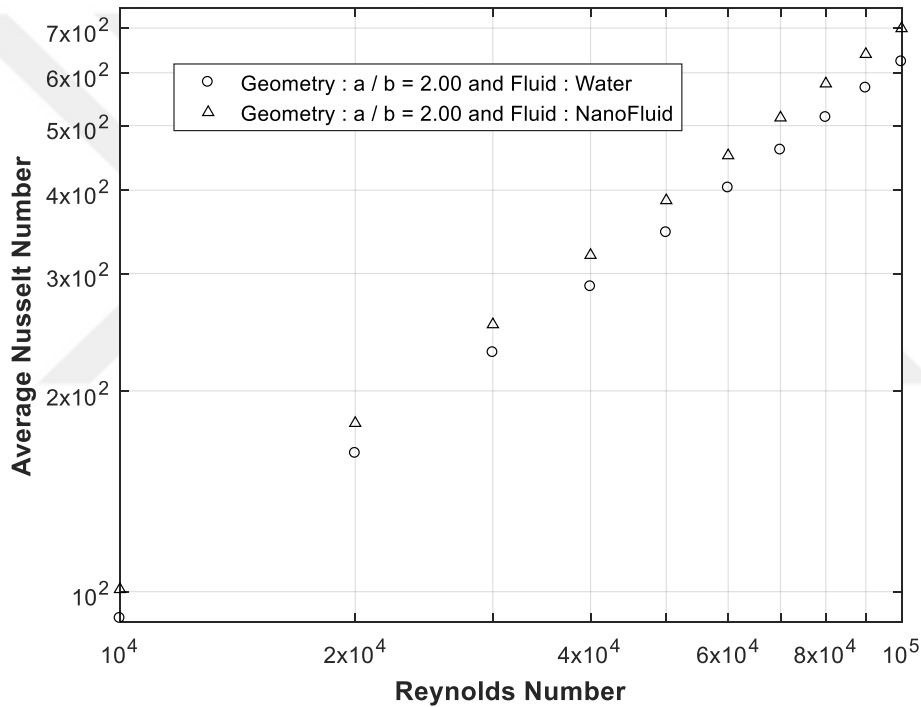
Figure 95. Comparison of Average Nusselt Numbers in both working fluid for a/b=2.00

Table 10. Average Darcy Friction Factor at specified Reynolds Numbers for different a/b ratios and Base Water and Nanofluid

a/b Ratios	Reynolds Number 20000		Reynolds Number 60000		Reynolds Number 100000	
	Water	Nanofluid	Water	Nanofluid	Water	Nanofluid
2.00	0.0266	0.0275	0.0199	0.0204	0.0177	0.0180
2.25	0.0265	0.0279	0.0199	0.0205	0.0176	0.0181
2.50	0.0269	0.0276	0.0202	0.0204	0.0179	0.0181
2.75	0.0268	0.0278	0.0201	0.0205	0.0179	0.0181
3.00	0.0277	0.0274	0.0204	0.0204	0.0180	0.0180
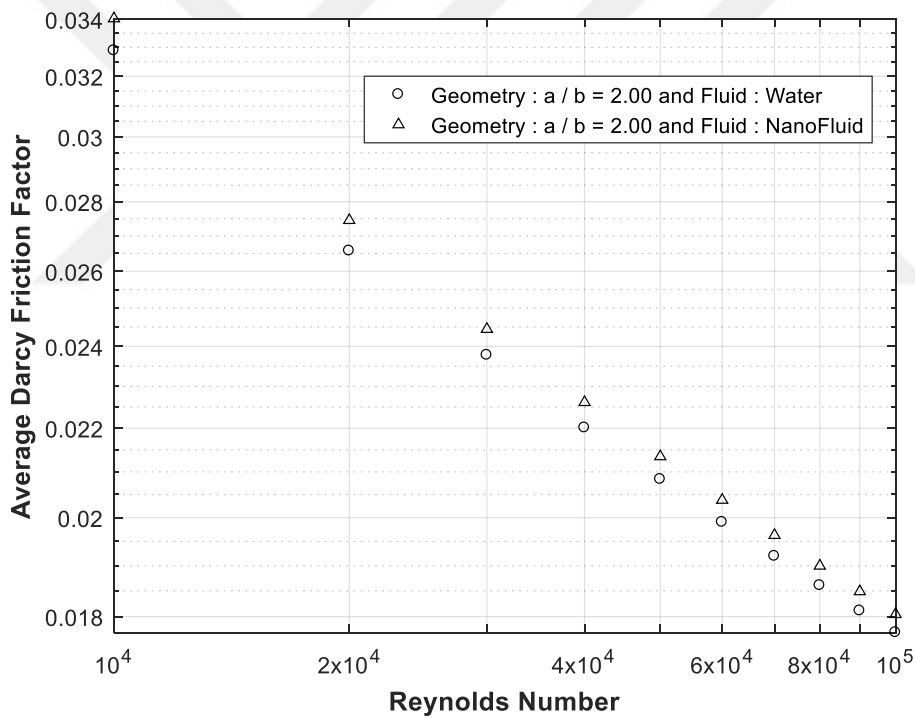
Figure 96. Comparison of Average Darcy Friction Factors in both working fluid for a/b=2.00

114

Effectiveness of Water and Nanofluid

In channel designing for heat transfer applications, average Nusselt number should be maximized and friction factor should be minimized as much as possible. So, ratio of these two parameters make sense to decide which working fluid is better. To compare, function of average Nusselt number to average friction factor was examined. Effectiveness parameter can be used for this purpose and it is defined as η: [13], [19]

$$\eta = \frac{Nu_m/Nu_{mo}}{[f_m/f_{mo}]^{1/3}} \qquad\qquad 6.4$$

As seen in the equation 6.4, heat transfer and pressure drop are defined as dimensionless form and in terms of average Nusselt number and average Darcy friction factor. In this equation, Nu_m and f_m belongs to nanofluid cases and Nu_{mo} and f_{mo} belongs to water cases.

As seen in the Figure 97, value of η always higher than unity as expected. Also, when flow is more turbulent, value of η is increasing. As a result, use of nanofluid in heat transfer applications is crucial, especially in turbulent flow. With nanofluids, less pump power is required to obtain same amount of heat transfer rate. Moreover, effect of nanofluid in a/b=3.00 is highest. The results show that the use of nanofluids provide an improvement of approximately 11% in heat transfer applications.

Figure 97. Effectiveness of Water and Nanofluid

7.   CONCLUSION AND DISCUSSION

In this study, numerical analysis of convective heat transfer with turbulent flow under constant temperature boundary conditions in elliptical cross-section channel with different aspect ratios was performed by using ANSYS Fluent 17.0 software. The range of Reynolds number $10000 \leq Re \leq 100000$ in the study was examined. Both water and Al_2O_3 + Water nanofluid were used as working fluid under the same conditions. Therefore, the results of the study were examined in two separate sections, one for water and one for Al_2O_3 + Water nanofluid.

After the end of numerical simulations, average Nusselt number and average Darcy friction factor with respect to different Reynolds numbers were obtained and they were compared with correlations which are commonly used in the literature. It was seen that the obtained results are consistent with the results in the literature with deviation 8% approximately in average Nusselt number and with deviation 3% approximately in average Darcy friction factor. When the average Nusselt numbers and the average Darcy friction factors were examined, it was seen that the results did not change much with respect to the aspect ratios. In addition, the local Nusselt numbers and the local Darcy friction factors at certain x-distances along the channel are graphically shown. Also velocity and dimensionless temperature profiles are plotted at certain planes. The point where the fluid becomes hydrodynamically and thermally developed is farther away in nanofluid cases because of effect of viscosity.

While comparing results between water and Al_2O_3 + Water, the design a / b =2.00 was used. After the end of numerical simulations for Al_2O_3 + Water, average Nusselt number with respect to different Reynolds numbers were obtained and they were compared with correlations which are commonly used in the literature. It is seen that the obtained results are consistent with the results in the literature.

117

According to the results, using of nanofluid increases average Nusselt number significantly. However, it leads to an increase in pressure drop inside the tube. So, it causes an increase in average friction factor. To find out how effective the use of nanofluid is, the effectiveness parameter is used.

The results show that the use of nanofluids provide an improvement of approximately 11% in heat transfer applications. Also, when flow is more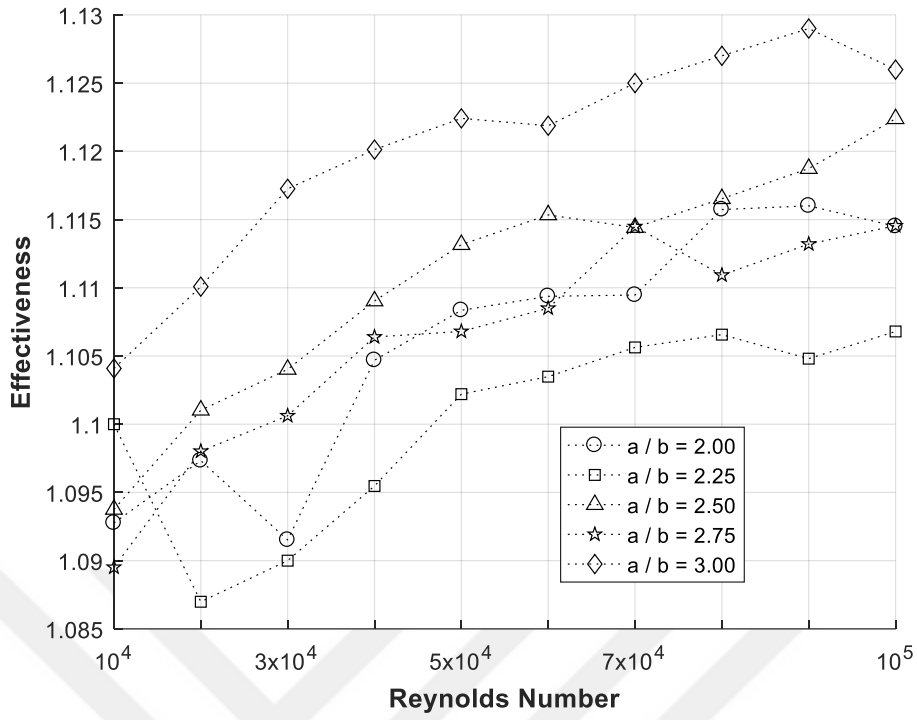 turbulent, effectiveness of use of nanofluid is increasing. As a result, use of nanofluid in heat transfer applications is crucial, especially in turbulent flows. With nanofluids, less pump power is required to obtain same amount of heat transfer rate.

In this study, numerical analysis of convective heat transfer with turbulent flow under constant temperature boundary conditions in elliptical cross-section channel with different aspect ratios was investigated. Both water and Al_2O_3 + Water nanofluid were used as a working fluid. With a similar study, changing aspect ratios at larger intervals can be examined. In addition, it is known that the diameter of the nanoparticles, the volume concentrations, the particle materials and the base fluids change heat transfer characteristics. Therefore, another study can be made based on the effect of these parameters. Furthermore, how the geometries with different cross-sectional areas affect the heat transfer together with the use of nanofluids may be another work of study. Finally, rather than identifying the thermophysical properties of the nanofluids with a single-phase approaching, two-phase approaching can be used to achieve more realistic results.

REFERENCES

1. Bianco, V., Chiacchio, F., Manca, O., Nardini, S., "Numerical investigation of nanofluid forced convection in circular tubes", *Applied Thermal Engineering*, 29: 3632-3642 (2009).

2. Dawood, H.K., Mohammed, H.A., Sidik, C.A.N., Munisamy, K.M, "Numerical investigation of heat transfer and friction factor characteristics of laminar and turbulent flow in an elliptic annulus utilizing nanofluid", *International Communication in Heat and Mass Transfer*, 66: 148-157 (2015)

3. Vajjha, S.R., Das, K.D., Ray, R.D., "Development of new correlations for the Nusselt number and the friction factor under turbulent flow of nanofluid in flat tubes", *Internatiol Journal of Heat and Mass Transfer*, 80: 353-367 (2015)

4. Shariat, M., Akbarinia, A., Nezhad, H.A., Behzadmehr, A., Laur, R., "Numerical study of two phase laminar mixed convection nanofluid in elliptic ducts", *Applied Thermal Engineering*, 31: 2348-2359 (2011)

5. Hussein, M.A., Sharma, V.K., Bakar, A.R, Kadirgama, K., "The effect of cross sectional area of tube on friction factor and heat transfer nanofluid turbulent flow", *International Communication in Heat and Mass Transfer"*, 47: 49-55 (2013)

6. Namburu, K.P, Das, K.D., Tanguturi, M.K., Vajjha, S.R., "Numerical study of turbulent flow and heat transfer characteristics of nanofluids considering variable properties", *International Journal of Thermal Sciences*, 48: 209-312 (2009)

7. Yarmand, H., Gharehkhani, S., Kazi, N.S., Sadeghinezhad, E., Safaei, R.M., "Numerical investigation of heat transfer enhancement in a rectangular heated pipe for turbulent nanofluid", *The Scientific World Journal*, Article ID:369593 (2014)

8. Abdel-Wahed, M.R, Attia, E.A., Hifni, A.M., "Experiments of laminar flow and heat transfer in an elliptical duct", *International Journal Heat Mass Transfer*, 27-12: 2397-2413 (1984)

9. Ebadian, A.M., Topakoglu, C.H., Arnas A.O., "On the convective heat transfer in a tube of elliptic cross section maintained under constant wall temperature", *Journal of Heat Transfer*, 108:33-39 (1986)

10. Bhatti, S.M., "Laminar flow in the entrance region of elliptical ducts", *Transaction of ASME*", 105:290-296 (1983)

11. Dunwoody, T.N., "Thermal results for forced heat convection through elliptical ducts", *Journal of Applied Mechanics*, March (1962)

12. Abbott, P., "On the perimeter of an ellipse", *The Mathematica Journal*, 11:2 (2009)

13. Xu, K., Ruan, B., Meng, H., "A thermal performance factor for evaluation of active engine cooling with asymmetric heating", *Applied Thermal Engineering*, 351:356-73 (2014)

14. Onur, N., Turgut, O., Arslan, K., Kurtul, Ö., "An experimental and three-dimensional numerical study on the convective heat transfer inside a trapezoidal duct under constant wall temperature", *Heat Mass Transfer*, 45:263-274 (2009)

15. Incropera, F.P., Dewitt, D., P., Bergman, T., L., Lavine, A. S., "Fundamentals of Heat and Mass Transfer Yth 6th ed.", *John Wiley&Sons Inc.*, New York, 486-533 (2007)

16. Verteg, H.K., Malalasekera, W., "An Introduction to Computational Fluid Dynamics-The Finite Volume Method 2nd ed.", *Pearson Inc.* England, 9-115 (2007)

17. Kakaç, S., Yener, Y., Pramuanjarıenkij, A., "Convective Heat Transfer 3rd ed." *CRC Press Taylor & Francis Group*, New York, 517-559 (2014)

18. Çengel, A.Y, Ghajar J. A., "Heat and Mass Transfer-Fundamentals & Applications 5th ed." *McGraw Hill Education*, New York, 1-51 (2015)

19. Arslan, K., "Experimental and numerical investigation of flow and heat transfer in rectangular corss-sectioned duct with mounted baffles on the bottom surface with different inclination angles under turbulent flow conditions", Ph.D. Dissertation, **Gazi University Instutute of Science and Technology**, Ankara, 171-173 (2010)

20. Introduction to ANSYS Fluent, Turbulence Modeling-Lecture 7, *ANSYS Inc.*, (2015)

21. ANSYS Fluent Theory Guide, *ANSYS Inc.*, 39-129 (2015)

Appendix-A / Calculation of Thermophysical Properties of Nanofluid

Calculation of thermophysical properties of Al_2O_3 + Water nanofluid is given below.

<u>Thermal Conductivity</u>

$$k_{eff} = k_{static} + k_{Brownian}$$

$$k_{static} = k_{bf} \left[\frac{(k_{np} + 2k_{bf}) - 2\phi(k_{bf} + 2k_{np})}{(k_{np} + 2k_{bf}) + \phi(k_{bf} + 2k_{np})} \right]$$

$$k_{static} = 0.613 \left[\frac{(40 + 2 \times 0.613) - 2 \times 0.06 \times (0.613 + 2 \times 40)}{(40 + 2 \times 0.613) + 0.06 \times (0.613 + 2 \times 40)} \right]$$

$$k_{static} = 0.42 \ W/m \cdot K$$

$$k_{Brownian} = 5 \times 10^4 \beta \phi \rho_{bf} c_{pbf} \sqrt{\frac{kT}{2\rho_{np}R_{np}}} f(T, \phi)$$

$$f(T, \phi) = (0.0.028217\phi + 0.003917) \frac{T}{T_o} + (0.030669\phi - 0.00391123)$$

$$f(T, \phi) = (0.0.028217 \times 0.06 + 0.003917) \frac{298}{298} + (0.030669 \times 0.06 - 0.00391123) = 0.0035$$

$$\beta = 8.4407 \, (100\phi)^{-1.07304}$$

$$\beta = 8.4407 \times (100 \times 0.06)^{-1.07304} = 1.2342$$

$$k_{Brownian} = 5 \times 10^4 \times 1.2342 \times 0.06 \times 1000 \times 418 \times \sqrt{\frac{1.3807 \times 10^{-23} \times 298}{2 \times 3970 \times 25 \times 10^{-9}}}$$

$$\times 0.0035$$

$$k_{Brownian} = 0.25 \ W/m \cdot K$$

$$k_{eff} = k_{static} + k_{Brownian} = 0.42 + 0.25 = 0.67 \ W/m \cdot K$$

Dynamic Viscosity

$$\mu_{nf} = (1 + 2.5\phi + 150\phi^2)\mu_f$$
$$\mu_{nf} = (1 + 2.5 \times 0.06 + 150 \times 0.06^2) \times 0.001$$
$$\mu_{eff} = 0.0018 \ N \cdot s/m^2$$

Density

$$\rho_{eff} = (1 - \phi)\rho_{bf} + \phi\rho_{np}$$

$$\rho_{eff} = (1 - 0.06) \times 1000 + 0.06 \times 3970 = 1178.2 \ kg/m^3$$

Specific Heat

$$(c_p)_{eff} = \frac{(1 - \phi)(\rho c_p)_{bf} + \phi(\rho c_p)_{np}}{(1 - \phi)\rho_{bf} + \phi\rho_{np}}$$

$$(c_p)_{eff} = \frac{(1 - 0.06) \times (1000 \times 4181) + 0.06 \times (3970 \times 765)}{(1 - 0.06) \times 1000 + 0.06 \times 3970}$$

$$(c_p)_{eff} = 3490.4 \ J/kg \cdot K$$

Appendix-B / Calculation of Inlet Velocities

In order to find out inlet velocity, sample calculation for design of a/b=2.00 at Reynolds number=100000 given below

Sample Calculation for Design of a/b=2.00 at Reynolds number=100000 for Water

We need only to know inlet velocity to carry out a simulation and we can calculate it by using Reynolds Number equation. In that equation, Reynolds numbers, density of fluid, dynamic viscosity of fluid and hydraulic diameter are known. Only velocity is unknown and we can calculate it as below:

$$Re_D = \frac{\rho \cdot V_i \cdot D_h}{\mu}$$

$$V_i = \frac{Re_D \cdot \mu}{\rho \cdot D_h}$$

Calculation of Hydraulic Diameter as follows [12];

$$h = \frac{(a - b)^2}{(a + b)^2}$$

$$h = \frac{(0.020 - 0.010)^2}{(0.020 + 0.010)^2}$$

$$h = 0.111$$

$$P = \pi(a + b) \sum_{n=0}^{\infty} \binom{0.5}{n}^2 h^n$$

$$P = \pi(a + b) \left(1 + \frac{1}{4}h + \frac{1}{64}h^2 + \frac{1}{256}h^3 + \cdots \right)$$

124

$$P \cong \pi(0.020 + 0.010)\left(1 + \frac{1}{4}0.111 + \frac{1}{64}0.111^2 + \frac{1}{256}0.111^3\right)$$

$$P \cong 0.09688 \, m$$

$$A_c = \pi ab$$

$$A_c = \pi \times 0.020 \times 0.010$$

$$A_c = 6.2832 \times 10^{-4} \, m^2$$

$$D_h = \frac{(4 \cdot A_c)}{P}$$

$$D_h = \frac{4 \times 6.2832 \times 10^{-4}}{0.09688}$$

$$D_h = 0.02594 \, m$$

$$V_i = \frac{Re_D \cdot \mu}{\rho \cdot D_h} = \frac{100000 \cdot 0.001002}{998.2 \cdot 0.02594} = 3.87 \, m/s$$

Likewise, all other inlet velocities can be calculated. In order to obtain specified Reynolds Number, inlet velocities must be calculated.

Sample Calculation for Design of a/b=2.00 at Reynolds number=100000 for Al_2O_3 + Water Nanofluid

$$Re_D = \frac{\rho \cdot V_i \cdot D_h}{\mu}$$

$$V_i = \frac{Re_D \cdot \mu}{\rho \cdot D_h}$$

Calculation of Hydraulic Diameter as follows [12];

$$h = \frac{(a-b)^2}{(a+b)^2}$$

$$h = \frac{(0.020 - 0.010)^2}{(0.020 + 0.010)^2}$$

$$h = 0.111$$

$$P = \pi(a+b)\sum_{n=0}^{\infty}\binom{0.5}{n}^2 h^n$$

$$P = \pi(a+b)\left(1 + \frac{1}{4}h + \frac{1}{64}h^2 + \frac{1}{256}h^3 + \cdots\right)$$

$$P \cong \pi(0.020 + 0.010)\left(1 + \frac{1}{4}0.111 + \frac{1}{64}0.111^2 + \frac{1}{256}0.111^3\right)$$

$$P \cong 0.09688\,m$$

$$A_c = \pi ab$$

$$A_c = \pi \times 0.020 \times 0.010$$

$$A_c = 6.2832 \times 10^{-4} \, m^2$$

$$D_h = \frac{(4 \cdot A_c)}{P}$$

$$D_h = \frac{4 \times 6.2832 \times 10^{-4}}{0.09688}$$

$$D_h = 0.02594 \, m$$

$$V_i = \frac{Re_D \cdot \mu}{\rho \cdot D_h} = \frac{100000 \cdot 0.0018}{1178.2 \cdot 0.02594} = 5.89 \, m/s$$

Appendix-C / MATLAB Script of Calculation of Average Nusselt Number and Average Darcy Friction Factor

```
clc
clear all
close all

%Properties of Water
rho=998.2;
mu=0.001003;
cp=4182;
k=0.6;
Pr=mu*cp/k;

% Major and Minor Axis Lengths of the Ellipces
a=[0.020 0.027 0.030 0.033 0.030];
b=[0.010 0.012 0.012 0.012 0.010];

L=3; %Length of the Tube

Tmi=298.15; % Inlet Temperature
Ts=398.15; % Wall Temperature
B=Ts-Tmi;

Re=[10 20 30 40 50 60 70 80 90 100].*1000; % Reynolds Numbers
```

% Outlet Temperatures at Every a / b

```matlab
Tmo=[343.46 339.50 337.72 335.92 334.85 334.05 333.39 332.80 332.35 331.95;...
    335.87 333.11 331.26 330.01 329.08 328.39 327.79 327.31 326.92 326.54;...
    335.81 332.35 330.52 329.30 328.43 327.72 327.19 326.70 326.32 326.027;...
    335.45 331.98 330.16 328.94 328.05 327.35 326.78 326.30 325.92 325.56;...
    340.47 336.74 334.52 333.22 332.27 331.50 330.40 329.95 329.77 329.61];
```

% Pressure Drops at Every a / b

```matlab
Pi=[284.8 920.4 1853.3 3049.5 4510.5 6205.0 8145.7 10312.5 12704.4 15325.4;...
    150.1 486.9 979.9 1615.4 2385.3 3287.6 4309.9 5446.1 6727.7 8097.8;...
    142.7 462.4 930.4 1533.9 2266.1 3119.8 4100 5185.1 6387.9 7712.8;...
    135.1 437.1 878.4 1449.9 2141.7 2950.1 3869.4 4896.4 6037.1 7274.8;...
    232.07 747.48 1478.49 2433.58 3590.76 4937.45 6474.53 8193.62 10080.23
12152];
```

```matlab
for j=1:length(a)

    h(j)=(a(j)-b(j))^2/(a(j)+b(j))^2;
    P(j)=pi*(a(j)+b(j))*(1+1/4*h(j)+1/64*h(j)^2+1/256*h(j)^3);
    A_c(j)=pi*a(j)*b(j);
    D(j)=4*A_c(j)/P(j);

    for i=1:length(Re)

        V(j,i)=Re(i)*mu/(rho*D(j));

        m(j,i)=rho*V(j,i)*A_c(j);

        A(j,i)=Ts-Tmo(j,i);

        LMTD(j,i)=log(B/A(j,i));

        h(j,i)=LMTD(j,i)*m(j,i)*cp/(P(j)*L);

        Nu(j,i)=h(j,i)*D(j)/k; % Our Calculation

        Dittus(j,i)=0.0243*Re(i)^(0.8)*Pr^(0.4); % Dittus-Boelter

        f(j,i)=(0.79*log(Re(i))-1.64)^(-2); % Petukhov

        f_kp(j,i)=(D(j)/L)*(Pi(j,i)/(998.2*0.5*V(j,i)^2)); % Our Calculation
```

```matlab
        Nu_yeni(j,i)=((f(j,i)/8)*(Re(i)-1000)*Pr)/(1+(12.7*(f(j,i)/8)^0.5*...
                (Pr^(2/3)-1)));  % Gnielinski

    end
end


loglog(Re,Nu(5,:),'ko','MarkerFaceColor','k')
hold on
loglog(Re,Dittus(5,:),'ks','MarkerFaceColor','k')
hold on
loglog(Re,Nu_yeni(5,:),'k^')
grid on
xlabel('Reynolds Number','FontWeight','b')
ylabel('Average Nusselt Number','FontWeight','b')
legend('CFD','Dittus-Boelter','Gnielinski')


figure

loglog(Re,f_kp(1,:),'ko','MarkerFaceColor','k')
hold on
loglog(Re,f(1,:),'k^')
grid on
xlabel('Reynolds Number','FontWeight','b')
ylabel('Average Darcy Friction Factor','FontWeight','b')
legend('CFD','Petukhov')
```

Appendix-D / MATLAB Script of Calculation of Local Nusselt Number and Local Darcy Friction Factor

```
clc
clear
close all

a=[0.020 0.027 0.030 0.033 0.030];
b=[0.010 0.012 0.012 0.012 0.010];

rho=998.2;
mu=0.001003;
k=0.6;

Ts=398.15;

Re=[10 20 30 40 50 60 70 80 90 100].*1000;

for j=1:length(a)

    h(j)=(a(j)-b(j))^2/(a(j)+b(j))^2;
    P(j)=pi*(a(j)+b(j))*(1+1/4*h(j)+1/64*h(j)^2+1/256*h(j)^3);
    A_c(j)=pi*a(j)*b(j);
    D(j)=4*A_c(j)/P(j);

    for i=1:length(Re)

        V(j,i)=Re(i)*mu/(rho*D(j));

    end
end


% ----------------- LOCAL DIMENSIONLESS NUMBERS --------------------- %

x=[3000 2950 2900 2850 2800 2750 2700 2650 2600 2550 2500 2450 2400 2350 ...
   2300 2250 2200 2150 2100 2050 2000 1950 1900 1850 1800 1750 1700 1650 ...
   1600 1550 1500 1450 1400 1350 1300 1250 1200 1150];

x=((3000-x).*0.001);

T1=xlsread('dimensionless.xlsx', 1, 'C52:C89');
qw1=xlsread('dimensionless.xlsx', 1, 'D52:D89');
tau1=xlsread('dimensionless.xlsx', 1, 'E52:E89');
```

```matlab
 T2=xlsread('dimensionless.xlsx', 1, 'C4:C41');
qw2=xlsread('dimensionless.xlsx', 1, 'D4:D41');
tau2=xlsread('dimensionless.xlsx', 1, 'E4:E41');

T6=xlsread('dimensionless.xlsx', 1, 'F4:F41');
qw6=xlsread('dimensionless.xlsx', 1, 'G4:G41');
tau6=xlsread('dimensionless.xlsx', 1, 'H4:H41');

T10=xlsread('dimensionless.xlsx', 1, 'I4:I41');
qw10=xlsread('dimensionless.xlsx', 1, 'J4:J41');
tau10=xlsread('dimensionless.xlsx', 1, 'K4:K41');

for i=1:length(x)

   T_theta1(i)=(Ts-T1(i))/(qw1(i)*D(1))*k;

   hx1(i)=qw1(i)/(Ts-T1(i));

   Nux1(i)=hx1(i)*D(1)/k;

   fx1(i)=tau1(i)/(1/2*rho*V(1,1)*V(1,1));

   T_theta2(i)=(Ts-T2(i))/(qw2(i)*D(1))*k;

   hx2(i)=qw2(i)/(Ts-T2(i));

   Nux2(i)=hx2(i)*D(1)/k;

   fx2(i)=tau2(i)/(1/2*rho*V(1,2)*V(1,2));

   T_theta6(i)=(Ts-T6(i))/(qw6(i)*D(1))*k;

   hx6(i)=qw6(i)/(Ts-T6(i));

   Nux6(i)=hx6(i)*D(1)/k;

   fx6(i)=tau6(i)/(1/2*rho*V(1,6)*V(1,6));

   T_theta10(i)=(Ts-T10(i))/(qw10(i)*D(1))*k;

   hx10(i)=qw10(i)/(Ts-T10(i));

   Nux10(i)=hx10(i)*D(1)/k;

   fx10(i)=tau10(i)/(1/2*rho*V(1,10)*V(1,10));

end
```

131

```matlab
 for i=1:length(x)-1

    AA(i)=(abs(Nux1(i)-Nux1(i+1))/Nux1(i));

end

stop=ones(1,length(10:length(x))).*0.0005;

hold on
plot(x(1,10:length(x))/D(1),AA(1,9:length(AA)),'-.k','Linewidth',2)
plot(x(1,10:length(x))/D(1),stop,'k-')
xlabel('x / D_h','FontWeight','b')
ylabel('Relative Percentage Change','FontWeight','b')
legend('Relative Change in Nu_x at Re=10000','Stopping Criteria = 0.0005')
grid on

figure

hold on

plot(x/D(1),Nux1','+k','markersize',4)
plot(x/D(1),Nux2','ok','markerfacecolor','k','markersize',4)
plot(x/D(1),Nux6','^k','markersize',4)
plot(x/D(1),Nux10','sk','markerfacecolor','k','markersize',4)
legend('Re = 10000','Re = 20000','Re = 60000','Re = 100000')
grid on
xlabel('x / D_h','FontWeight','b')
ylabel('Nu_x','FontWeight','b')

figure

hold on

plot(x/D(1),fx1,'+k','markersize',4)
plot(x/D(1),fx2,'ok','markerfacecolor','k','markersize',4)
plot(x/D(1),fx6,'^k','markersize',4)
plot(x/D(1),fx10,'sk','markerfacecolor','k','markersize',4)
legend('Re = 10000','Re = 20000','Re = 60000','Re = 100000')
grid on
xlabel('x / D_h','FontWeight','b')
ylabel('C_f_x','FontWeight','b')
```

CURRICULUM VITAE

PERSONAL INFORMATION

Surname, Name: Peneklioğlu, Kağan

Date and Place of Birth: 16 Feb 1989, Ankara

Marital Status: Married

Email: kaganpe@gmail.com

EDUCATION

Degree	Institution	Year of Graduation
M.Sc.	Çankaya University Mechanical Engineering	2017
B.Sc.	Hacettepe University, Nuclear Energy Engineering	2013

WORK EXPERIENCE

Year	Place	Enrollment
2013- Present	Figes Engineering	CFD Application Engineer

FOREIN LANGUAGES

English

PUBLICATIONS

1. Öztürk, İ., Koyuncu, A., **Peneklioğlu, K.**, Karaismail, E., "Effect of Radiator Cooling Package Alignment on Underhood Cooling Performance of an Agricultural Tractor", International Conference on Advances in Automotive Technologies, 10-11 October 2016, Yıldız Technical University, İstanbul / Turkey